ORNL/TM-6659

High Voltage Research (Breakdown Strengths of Gaseous and Liquid Insulators)

Semiannual Report (April 1-September 30, 1978)

L. G. Christophorou
D. R. James
R. Y. Pai
R. A. Mathis
I. Sauers
M. O. Pace
D. W. Bouldin
A. A. Christodoulides
C. C. Chan

OAK RIDGE NATIONAL LABORATORY
OPERATED BY UNION CARBIDE CORPORATION · FOR THE DEPARTMENT OF ENERGY

DISCLAIMER

Printed in the United States of America. Available from
National Technical Information Service
U.S. Department of Commerce
5285 Port Royal Road, Springfield, Virginia 22161
Price: Printed Copy $7.25; Microfiche $3.00

ORNL/TM-6659

Contract No. W-7405-eng-26
Activity No. C1 01 01 04 0

HEALTH AND SAFETY RESEARCH DIVISION

ATOMIC, MOLECULAR AND HIGH
VOLTAGE PHYSICS GROUP

HIGH VOLTAGE RESEARCH (BREAKDOWN STRENGTHS OF GASEOUS AND LIQUID INSULATORS)

Semiannual Report
(April 1 - September 30, 1978)

L. G. Christophorou

D. R. James
R. Y. Pai
R. A. Mathis
I. Sauers (Postdoctoral Fellow)
M. O. Pace (part time)
D. W. Bouldin (part time)
A. A. Christodoulides (alien guest)
C. C. Chan (student)

Date Published: January 1979

NOTICE This document contains information of a preliminary nature. It is subject to revision or correction and therefore does not represent a final report.

OAK RIDGE NATIONAL LABORATORY
Oak Ridge, Tennessee 37830
operated by
UNION CARBIDE CORPORATION
for the
DEPARTMENT OF ENERGY

THIS PAGE

WAS INTENTIONALLY

LEFT BLANK

CONTENTS

ABSTRACT

The work on gas dielectric mixtures continued to focus on carefully chosen combinations of electron attaching and electron slowing-down gases. Experimental evidence relating the electron attachment cross section to the dielectric strength is discussed. Conclusions are reached as to the relation of molecular structure to the electron attaching properties of dielectric gases.

A variety of mixtures of SF_6, Ar, Ne, and N_2 have been studied to determine the relative importance of electron impact ionization and electron scattering on the breakdown voltage, V_S. Very interestingly, electron scattering (especially in the subexcitation energy range) was found to influence V_S much more critically than electron impact ionization. Preliminary studies involving mixtures of the polar molecules (1,1,1-CH_3CF_3, CHF_3, and CH_2F_2 with SF_6 and N_2 showed that electron-dipole scattering does not significantly affect V_S. Field-induced electron detachment from negative ions--which has often been cited as a possible cause of a host of phenomena in gas breakdown studies--has been investigated, and the results of this investigation are reported.

The temperature range of the high pressure, variable temperature apparatus has been extended to ∿150°C by irradiation of the high-voltage cable. Preliminary data indicate that there is no appreciable change in the uniform-field breakdown voltage over the range of temperatures from 18 to ∿150°C for 100% SF_6 and a 30% SF_6 + 70% N_2 mixture. The V_S of C_2F_6 and n-C_4F_{10} was measured and found to be, respectively, 0.80 and 1.32 relative to that of SF_6.

In the environmental effects area, results are presented on the initial

decomposition of a number of fluorocarbons. Results are also presented on stressed and/or sparked perfluorocarbons and SF_6 as well as on breakdown solid residues and toxicity tests.

In the practical conditions test facility using cylindrical electrodes, tests have essentially been completed for SF_6/N_2, $c\text{-}C_4F_8/N_2$, $2\text{-}C_4F_8/N_2$, and $2\text{-}C_4F_6/N_2$ mixtures. Three different inner radii, both polarities, and a comprehensive set of mixture proportions were used in these studies. To investigate the effects of surface roughness, these mixtures were tested with three different cylindrical electrodes identical except for the degree of carefully produced roughness. The effects of electrode material composition and particle contamination were also studied for these mixtures.

The purification system for our liquid dielectrics studies has been fabricated and tested, and the breakdown cell has been successfully operated. The apparatus for impulse testing of gases/mixtures has been assembled, tested, and put into regular operation. The first tests have been on SF_6/N_2 mixtures in point-plane geometry, with both switching surge and lightning waveforms with the plan of compiling careful impulse test results on a variety of dielectric gas mixtures *under identical conditions* to provide meaningful comparisons.

I. INTRODUCTION

The Oak Ridge National Laboratory's dielectrics program is *comprehensive*. It embraces

1. basic studies,
2. applied testing,
3. environmental effects and long-range stability studies, and
4. efforts for industrial interfacing.

Work on items 1 and 2 continued with vigor. Work on item 3 is currently being intensified. It is hoped that work on item 4 will commence in the near future.

II. BASIC STUDIES OF GASEOUS DIELECTRICS

A. The Magnitude and Energy Dependence of the Electron Attachment Cross Section for Highly Electronegative Gaseous Dielectrics

During this six-month period we (1) concentrated on analyzing the full range of our data on electron attachment to perfluorocarbon molecules with the view of presenting a coherent picture of the influences of the various aspects of molecular structure on the attachment of slow electrons to perfluorocarbon compounds and (2) continued to measure electron attachment rates and cross sections for other perfluorocarbons.

In connection with (1) two papers entitled: "Electron attachment to perfluorocarbon compounds: Part I: c-C_4F_6, 2-C_4F_6, 1,3-C_4F_6, c-C_4F_8, and 2-C_4F_8" and "Electron attachment to perfluorocarbon compounds: Part II: c-C_5F_8 and c-C_6F_{10}, c-C_6F_{12}, C_7F_8, and C_8F_{16} - Relevance to Gaseous Dielectrics" have been submitted and have been accepted for publication in the *Journal of Chemical Physics*. These comprehensive studies clearly show some of the distinct advantages of many perfluorocarbon compounds (PFCs) for use as unitary gases and/or as additives to multicomponent gas dielectrics. Thus, the average value of the energy integrated attachment cross section from thermal energy to 1.4 eV [i.e., $\int_{0.04\ \mathrm{eV}}^{1.4\ \mathrm{eV}} \sigma_a(\varepsilon)d\varepsilon$] is 0.83 x 10^{-15} cm^2 eV for perfluorocarbons whose mean V_s is $\sim$1.5 times that of SF_6 and 1.8 x 10^{-15} cm^2 eV for perfluorocarbons whose V_s is $\sim$2.3 times that of SF_6. Large electron attachment cross sections extending to as high an electron energy range as possible are crucial in effecting a high dielectric strength. Other conclusions drawn from those comprehensive studies are: (i) open-chain saturated PFCs do not attach electrons as efficiently as the

unsaturated PFCs; (ii) for saturated PFCs an increase in molecular size (chain length) increases the attachment rate; (iii) the presence of multiple bonds in the molecule dramatically increases the magnitude of the electron attachment rate for the saturated open-chain PFCs, but it has only a small effect for cyclic PFCs; (iv) the cyclic nature of the PFCs seems to increase greatly the electron attachment cross section; and (v) for single-bonded cyclic PFCs, substitution of CF_3 groups for F atoms increases electron attachment at thermal electron energies more than does an increase in molecular size; in double-bonded cyclic compounds, increase in ring size increases the attachment cross section at thermal energies.

In connection with (2) a swarm study on the attachment of slow electrons ($\lesssim$3 eV) to c-C_7F_{14} (perfluoromethylcyclohexane) and 1-C_7F_{14} (perfluoro-1-heptene) has been completed. For both molecules the attachment cross sections show resonance maxima at 0.07 and 0.25 eV, and they are much larger for the cyclic isomer. The energy integrated attachment cross section from thermal energy to 1.4 eV [i.e., $\int_{0.04\ eV}^{1.4\ eV} \sigma_a(\varepsilon)d\varepsilon$] is 2.6 x 10^{-15} cm^2 eV for c-C_7F_{14} and $\sim$0.5 x 10^{-15} cm^2 eV for 1-C_7F_{14}, while the thermal value of the electron attachment rate for c-C_7F_{14} is 18.3 x 10^8 sec^{-1} $torr^{-1}$ [i.e., 14 times larger than that (1.33 x 10^8 sec^{-1} $torr^{-1}$) for 1-C_7F_{14}]. These findings are consistent with the higher dielectric strength of c-C_7F_{14} relative to 1-C_7F_{14}. The relative direct current (DC) breakdown voltages for c-C_7F_{14}, 1-C_7F_{14} and SF_6 are: 2.2, 1.2, and 1.0, respectively. This work is fully described in a paper submitted for publication to *Chemical Physics Letters* which is attached as Appendix A.

B. The Role of the Electron Impact Ionization Cross Section in the Breakdown Strength of Dielectric Gases

Our systematic studies on the role of the electron impact ionization cross section, $\sigma_i(\varepsilon)$, as a function of electron energy ε in the breakdown strength, V_S, of gases/mixtures continued with extreme vigor. Four gases (Ne, Ar, N_2, and SF_6) were chosen for which the $\sigma_i(\varepsilon)$ and the total electron scattering cross section, $\sigma_{sc}(\varepsilon)$, at low energies are known. Measurements of DC breakdown strengths on Ne, Ar, Ne + N_2, Ar + N_2, Ne + SF_6, Ar + SF_6, N_2 + Ne + SF_6, and N_2 + Ar + SF_6 have been completed and are reported, using sphere on sphere-sphere and/or square rod-plane electrode geometries. Also DC breakdown strength measurements have been made on pure Ne and pure Ar using plane-plane electrode geometry (see Fig. 1). Additionally, electron energy distribution functions have been computed for a number of values of E/P (pressure-reduced electric field) for Ne and Ar. On the basis of these measurements, calculations, and data on $\sigma_{sc}(\varepsilon)$ and $\sigma_i(\varepsilon)$, it was concluded that the magnitude of $\sigma_{sc}(\varepsilon)$ at subionization ($\varepsilon < I$) and especially at subexcitation ($\varepsilon <$ energy of lowest excited electronic state) energies is much more significant in effecting high values of V_S than $\sigma_i(\varepsilon)$. The *general* conclusion can be drawn that large electron scattering cross sections in the *subexcitation* energy range is *the* most significant factor in effecting a high V_S besides large electron attachment cross sections. These significant findings are described in a paper being submitted for publication in the *Journal of Physics D (Applied Physics)*; the paper is attached to this report as Appendix B. In this paper the effect of the static polarizability and perfluorination on $\sigma_i(\varepsilon)$ is also discussed. Thus, it was found that the size of the ionization cross section for

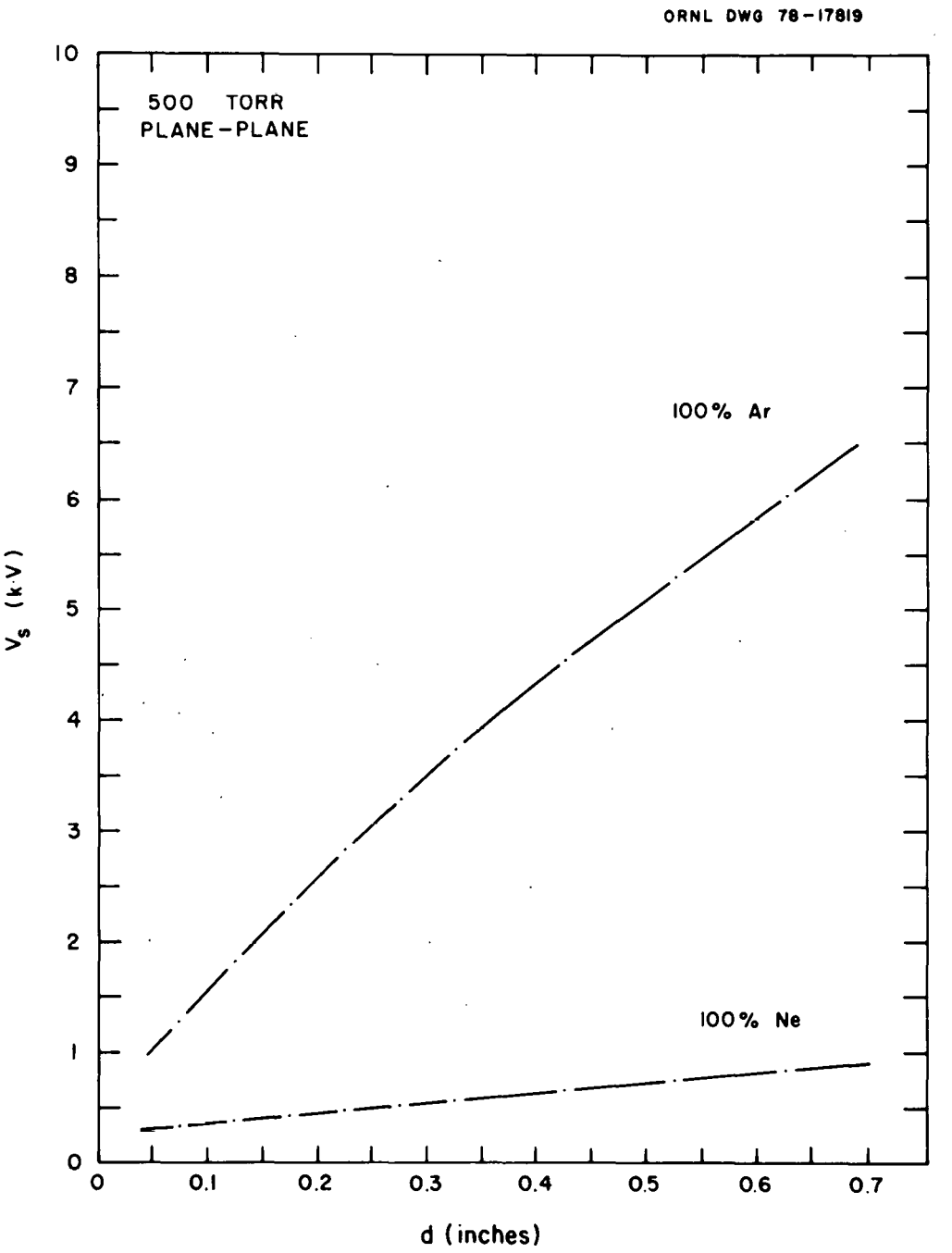

Fig. 1. V_S vs d for pure Ar and pure Ne. (Pressure = 500 torr; T ≃ 296°K; plane-plane electrode geometry.) The breakdown voltages for 100% Ar reflect a greater uncertainty than for any other gas we investigated. For a given electrode separation the V_S was observed to increase with time on the order of 5 to 10% over the course of ∿30 min. Also when the V_S of a given Ar sample was measured on succeeding days a difference in V_S of as much as 20% was noted.

most molecules tends to increase with the size of their respective static polarizabilities. For a given value of the static polarizability it was found that perfluorination of a hydrocarbon reduces the size of the ionization cross section, especially near the ionization threshold energy. It was found, also, that for perfluorinated hydrocarbons the ionization thresholds are higher, and ionization cross sections are lower, than those of their respective nonfluorinated analogs. This is attributable to the high electronegativity and high ionization threshold energy of the ground state F atom.

Not included in the *Journal of Physics D* paper are the V_S vs Pd data on the Ne + N_2 and Ar + N_2 mixtures which are shown in Fig. 2.

C. Effect of Dipole Scattering on V_S

Gas dielectric components comprising molecules with permanent electric dipole moments may prove beneficial in increasing the breakdown voltage, V_S, of multicomponent gaseous insulators in two ways:

(1) via strong dipole scattering of low-energy electrons and

(2) via clustering effects involving ions and dipolar molecules.

In this reporting period we began investigating (1), and some of our initial findings are briefly outlined below.

The cross sections for electron-dipolar molecule scattering at near thermal electron energies are large and increase approximately as the square of the size of the permanent electric dipole moment D (see for example refs. 1-3). The electron-dipole scattering cross section falls off as $1/v^2$ (v is the electron velocity), but the extent of electron energies above thermal over which this velocity dependence of the

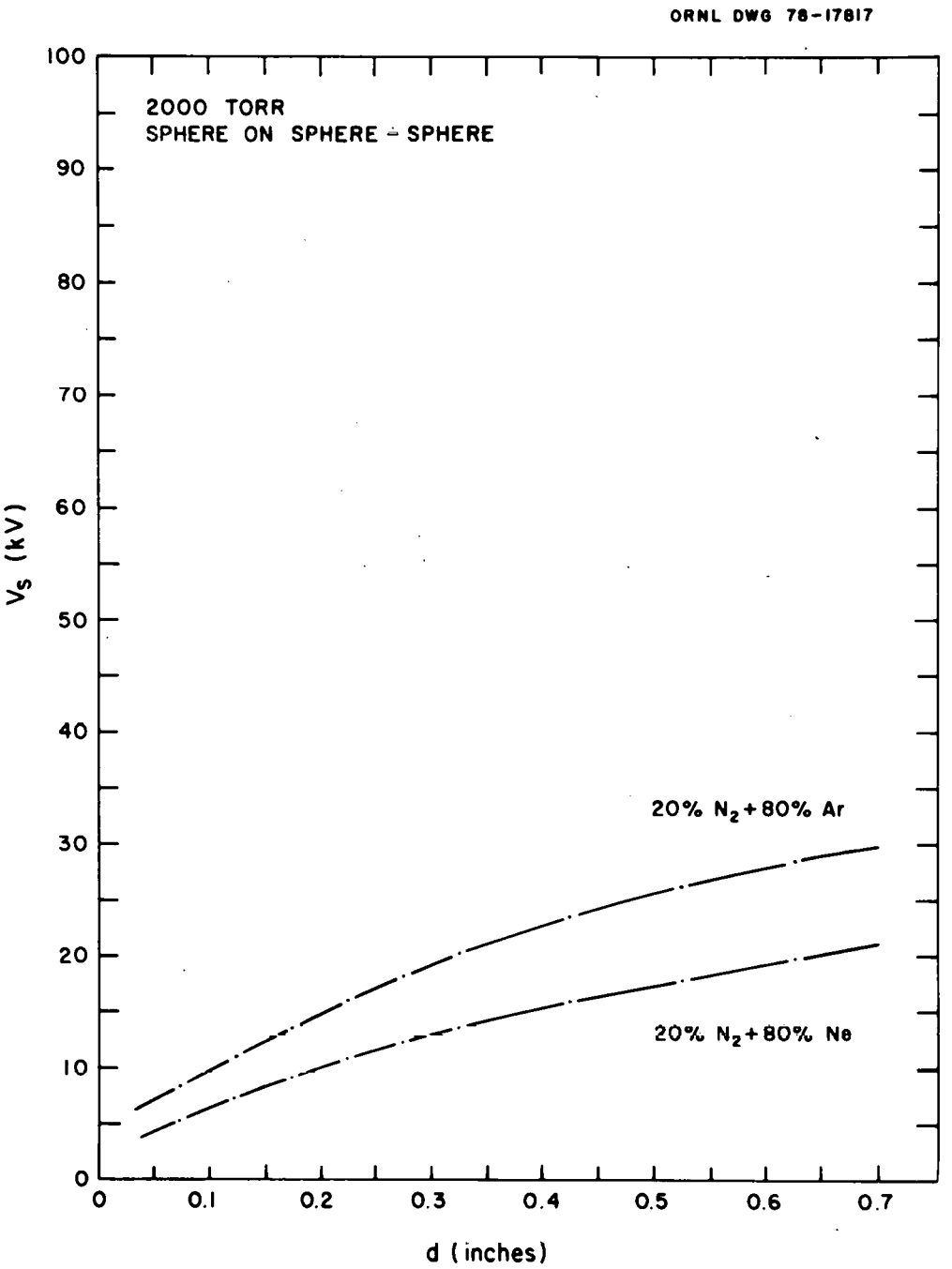

Fig. 2. V_S vs d for 20% N_2 + 80% Ar and 20% N_2 + 80% Ne (total pressure = 2000 torr; T ≈ 296°K; sphere on sphere-sphere electrode geometry).

scattering cross section is valid is unknown. For D values of 2 to 3 debye, the scattering cross section is quite large ($>10^{-14}$ cm^2 for $\varepsilon < 0.9$ eV for D = 3 debye) and many molecules, convenient to use in multicomponent gas mixtures, exist with dipole moments of this size. Four such molecules with D in the range 0 to 2.32 debye were chosen, and their V_s in mixtures with SF_6 and $SF_6 + N_2$ have been measured. The results of these studies are summarized in Table 1 and Figs. 3 and 4. It can be seen from these findings that electron-dipole scattering does not significantly increase V_s. However, further work is needed and is in progress. Work is also in progress with regard to item (2) (i.e., the possible effect of clustering on V_s in multicomponent gas mixtures containing molecules with large D).

D. Electric Field-Induced Electron Detachment from Mononegative Ions

We have repeatedly pointed out in our earlier work (see, for example, refs. 4-6) that the most desirable way of removing electrons from a gaseous dielectric medium--in order to effect a higher dielectric strength--is capture of the electrons by the dielectric gas molecules forming negative ions. These ions diffuse to the walls and are destroyed there. If, however, the electrons are loosely bound to the atom, radical, or molecule (i.e., if the electron affinity, EA, of the capturing species is small, say, close to 3/2 kT), the ions, A^-, can be efficiently destroyed in collisions with neutral species, M ($A^- + M \rightarrow M + A + e$) and/or by electric fields (field-induced electron detachment) when the latter are large. It is of course possible that other electron detachment processes (e.g., photodetachment, associative, and nonassociative collisional

Table 1. Breakdown voltage, V_s, for mixtures containing component gases with permanent electric dipole moments, D

Percentage (%)			Dipole Moment of X (debye)	V_s (kV)[a] d(inches)								
SF_6	N_2	X		0.075	0.125	0.175	0.225	0.275	0.325	0.425	0.525	0.625
100					18.27	25.71	33.04	40.52	48.03			
30	70				15.07	21.14	27.24	33.30	39.43			
30		70 (CF_4)	0	7.58	12.31	17.15	21.87	26.75	31.50	41.12	50.80	60.33
30		70 (CHF_3)	1.65	8.00	12.77	17.92	22.93	27.91	33.02	43.07	53.23	63.24
30		70 (CH_2F_2)	1.97	7.65	12.46	17.27	22.15	27.01	31.89	41.61	51.39	61.15
30		70 (1,1,1-CH_3CF_3)	2.32	9.56	15.73	21.72	27.92	34.04	40.08	52.32	64.66	76.92
30	35	35 (CF_4)	0	8.75	14.47	19.87	25.37	30.97	36.55	47.70	58.90	69.98
30	35	35 (CHF_3)	1.65	8.74	14.41	20.01	25.63	31.27	36.87	48.18	59.39	70.63
30	35	35 (CH_2F_2)	1.97	8.43	13.84	19.35	24.62	30.22	35.52	46.47	57.38	68.42
30	35	35 (1,1,1-CH_3CF_3)	2.32	9.49	15.45	21.45	27.49	33.49	39.57	51.67	63.71	75.74

[a]Total pressure: 500 torr; T ≈ 296°K; plane-plane electrode geometry.

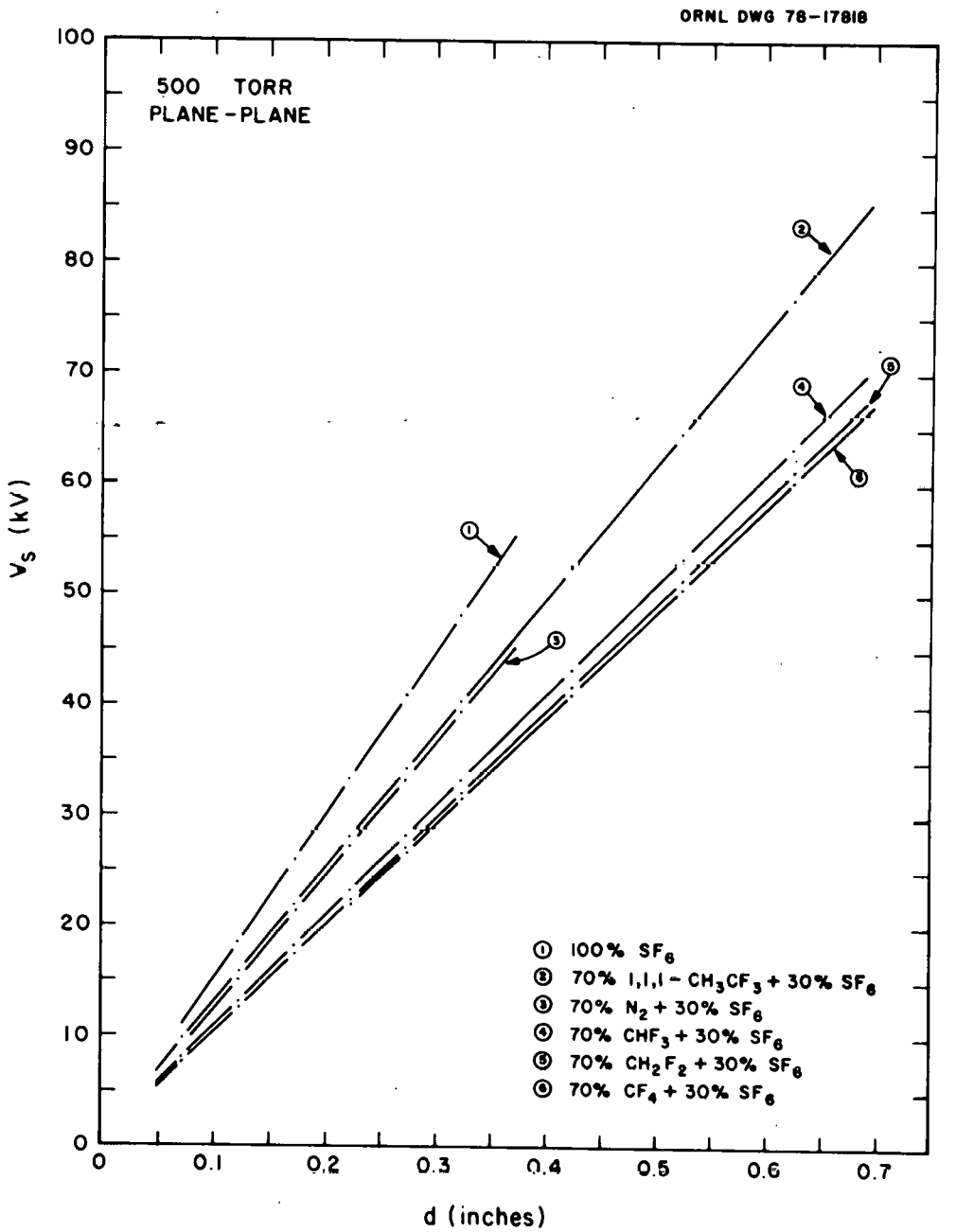

Fig. 3. V_S vs d for pure SF_6 and mixtures of SF_6 with polar and nonpolar component gases (see text and Table 1). (Total pressure = 500 torr; T ≈ 296°K; plane-plane electrode geometry.)

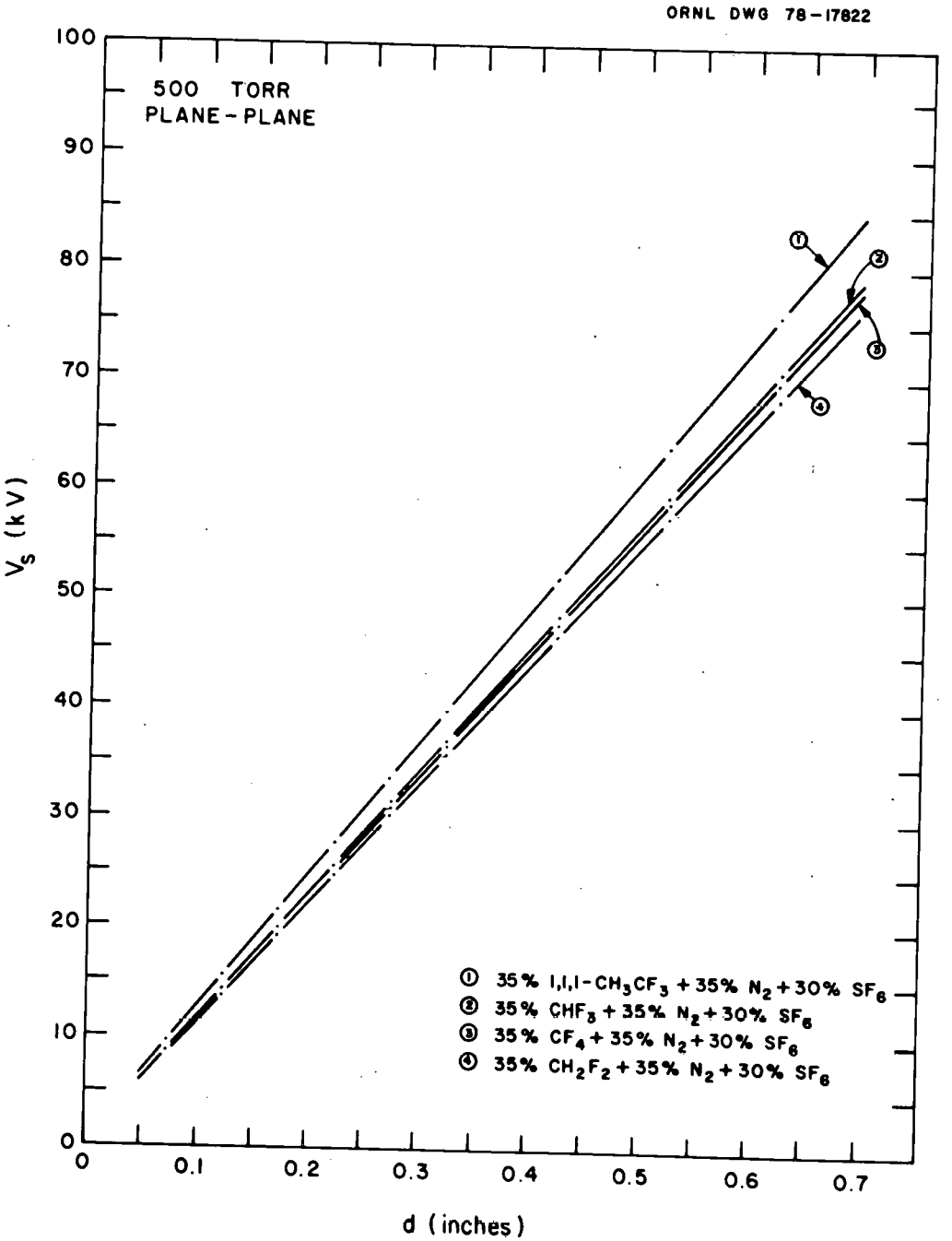

Fig. 4. V_s vs d for mixtures of polar fluorocarbons with 35% N_2 + 30% SF_6. (Total pressure = 500 torr; T ≈ 296°K; plane-plane electrode geometry.)

detachment, see Chapter 7 of ref. 1) can occur. Electron impact-induced collisional detachment ($e + A^- \rightarrow A + 2e$) may occur when a substantial fraction of the electrons in the stressed gas have high energies, as might be the case in high electric fields. Although little is known about this process in the energy range of interest to breakdown phenomena, it is clear that a repulsive Coulomb force exists between the electron and the anion--which is, of course, absent in other types of electron detachment processes such as photodetachment. Actually, the Bethe-Born approximation with a semiempirical correction for the $e - A^-$ repulsion was found to be in reasonable agreement at high energies with the experimental results on $e + H^- \rightarrow H + 2e$ and $e + O^- \rightarrow O + 2e$ (see ref. 1, Chapter 7 and ref. 7, pp. 500-512).

A host of observations in breakdown studies have been attributed to electric field-induced electron detachment from negative ions. Very little is indeed known about this process (see, however, ref. 7, pp. 495-500) and its implied role in breakdown phenomena. We addressed ourselves to this question, and our preliminary results are outlined below.

Schweinler (see Appendix C) considered field emission from atomic and molecular anions in s-states (angular momentum quantum number $\ell = 0$)[†] and obtained for the probability of electron detachment per second, p, the expression

$$p = \frac{\text{transition}}{\text{sec}} \simeq \left\{ f \exp\left[2(\tilde{EA})^{1/2} \frac{r_o}{a_H} \right] \right\} \times 2 \times 10^{16} \left\{ \frac{|\tilde{E}|}{(\tilde{EA})} \right\}^{1/2} \exp\left(-\frac{2}{3} \frac{(\tilde{EA})^{3/2}}{|\tilde{E}|} \right) \Bigg\}, \quad (1)$$

[†]Work on field-induced electron detachment from negative ion states with $\ell \geq 0$ is in progress.

where

f = fraction of probability density outside of the effective range, r_0, of the interaction potential (r_0 is roughly the radius of the negative ion; see Appendix C)

$\tilde{EA} = \frac{EA}{13.6}$; EA is the electron affinity of the capturing species in eV.

a_H = Bohr radius = 0.5292×10^{-8} cm

$\tilde{E} = \frac{E}{5 \times 10^9}$; E is the applied electric field in volts cm^{-1}.

Figure 5 shows p as a function of E for different values of EA for $x = r_0/a_H = 2$ and f = 0.01, and Fig. 6 shows p as a function of EA for various values of E. Since f in Eq. (1) is simply a multiplicative factor, the values of p in Figs. 5 and 6 will have to be multiplied by a factor of y/0.01 for values, y, of f. A value of f between 0.1 and 0.01 is considered reasonable. The effect of r_0 on p can be seen from the data in Tables 2 and 3 for x = 2 (Table 2) and x = 5 (Table 3). The former (x = 2) values may be considered typical of atomic anions and the latter (x = 5) typical of molecular anions.

To understand the role of field-induced electron detachment let us consider the reaction

$$e + AX \longrightarrow AX^{-*} \begin{cases} \rightarrow A + X^- & (2a) \\ \rightarrow AX^- & (2b) \end{cases},$$

where AX^{-*} is a transient (metastable) negative ion which dissociates (channel 2a); is stabilized (usually by collision)(channel 2b) or is destroyed by autodetachment [$AX^{-*} \rightarrow AX^{(*)} + e^{(\cdot)}$]. For pressures normally employed in practice (say $\sim$5 atm) the collision time, τ_{coll}, between AX^{-*} and AX (or a buffer gas molecule, Y) is of the order of 10^{-11}-10^{-12} sec, depending on AX^- and Y.† If AX^{-*} is stabilized with an efficiency

†If AX or Y is polar the collision time could be even shorter.

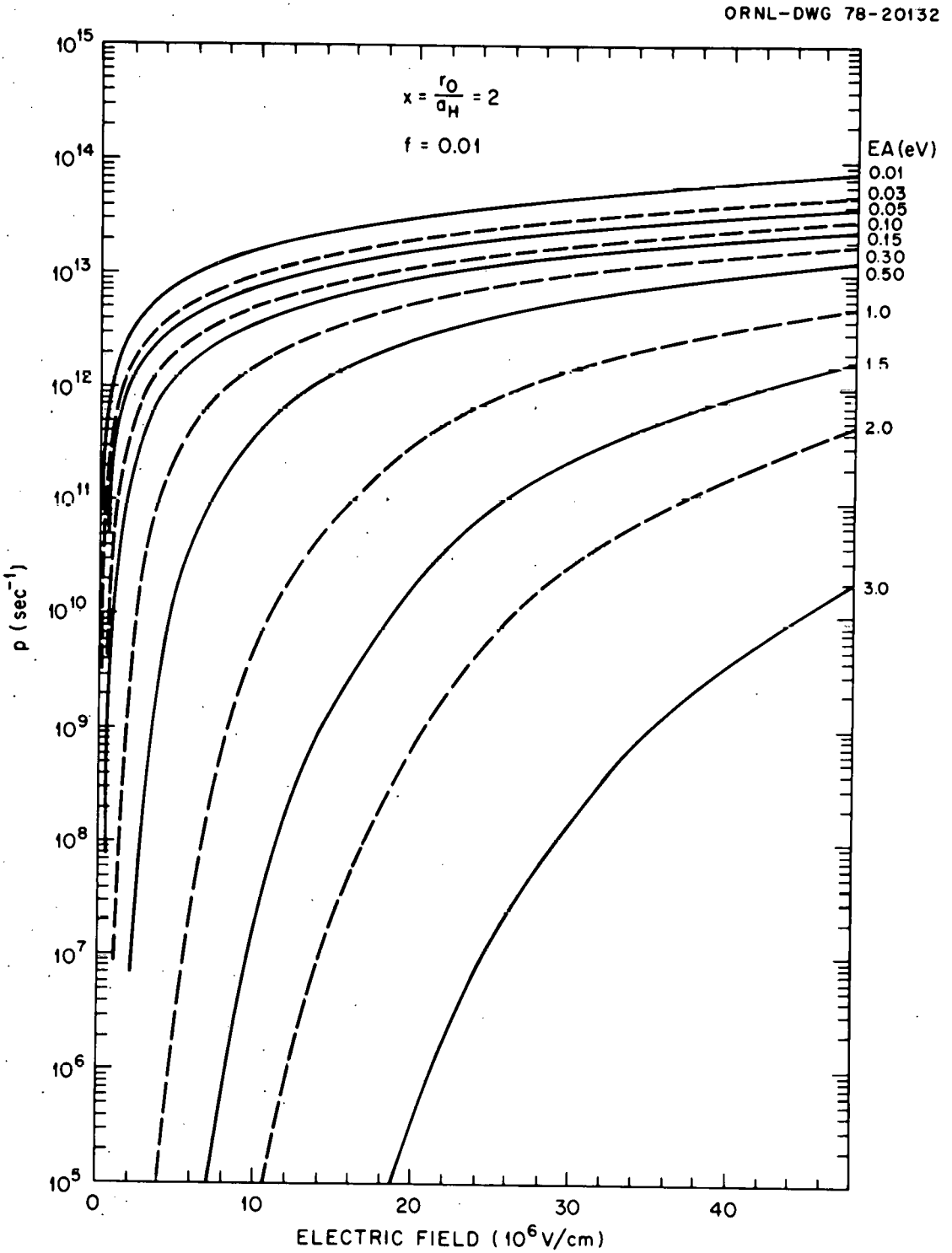

Fig. 5. p(sec^{-1}) vs E(10^6 V cm^{-1}) for various values of EA(eV); $x = r_0/a_H = 2$ and f = 0.01 (see text).

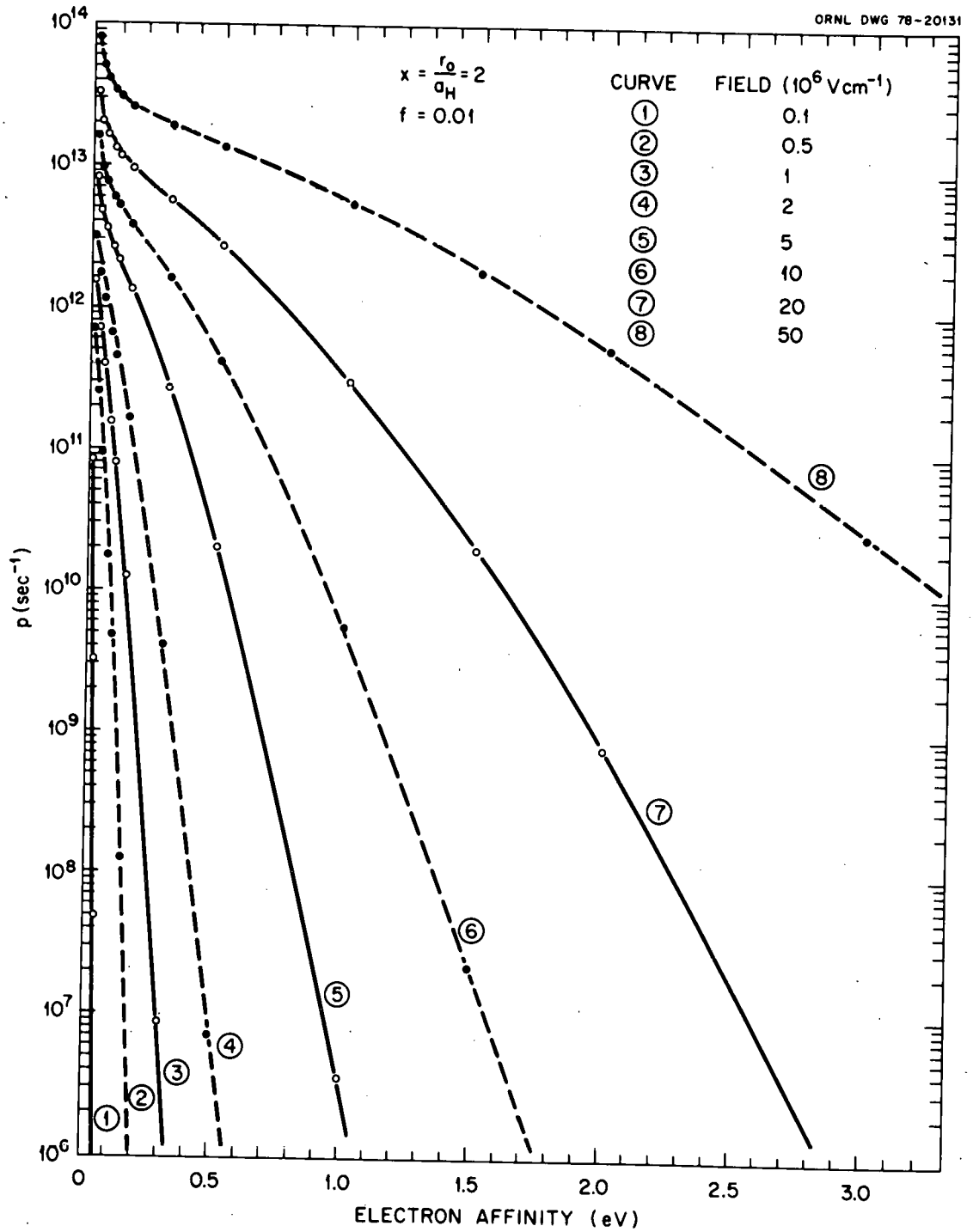

Fig. 6. p(sec^{-1}) vs EA(eV) for various values of E(10^6 V cm^{-1}); $x = r_o/a_H = 2$; f = 0.01 (see text).

Table 2. Values of p for various combinations of EA and E; x = 2 and f = 0.01[a]

	p(sec^{-1})							
	E (10^6 volts cm^{-1})							
EA(eV)	0.1	0.5	1	2	5	10	20	50
0.01	8.46×10^{10}	7.20×10^{11}	1.54×10^{12}	3.18×10^{12}	8.11×10^{12}	1.63×10^{13}	3.28×10^{13}	8.21×10^{13}
0.03	3.25×10^{9}	2.58×10^{11}	7.28×10^{11}	1.73×10^{12}	4.3×10^{12}	9.93×10^{12}	2.02×10^{13}	5.1×10^{13}
0.05	4.98×10^{7}	9.51×10^{10}	4.00×10^{11}	1.16×10^{12}	3.52×10^{12}	7.81×10^{12}	1.62×10^{13}	4.14×10^{13}
0.08	2.09×10^{4}	1.75×10^{10}	1.58×10^{11}	6.68×10^{11}	2.52×10^{12}	6.1×10^{12}	1.31×10^{13}	3.44×10^{13}
0.1	4.9×10^{1}	4.91×10^{9}	8.04×10^{10}	4.60×10^{11}	2.16×10^{12}	5.33×10^{12}	1.18×10^{13}	3.15×10^{13}
0.15	9.88×10^{-7}	1.28×10^{8}	1.22×10^{10}	1.68×10^{11}	1.34×10^{12}	3.94×10^{12}	9.56×10^{12}	2.68×10^{13}
0.3	1.82×10^{-37}	7.97×10^{1}	8.82×10^{6}	4.15×10^{9}	2.75×10^{11}	1.64×10^{12}	5.65×10^{12}	1.96×10^{13}
0.5		8.74×10^{-10}	2.80×10^{1}	7.10×10^{6}	2.04×10^{10}	4.28×10^{11}	2.77×10^{12}	1.40×10^{13}
1.0		4.08×10^{-47}	5.97×10^{-18}	3.23×10^{-3}	3.58×10^{6}	5.67×10^{9}	3.15×10^{11}	5.78×10^{12}
1.5			4.28×10^{-42}	2.79×10^{-15}	5.54×10^{1}	2.27×10^{7}	2.03×10^{10}	1.98×10^{12}
2.0				1.46×10^{-29}	1.14×10^{-4}	3.32×10^{4}	8.01×10^{8}	5.63×10^{11}
3.0				1.14×10^{-63}	2.81×10^{-18}	5.6×10^{-3}	3.53×10^{5}	2.79×10^{10}

[a]For f = 0.1 or generally for f = y the corresponding probabilities p will have to be multiplied by a factor of 10 or 10^{2y} respectively.

Table 3. Values of p for various combinations of EA and E; x = 5 and f = 0.01

	p(sec^{-1})							
	E (10^6 volts cm^{-1})							
EA(eV)	0.1	0.5	1	2	5	10	20	50
0.01	9.95×10^{10}	8.47×10^{11}	1.81×10^{12}	3.74×10^{12}	9.54×10^{12}	1.92×10^{13}	3.86×10^{13}	9.66×10^{13}
0.03	4.31×10^{9}	3.41×10^{11}	9.64×10^{11}	2.29×10^{12}	6.36×10^{12}	1.32×10^{13}	2.68×10^{13}	6.76×10^{13}
0.05	7.17×10^{7}	1.37×10^{11}	5.75×10^{11}	1.67×10^{12}	5.21×10^{12}	1.12×10^{13}	2.33×10^{13}	5.96×10^{13}
0.08	3.31×10^{4}	2.77×10^{10}	2.5×10^{11}	1.06×10^{12}	4.16×10^{12}	9.66×10^{12}	2.08×10^{13}	5.45×10^{13}
0.1	8.2×10^{1}	8.22×10^{9}	1.34×10^{11}	7.69×10^{11}	3.61×10^{12}	8.91×10^{12}	1.98×10^{13}	5.27×10^{13}
0.15	1.86×10^{-6}	2.41×10^{8}	2.29×10^{10}	3.16×10^{11}	2.51×10^{12}	7.4×10^{12}	1.8×10^{13}	5.04×10^{13}
0.3	4.44×10^{-37}	1.94×10^{2}	2.15×10^{7}	1.01×10^{10}	6.69×10^{11}	3.99×10^{12}	1.38×10^{13}	4.78×10^{13}
0.5		2.76×10^{-9}	8.85×10^{1}	2.24×10^{7}	6.46×10^{10}	1.35×10^{12}	8.77×10^{12}	4.44×10^{13}
1.0		2.08×10^{-46}	3.04×10^{-17}	1.64×10^{-2}	1.87×10^{7}	2.88×10^{10}	1.60×10^{12}	2.94×10^{13}
1.5			3.14×10^{-41}	2.05×10^{-14}	4.14×10^{2}	1.66×10^{8}	1.49×10^{11}	1.45×10^{13}
2.0				1.46×10^{-28}	1.13×10^{-3}	3.31×10^{5}	7.99×10^{9}	5.62×10^{12}
3.0				1.91×10^{-62}	4.71×10^{-17}	9.37×10^{-2}	5.92×10^{6}	4.67×10^{11}

f' at each collision with AX or Y then the time, τ_{st}, for collisional stabilization of AX^{-*} is

$$\tau_{st} = \tau_{coll}/f' \quad . \tag{3}$$

If AX and Y are large molecular systems, values of f' between 0.5 and 1 are not unreasonable (see ref. 8). Then, taking $f' = 1$, a time of $\leq 10^{-11}$ sec is roughly needed for AX^{-*} to be stabilized and yield a stable AX^- in which the attached electron is bound by an energy equal to the electron affinity EA(AX) of the molecule AX. If, on the other hand, dissociative attachment (channel 2a) takes place, the fragment X^- usually is stable by EA(X), the electron affinity of X, if X is an atom; if X is a radical, it may still require further stabilization collisionally, and the time required for this stabilization may again be taken to be of the order of $\leq 10^{-11}$ sec. Thus the final, stable, products AX^- and X^- of electron attachment are formed, as a rule, within 10^{-11} to 10^{-12} sec of the initial electron capture event. These stabilized ions, AX^- and X^-, will drift under the influence of the electric field to the walls of the gas container and be destroyed there. The time, τ_{wall}, required for this drift to the walls is of course determined by the respective ionic mobilities, the distance of the ions from the walls, and the effective value of E/P. We may take as a typical average value of $\tau_{wall} \sim 10^{-5}$ sec.

Hence, the probability, p', that the electron will be detached by the electric field from the stable AX^- and X^- ions before they reach the wall is[†]

$$p' \simeq p\, \tau_{wall} \quad . \tag{4}$$

[†]This is of course for a uniform electric field. For nonuniform electric fields both p and τ_{wall} will vary considerably depending on the field region in which the ions are formed.

From the data in Figs. 5 and 6 and Tables 2 and 3, it is seen that for fields normally expected in practice ($\lesssim 1 \times 10^6$ V cm^{-1}) $p' \ll 1$, if EA(AX) or EA(X) is $\gtrsim$0.5 eV. Thus, unless the EA of AX and X is small (<0.2 to 0.3 eV), the process of field-induced electron detachment must be considered unimportant.

Now, it can be seen from Eq. (2) (and from many earlier discussions; see, for example, ref. 1) that the production of the final stable ions AX^- and X^- proceeds via the intermediate state AX^{-*}. In this intermediate state the electron is bound to the molecule instantaneously very weakly and with a spectrum of binding energies. The ionization energy, $I(AX^{-*})$, of AX^{-*} varies from -3/2 kT to +EA(AX), the value of $I(AX^{-*})$ depending on the various phases of the vibrational cycle of AX^{-*} and being closer to -3/2 kT than to +EA(AX). It is seen from Tables 2 and 3 that p can be very large when EA is very small.† Hence, although the intermediate AX^{-*} may have a lifetime, τ_a, of $<10^{-12}$ sec, the product

$$p' = p\,\tau_a \tag{5}$$

can be large. In practical situations, therefore, it is most likely that it is the effect of the electric field on AX^{-*} rather than on the stable AX^- or X^- which determines the probability of field-induced detachment, (i.e., the detachment of the loosely bound electron from the high-lying levels of AX^{-*} that is very sensitive to electric fields).

†It is noted that although the probability, p, of field emission is very much higher when $I(AX^{-*})$ is instantaneously close to zero, the ergodic factor may reduce p.

III. DIRECT CURRENT BREAKDOWN STRENGTHS OF GASES/MIXTURES

A. Unitary Gases

During this reporting period a number of unitary gases were studied. To provide additional information on the dielectric characteristics of fluorocarbon gases, we measured the breakdown voltages of C_2F_6 (hexafluoroethane, Freon 116) and n-C_4F_{10} (perfluoro-n-butane). The uniform-field dielectric strengths relative to SF_6 of C_2F_6 and n-C_4F_{10} were found to be 0.80 and 1.32, respectively. The breakdown voltages of C_2F_6 and some of its mixtures with SF_6 and N_2 are given in Fig. 7. Similarly, in Fig. 8 are shown V_S versus Pd for pure n-C_4F_{10}, pure SF_6, and 50% C_4F_{10} + 50% SF_6. The relative strengths were determined by taking the ratio of the slopes of the least squares fit lines for the breakdown voltages. A thorough study of these gases and their mixtures in nonuniform fields (rod-plane, point-plane, concentric cylinders) is planned. Camilli et al.[9] indicated that n-$C_4F_{10}$and n-C_4F_{10}/N_2 mixtures are superior to SF_6 in nonuniform fields.

Additionally, we have studied extensively the rare gases Ar and Ne both in pure form and in mixtures with N_2 and SF_6 (see Sect. II B and Appendix B). These rare gases are poor dielectrics, as expected. However, their study is useful since a great deal of basic physical data on them already exists, in particular on electron-impact ionization and electron scattering cross sections. The significance of ionization and scattering to the dielectric strength is discussed in detail in Sect. II B and Appendix B.

Several other new compounds have been studied only in mixtures and the results of these studies are discussed in the next section.

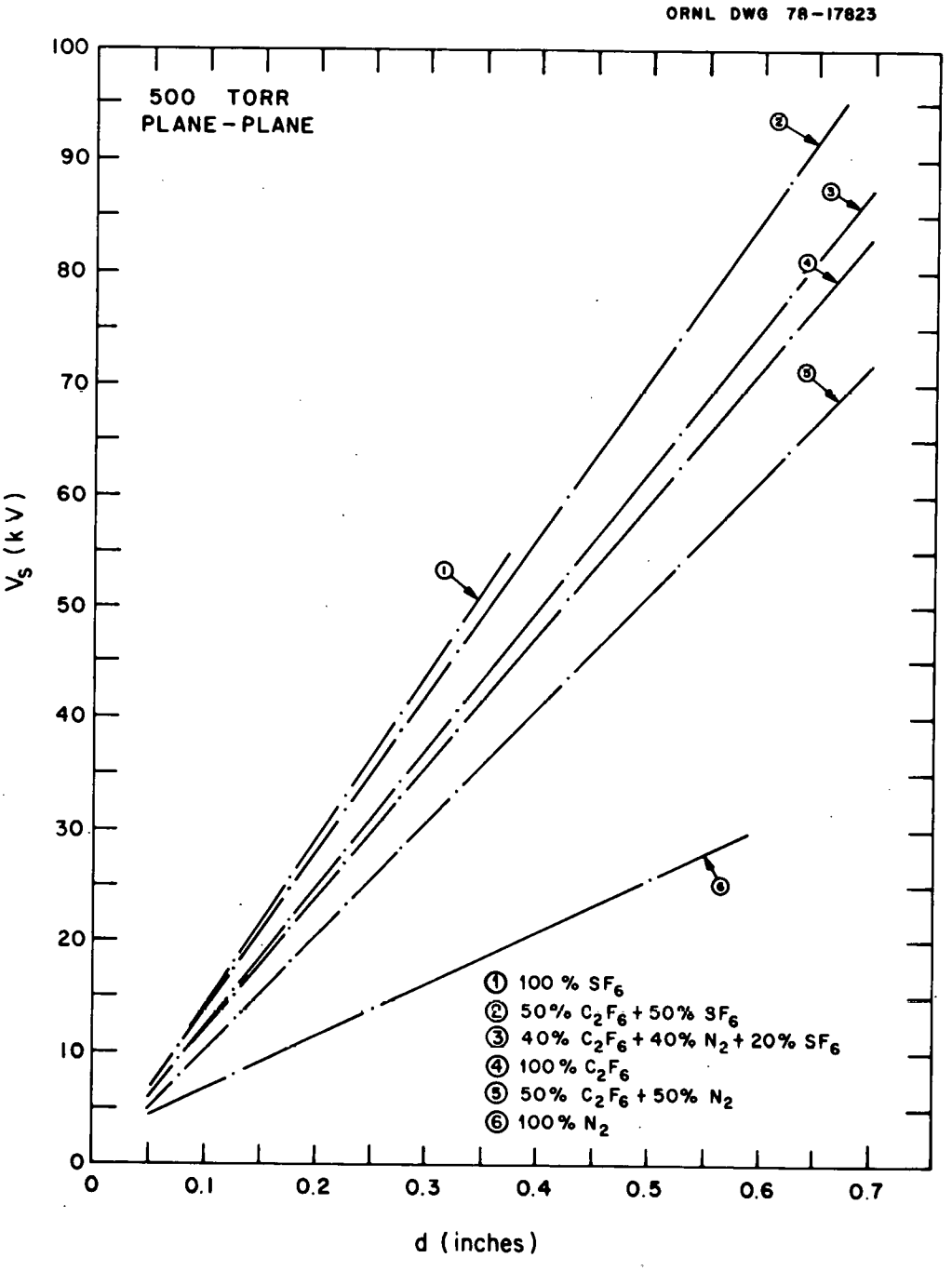

Fig. 7. V_S vs d for pure SF_6, C_2F_6 and N_2 and mixtures of C_2F_6 with N_2 and SF_6 (see text and Table 4) (total pressure = 500 torr; T ≈ 296°K; plane-plane electrode geometry).

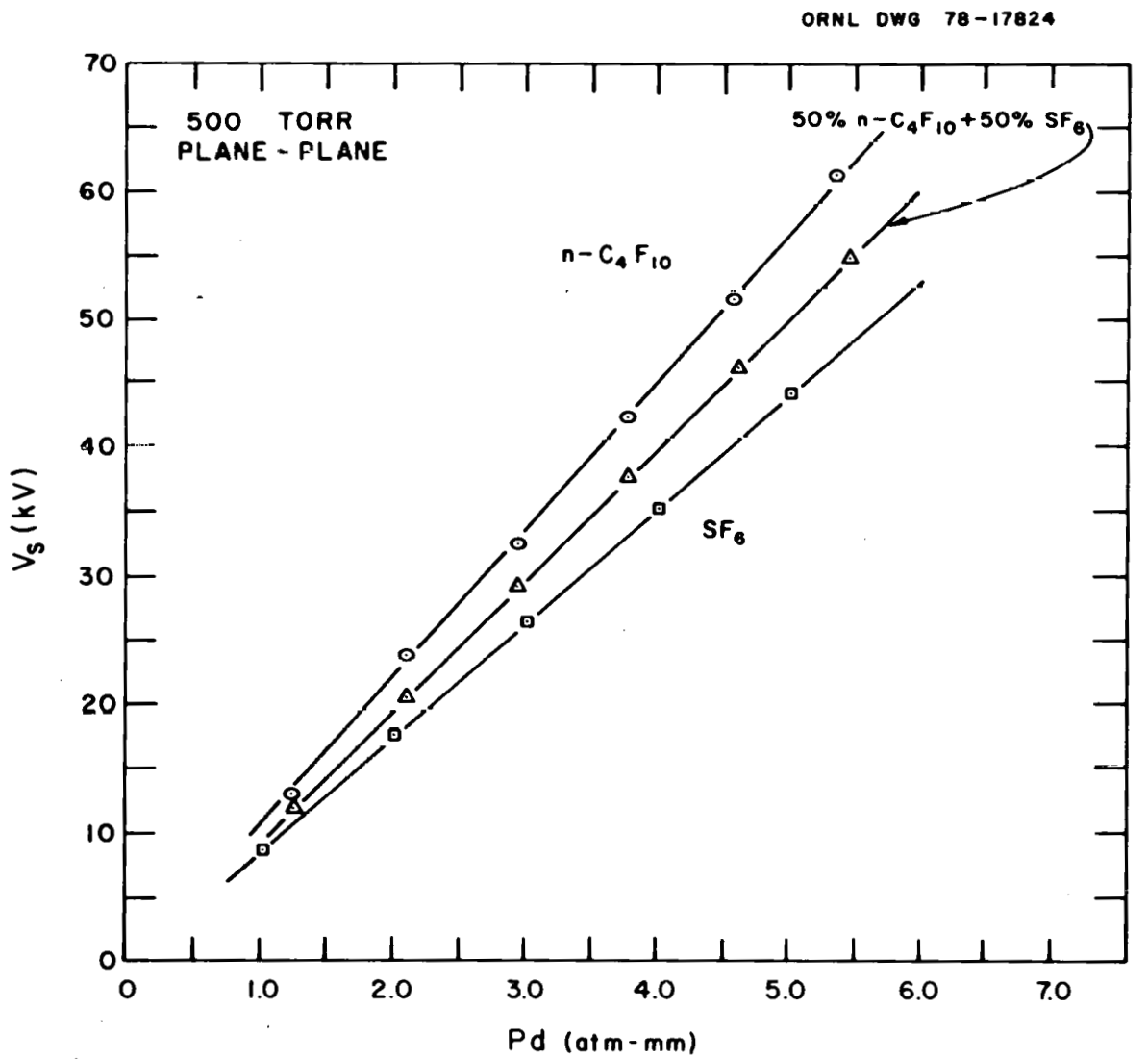

Fig. 8. V_S vs d for n-C_4F_{10}, SF_6 and 50% n-C_4F_{10} + 50% SF_6 (total pressure = 500 torr; T ≃ 296°K; plane-plane electrode geometry).

B. Gas Mixtures

In Fig. 7 the V_S vs d data for the mixtures of C_2F_6 with N_2 and SF_6 are shown, and in Table 4 the slopes and intercepts of the V_S versus d lines as well as the relative breakdown strengths, $(V_S)_R$, are listed. The $(V_S)_R$ were calculated in this case by taking the ratio of the slopes of the respective gas/mixture to that of SF_6 except for N_2. In Table 4 of ref. 4, even though the slopes and intercepts were given, all of the relative strengths were obtained by averaging the ratios of the breakdown voltages over the corresponding range of Pd's. For gases which have a relatively large intercept, the ratio of its slope to that of SF_6 does not always give the same relative breakdown strength as in taking the ratios of the individual V_S values at the corresponding Pd's. For example, N_2 as reported in ref. 4 has a $(V_S)_R$ of 0.40 when calculated from individual V_S values, but it has a $(V_S)_R$ of 0.31 when the slopes are used. When the intercept is negligible compared to the actual breakdown voltage, the relative breakdown strength may be accurately obtained by taking the ratio of the slopes. In many small-scale laboratory tests, however, the voltages used are less than 100 kV and frequently less than 50 kV, which is the case for N_2 in Fig. 7. In these situations the $(V_S)_R$ is best represented by calculating the ratio of the V_S at each Pd value used and then taking an average. This procedure will be followed whenever the ratios of the slopes do not give an accurate $(V_S)_R$. Hence the value of 0.40 is used for N_2 in this case.

From Fig. 7 and Table 4 we see a synergistic effect in the 50% C_2F_6 + 50% N_2 mixture. The mixture has a relative strength of 0.69, which lies well above the value of 0.60 obtained by a weighted average of the V_S of

Table 4. Uniform field breakdown voltages for C_2F_6, n-C_4F_{10}, and some of their mixtures with SF_6 and N_2 (P = 500 torr; T = ≈23°C)

Gas	Slope[a] (kV/in)	Intercept (kV)	$(V_s)_R$
100% C_2F_6	118.76	0.48	0.80
100% N_2	46.46	2.53	0.40
100% SF_6	148.69	-0.34	1.00
40% C_2F_6 + 40% N_2 + 20% SF_6	125.12	0.12	0.84
50% C_2F_6 + 50% N_2	102.16	0.52	0.69
50% C_2F_6 + 50% SF_6	141.60	0.07	0.95
100% n-C_4F_{10}	196.18	-1.68	1.32[b]
50% n-C_4F_{10} + 50% SF_6	170.06	-0.55	1.14[b]

[a]Slopes may be converted to units of kV/atm-mm by multiplying by 5.984×10^{-2}.

[b]Measured on high pressure, variable temperature apparatus.

the separate components. Similarly, a synergistic effect is observed for the 50% C_2F_6 + 50% SF_6 mixture, the $(V_s)_R$ of 0.95 being higher than the expected 0.90. Also the 40% C_2F_6 + 40% N_2 + 20% SF_6 mixture at 0.84 lies well above the weighted average value of 0.68. However, in the case of n-C_4F_{10} in Fig. 8, no synergism is evident in the 50% n-C_4F_{10} + 50% SF_6 mixture. Further data on mixtures and measurements of the electron attachment properties of C_2F_6 and n-C_4F_{10} are necessary to interpret these findings .

A number of mixtures were investigated using gases with large dipole moments in combination with SF_6 and N_2. The gases used were 1,1,1-CH_3CF_3, CHF_3, CH_2F_2, and CF_4. These gas mixtures were studied to determine the

effect of dipole scattering on breakdown strength (see Sect. II C). Figures 3, 4, 9, and 10 give the results of these breakdown measurements. The mixtures involving CF_4 and CHF_3 suggest a slight synergism with N_2; however, the effect is quite small, and it could very well fall within the experimental error. Hence no conculsions can be made about synergistic effects in these mixtures at the present time. The effect of dipole scattering on the dielectric strength has been elaborated upon in Sect. II C.

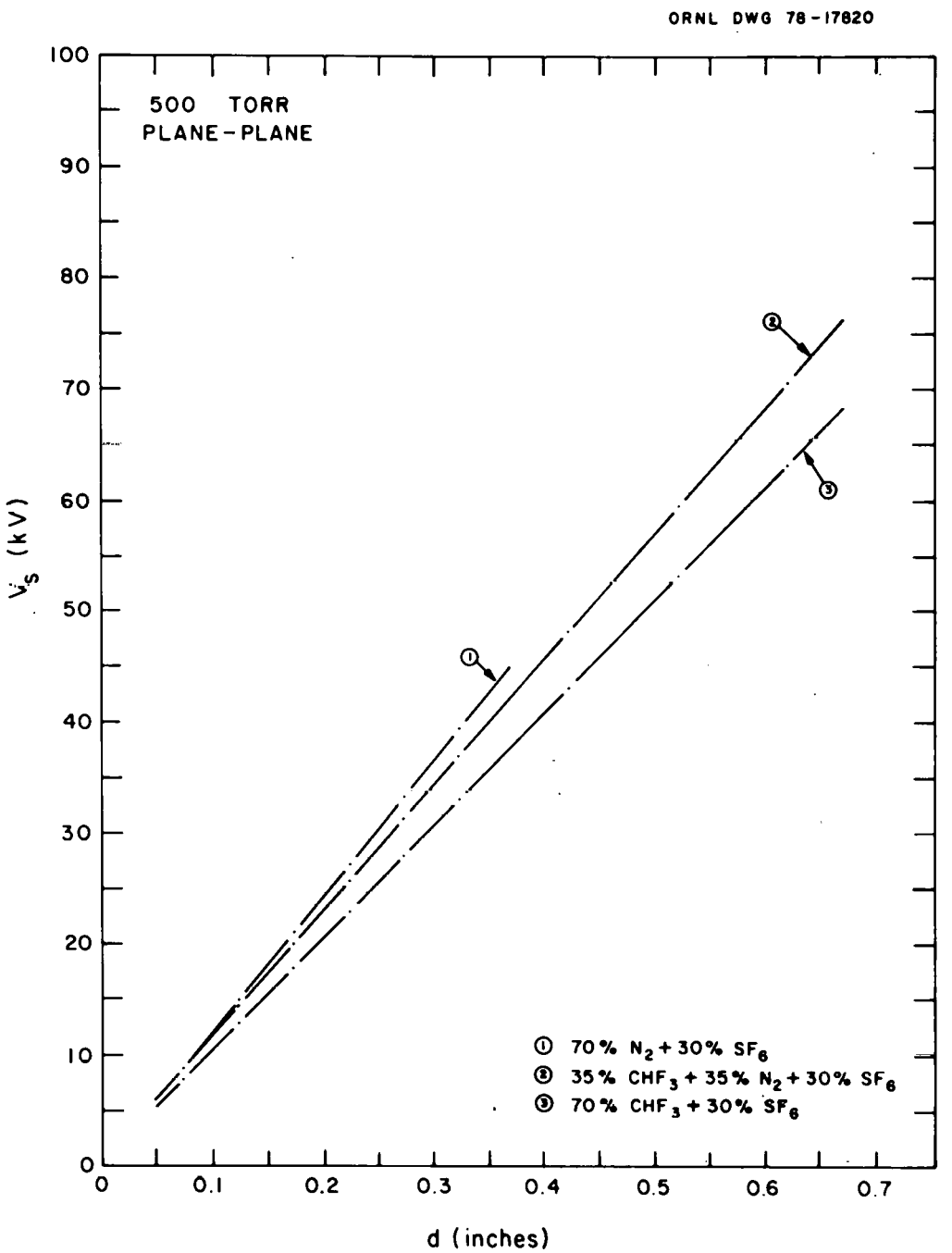

Fig. 9. V_s vs d for 70% N_2 + 30% SF_6, 70% CF_4 + 30% SF_6 and 35% CF_4 + 35% N_2 + 30% SF_6 (total pressure = 500 torr; T ≈ 296°K; plane-plane electrode geometry).

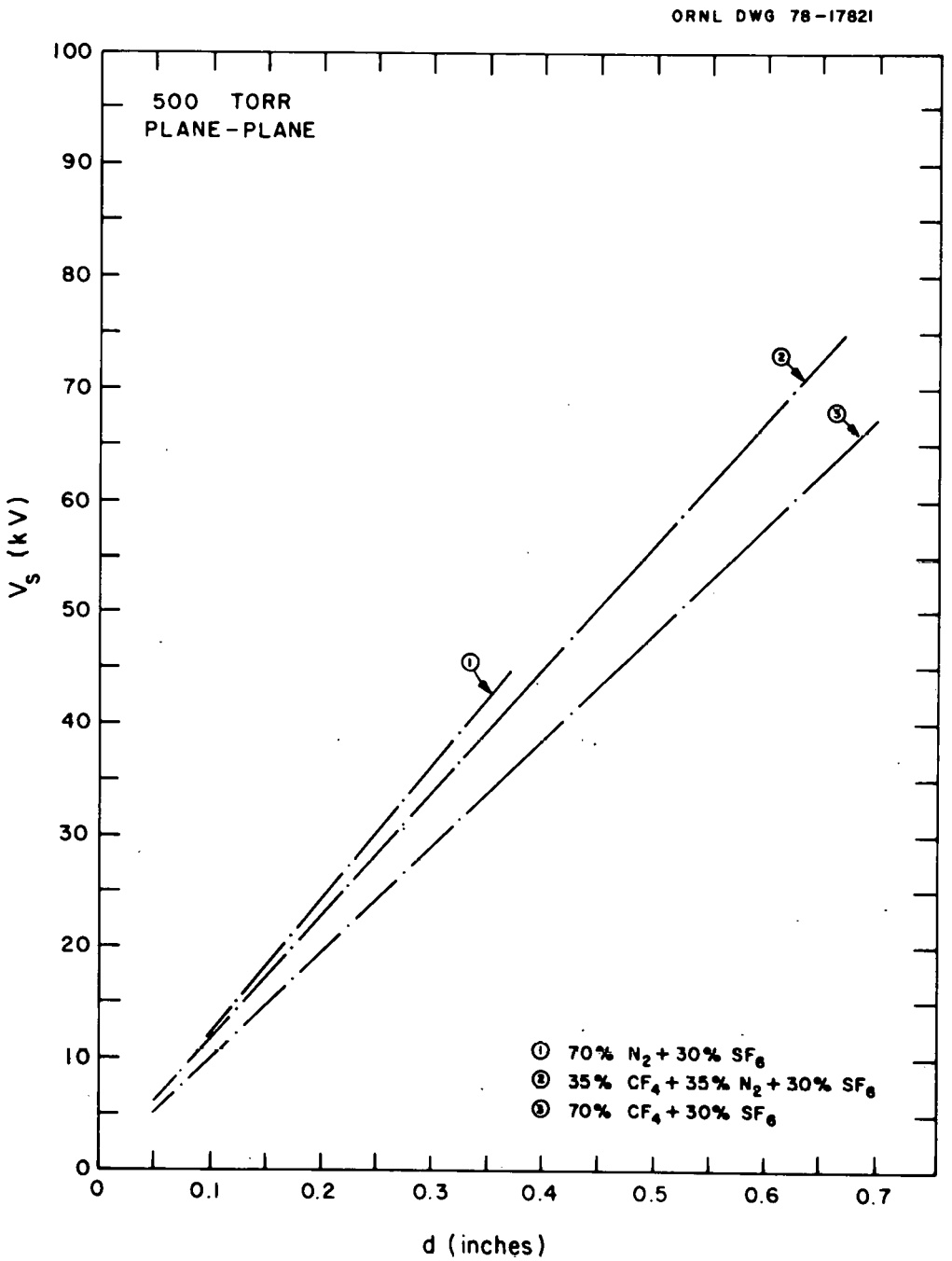

Fig. 10. V_S vs d for 70% N_2 + 30% SF_6, 70% CHF_3 + 30% SF_6 and 35% CHF_3 + 35% N_2 + 30% SF_6 (total pressure = 500 torr; T ≃ 296°K; plane-plane electrode geometry).

IV. EFFECTS OF TEMPERATURE ON THE DIELECTRIC STRENGTH OF GASEOUS DIELECTRICS

We have concentrated in this reporting period on the temperature range above room temperature (∿20°C). In previous work[5] we reported on breakdown measurements in the range -15°C to ∿+50°C for 100% SF_6 and 0°C to ∿85°C for 20% SF_6 + 80% N_2 mixture. In that work[5] no temperature dependence of the breakdown voltage was observed for 100% SF_6. However, a slight drop in V_S for the mixture was observed at the highest temperatures. Thus, further investigations at higher temperatures were required, and to go to higher temperatures modification of our apparatus was necessary.

The high voltage feedthrough for the chamber is an internal type in which the high voltage cable extends about 1 ft inside the chamber itself. The pressure seal is made by an O-ring contained in a housing bolted onto the top flange of the chamber. In a preliminary test of a small section of cable we found that the cable began to melt at ∿90°C. Further testing indicated that gamma irradiation could raise the melting point of the cable well above 150°C. Hence to achieve temperatures on the order of 150°C it was necessary to have one end of our power supply cable irradiated (see Sect. IX for details).

During preliminary checkout runs at elevated temperatures a substantial temperature gradient was found to exist between the bottom and the top of the chamber even though the oven completely enclosed the chamber. The gradient is evidently caused by convection resulting in a "smokestack" effect. It was not possible to seal the oven tightly enough to completely eliminate the problem. As a temporary means of coping with the problem we wrapped heating tapes around the bottom one third of the chamber which

could be regulated separately from the strip heaters in the oven. By this additional heating of the bottom of the chamber we were essentially able to eliminate the gradient. The temperatures were monitored by a thermocouple placed inside the chamber below the ground electrode and a second thermocouple located inside the chamber approximately 4 in. below the top flange. The temperature difference between the two points was kept less than 2°C over the entire range of temperatures.

Table 5 gives preliminary results on the breakdown voltages for 100% SF_6 and 30% SF_6 + 70% N_2 for three temperatures. Uniform-field electrodes were used. These measurements were made at a constant number density of 1.65×10^{19} cm^{-3}, calculated by assuming ideal gas law behavior. This number density corresponds to 500 torr pressure at ∿20°C. The data indicate that to within experimental error there is no dependence of the breakdown voltage for these gases on temperature. At each temperature, new gas was introduced into the chamber, allowed to reach thermal equilibrium, and the pressure was adjusted to obtain the correct number density. The temperatures given in Table 5 are the averages of the top and bottom thermocouple readings immediately before and immediately after a set of 15 sparks was made. Further study at higher number densities is planned.

Table 5. Preliminary breakdown measurements at high temperatures for uniform-field electrodes at constant number density, $N = 1.65 \times 10^{19}$ cm^{-3}

Gas/Mixture	T(°C)	V_S (kV) Gap spacing (inches)					
		0.075	0.125	0.175	0.225	0.275	0.325
100% SF_6	19	10.8	18.0	25.5	33.0	40.5	47.9
	82	10.7	18.2	25.6	33.2	40.7	48.4
	154	10.8	18.2	26.0	33.5	41.2	48.8
30% SF_6 + 70% N_2	82	8.9	14.9	20.9	26.9	33.0	39.0
	154	8.8	14.7	20.7	26.7	32.8	38.8

V. IMPULSE STUDIES

The thrust of our impulse studies is bidirectional. One direction is to test the impulse withstand behavior of new gases and gas mixtures as a function of the various practical parameters (e.g., pressure, electrode separation, electrode geometry, etc.) with a view toward practical application of these new gases and gas mixtures; impulse testing may well prove to be the crucial test for dielectric gases since the primary source of over voltage in electrical power apparatus is due to lightning and switching surges. The other direction of our impulse work is toward improving the understanding of the dynamics of the breakdown processes in gases. A better understanding of the dynamics of breakdown can lead to improvements in the use of dielectric gases and gas mixtures.

The complexity of the impulse behavior in dielectric gases makes it difficult to evaluate the relative merits of different gases unless all of the parameters are kept the same or are properly controlled. With this in mind, we have initiated testing of dielectric gases by taking a set of reference data with N_2 and SF_6 and their mixtures so that direct comparisons (with all experimental variables kept identical) can be made with data on new gases/mixtures. Measurements have been made of V_{50} (voltage with 50% probability of breakdown), V_{10X} (voltage with ten consecutive breakdowns), and a lower voltage limit for ten impulses with no breakdown.

Figure 11 shows a typical data run at 0.625 in. gap setting for 20% SF_6 + 80% N_2 (304 torr SF_6 + 1216 torr N_2), positive polarity in a point-plane geometry with a lightning waveform (1.2 μsec rise time and 50 μsec decay time). (The "point" electrode is a 30° cone ending in a hemisphere of 1 mm radius to prevent sparks from changing the geometry of the "point.") The data

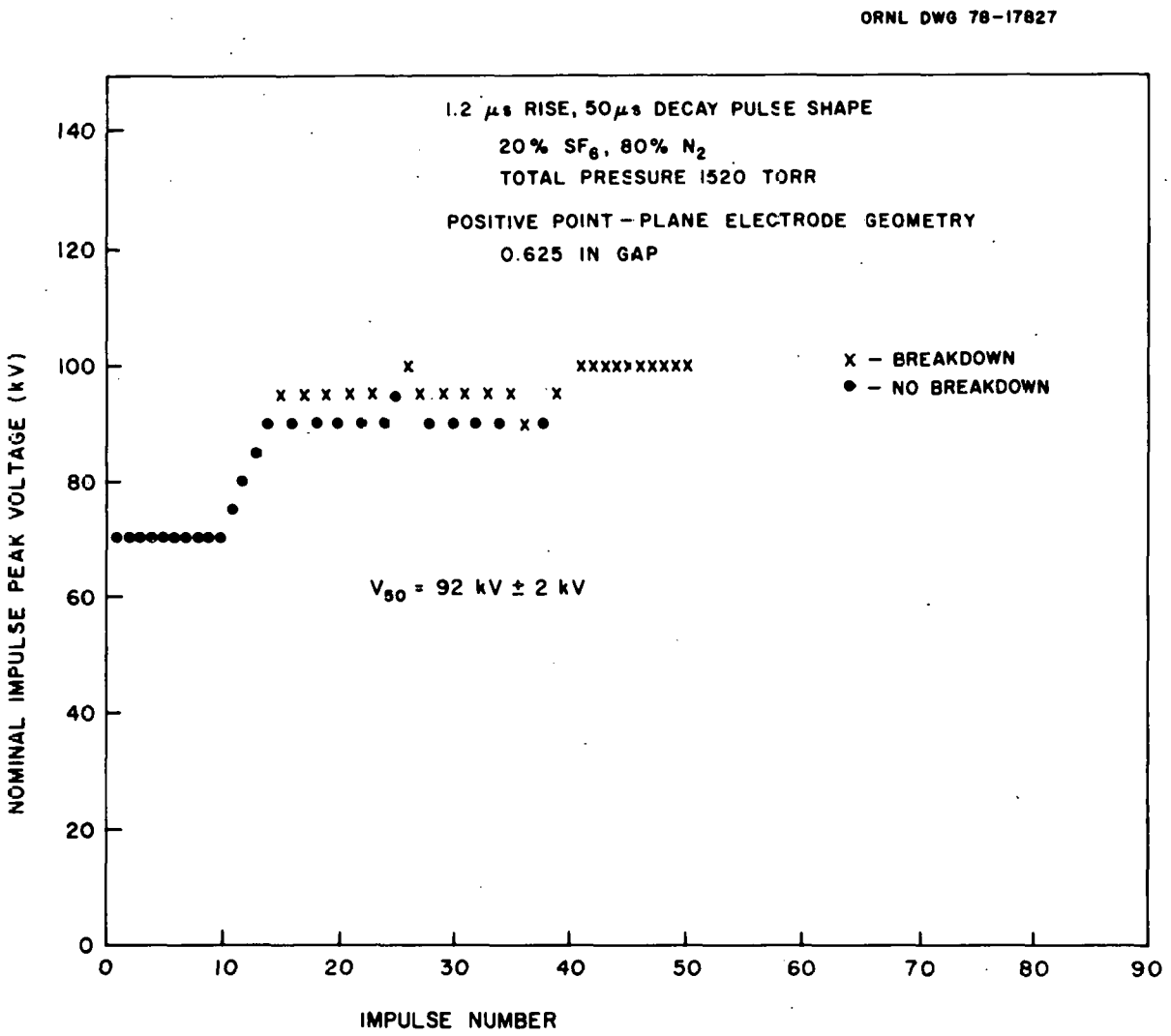

Fig. 11. Typical measurement run of nominal impulse peak voltage vs impulse number to determine one V_{50} value.

have been taken as follows:

(i) some suitably low value of the impulse voltage was chosen so that no breakdown occurred in ten consecutive impulses.

(ii) following (i), for a given impulse, if there was a breakdown, the impulse voltage was lowered by 5 kV; if there was no breakdown, the impulse voltage was raised by 5 kV. This technique automatically hunts for the voltage for 50% probability of breakdown, V_{50}, and explains why the V_{50} value is the most frequently measured voltage.

(iii) when a suitable number of impulses have been fired so that V_{50} can be determined accurately, the voltage at which ten consecutive breakdowns occurred was found.

Results for a series of gases, gaps, and polarities are given in Table 6.

Some of the salient features of the V_{50} values we have measured (see Table 6) for these gases are:

(i) For all gases tested, negative polarity V_{50} values tend to be independent of gap separation for larger gap values.

(ii) Positive polarity V_{50} values increase approximately linearly with gap spacing for the gaps used .

(iii) Increasing the percentage of SF_6 in N_2, increases the V_{50} for the N_2/SF_6 mixtures used .

(v) The V_{10X} voltage behaves similarly to V_{50} voltage (i.e., it changes very little with gap separation for negative polarity, and increases linearly with gap separation for positive polarity).

Studies of the dynamics of breakdown are being planned using the new image converter camera which we have just received (see Sect. IX on Apparatus).

Table 6. V_{50}, V_{N0} and V_{10X} for SF_6 and SF_6/N_2 mixtures for various electrode separations, polarities, electrode geometries and τ_1/τ_2[a]

Gas or Gas Mixture (Pressure in Torr)	Electrode Separation (inches)	V_{50} (kV)	V_{N0}[b] (kV)	V_{10X}[c] (kV)	τ_1/τ_2[a] (μsec)	Polarity	Geometry
SF_6 (760)	0.250	7.3	-	-	200/2000	+	S-P[d]
	0.375	10.5	-	-	"	+	"
	0.500	11.5	-	-	"	+	"
	0.625	11.8	-	-	"	+	"
SF_6 (1520)	0.250	8.0	-	9.0 (5)	1.2/50	-	Pt-P[e]
	0.375	9.0	-	11.0 (5)	"	-	"
	0.500	10.7	-	11.5 (5)	"	-	"
	0.625	11.5	-	13.0 (5)	"	-	"
	0.750	12.2	-	12.0 (5)	"	-	"
	0.875	12.0	-	12.0 (5)	"	-	"
SF_6 (1520)	0.250	8.3	-	8.5 (5)	1.2/50	+	Pt-P
	0.375	8.9	-	10.0 (5)	"	+	"
	0.500	10.7	-	11.5 (5)	"	+	"
	0.625	13.5	-	14.5 (5)	"	+	"
	0.750	15.2	-	16.5 (5)	"	+	"
	0.875	17.4	-	18.5 (5)	"	+	"
SF_6 (2280)	0.250	10.5	-	11.5 (5)	1.2/50	-	Pt-P
	0.375	12.0	-	-	"	-	"
	0.500	12.2	-	13.0 (5)	"	-	"
	0.625	12.0	-	13.0 (5)	"	-	"
	0.750	12.6	-	13.0 (5)	"	-	"
SF_6 (2280)	0.250	8.0	-	9.5 (5)	1.2/50	+	Pt-P
	0.375	10.8	-	12.0 (5)	"	+	"
	0.500	13.8	-	15.0 (5)	"	+	"
	0.625	15.8	-	-	"	+	"
SF_6 (608) N_2 (912)	0.250	8.0	5.5	8.0	1.2/50	-	Pt-P
	0.375	9.0	5.5	10.0	"	-	"
	0.500	8.9	6.0	10.0	"	-	"
	0.625	8.8	6.5	11.0	"	-	"
SF_6 (912) N_2 (1368)	0.250	9.5	5.5	11.0	1.2/50	-	Pt-P
	0.375	9.5	6.0	11.0	"	-	"
	0.500	(9.0-11.0)	6.0	12.0	"	-	"
	0.625	10.4	7.0	11.5	"	-	"
	0.750	10.5	7.5	11.5	"	-	"
SF_6 (912) N_2 (1368)	0.250	7.0	6.0	8.0	1.2/50	+	Pt-P
	0.375	8.5	6.5	9.5	"	+	"
	0.500	11.0	7.0	12.0	"	+	"
SF_6 (304) N_2 (1216)	0.375	6.0	5.0	6.5	1.2/50	+	Pt-P
	0.500	7.5	6.0	8.5	"	+	"
	0.625	9.2	7.0	10.0	"	+	"
SF_6 (304) N_2 (1216)	0.500	7.9	5.0	10.0	1.2/50	-	Pt-P
	0.625	7.8	5.5	11.0	"	-	"
	0.750	6.3	5.5	9.5	"	-	"
SF_6 (608) N_2 (1672)	0.250	8.2	6.0	11.0	1.2/50	-	Pt-P
	0.375	8.7	6.0	10.0	"	-	"
	0.500	9.0	6.5	10.5	"	-	"
	0.625	9.2	7.0	10.5	"	-	"
	0.750	9.8	7.0	12.0	"	-	"
SF_6 (608) N_2 (1672)	0.250	7.2	6.5	8.5	1.2/50	+	Pt-P
	0.375	8.5	6.0	9.5	"	+	"
	0.500	10.0	7.0	11.0	"	+	"
	0.625	11.3	7.5	12.5	"	+	"
SF_6 (456) N_2 (1824)	0.250	8.0	5.0	9.5	1.2/50	-	Pt-P
	0.375	8.5	5.5	10.0	"	-	"
	0.500	9.0	6.0	10.0	"	-	"
	0.625	9.2	6.5	11.5	"	-	"
SF_6 (456) N_2 (1824)	0.250	9.0	6.0	11.0	1.2/50	+	Pt-P
	0.375	10.2	7.0	11.5	"	+	"
	0.500	10.5	8.0	11.5	"	+	"
	0.625	11.7	8.0	12.5	"	+	"

[a] τ_1/τ_2 is the ratio of the rise time over the decay time of the impulse.

[b] V_{N0} is the lower limit for ten consecutive impulses with no breakdown.

[c] Some V_{10X} data were taken only five consecutive times; these are indicated by (5).

[d] Sphere-sphere.

[e] Point-plane.

VI. ENVIRONMENTAL EFFECTS STUDIES

The expanding use of dielectric gases and the introduction of new gases/mixtures to meet the varied and multiple needs for high voltage insulation, demand a *comprehensive* study of the environmental effects of gaseous dielectrics. Our program in this area can be summarized as in Table 7.

Table 7. Environmental effects studies

A.	Initial decomposition of dielectric under electron impact
B.	Decomposition under stress; long term electrical stress tests (accelerated "life-tests")
C.	Decomposition after breakdown
D.	Linking of A and C products
E.	Toxicity, etc.
F.	Assessment; environmental impact of wide-spread use of dielectric gases (in the future)

A. Initial Decomposition of the Gas Dielectric Under Electron Impact

Low-energy ($\lesssim$12 eV) electron impact induced fragmentation for the dielectric gases c-C_4F_6 and 1,3-C_4F_6 has been investigated employing time-of-flight mass spectrometry. Negative ion fragments have been identified, and their abundances have been measured as a function of electron energy. These results are shown in Figs. 12 and 13.

For the cyclic C_4F_6 the parent ion contributes 89.1% to the total ion yield. For electron energies below one electron volt no decomposition is observed. However, the data for 1,3-C_4F_6 indicate that practically all of the ions produced in the energy range studied (0-12 eV) are due to dissociative attachment. For electrons in the 1-2 eV energy range, 1,3-C_4F_6 is not

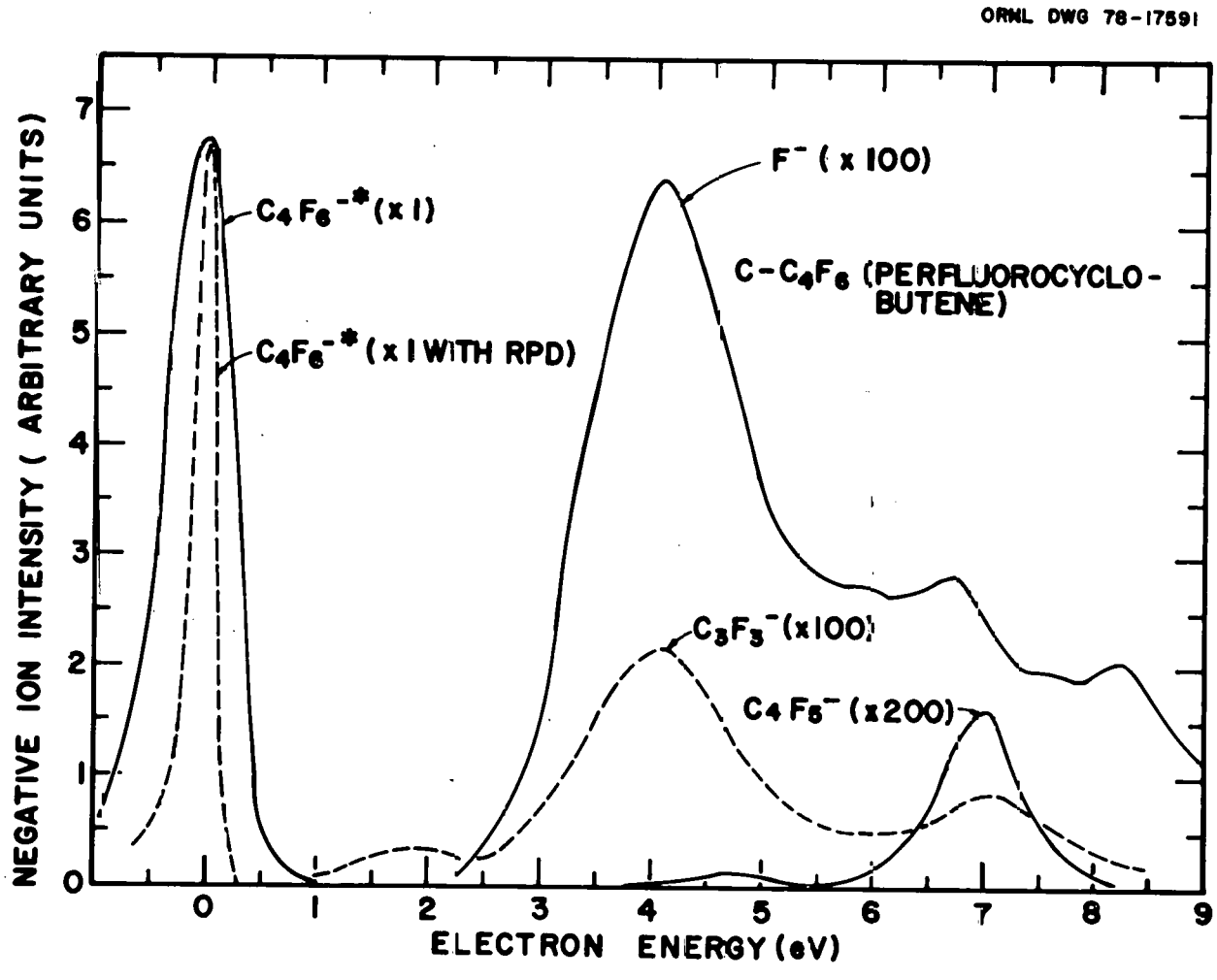

Fig. 12. Negative ion intensity as a functicn of electron impact energy for c-C_4F_6.

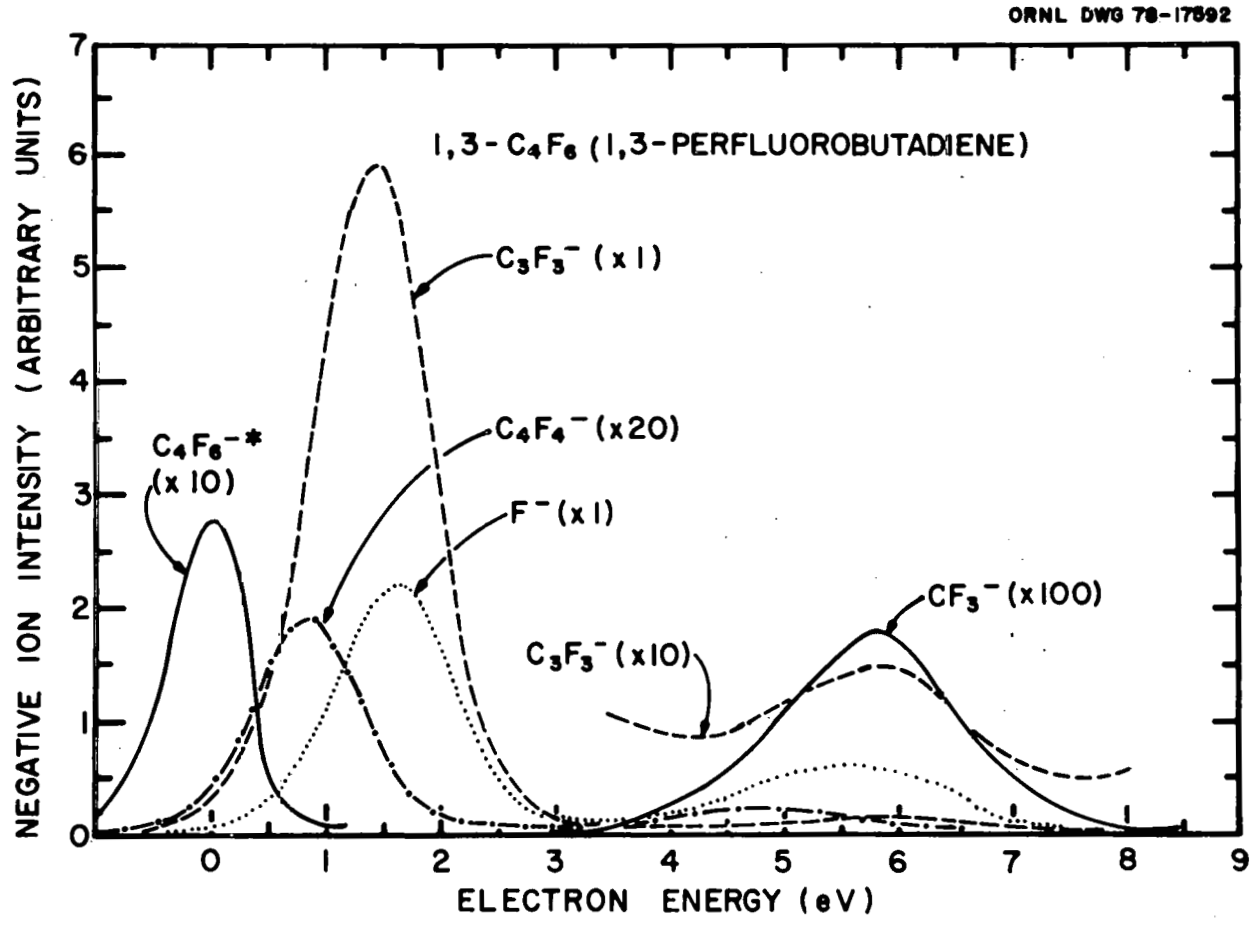

Fig. 13. Negative ion intensity as a function of electron impact energy for 1,3-C_4F_6

expected to be as stable as the isomers c-C_4F_6 and 2-C_4F_6 (ref. 5) with respect to decomposition by electrical breakdown.

This work, in addition to the results of initial fragmentation of c-C_4F_8, 2-C_4F_8, and 2-C_4F_6 (ref. 5), completes a systematic study of fragmentation patterns of perfluorinated four-carbon atom-containing (C_4) molecules.[10] Tabulated summaries are given in Tables 8 and 9. Some general conclusions may be drawn from this work as follows:

1. With the exception of 1,3-C_4F_6, perfluorinated C_4 molecules are stable dielectrics under electron bombardment.
2. When fragmentation does occur, perfluorinated C_4 molecules preferentially cleave at single bonds rather than at the multiple bonds.
3. No fragments are observed for the cyclic molecules below ~2 eV electron impact energy.
4. Aside from 2-C_4F_6, F^- production is most probable in the medium electron energy range (~4 - 12 eV).
5. Where fragments are produced by thermal energy electrons (non-cyclic isomers), long-term electrical stress tests are highly recommended for those systems and are planned.

B. Gaseous Dielectrics Under Prolonged Electrical Stress

Sulfur hexafluoride, subjected to electrical stress representing 75% breakdown voltage at a pressure of ~3 atm, was tested for durations of 6 and 9 days. No decomposition products could be observed. Tests for much longer durations at 50% breakdown voltages are currently in progress. Additional tests involving elevated temperatures and irradiation of the stressed gas by ultraviolet (UV) light are being initiated.

Table 8. Positions of resonance maxima in the fragmentation of perfluorinated C_4 molecules by direct electron impact

	2-C_4F_6 (eV)	c-C_4F_6 (eV)	1,3-C_4F_6 (eV)
$C_4F_6^{-*}$	∿0.0	∿0.0	∿0.0
$C_4F_5^-$		4.8, 7.0	
$C_4F_4^-$			0.8, 4.8
$C_3F_3^-$	1.5, 5.0	1.85, 4.0, 7.0	1.45, 5.9
CF_3^-	5.9		5.8
F^-	5.3	4.1, 6.0, 6.7, 7.6, 8.3	1.6, 5.6
	2-C_4F_8	c-C_4F_8	
$C_4F_8^{-*}$	∿0.0	∿0.0	
$C_4F_7^{-*}$	∿0.0		
$C_4F_6^{-*}$	∿0.0, 0.7		
$C_3F_5^{-*}$ [a]	2.3, 4.2	4.1	
C_3F_3	5.1		
C_2F_3	5.4	4.9, 7.9	
CF_3^-	5.3	4.8	
F^-	5.2	4.8, 6.5, 7.9, 10.2	

[a] Long-lived metastable in the case of 2-C_4F_8.

Table 9 Relative negative ion integrated intensity in the 0-12 eV energy range for perfluorinated C_4 molecules

	$2\text{-}C_4F_6$ (%)	$c\text{-}C_4F_6$ (%)	$1,3\text{-}C_4F_6$ (%)
$C_4F_6^-$*	96.3	98.6	1.9
$C_4F_5^-$		0.3	
$C_4F_4^-$			1.1
$C_3F_3^-$	2.5	0.9	64.5
CF_3^-	1.1		0.2
F^-	0.1	0.1	32.2
	$2\text{-}C_4F_8$	$c\text{-}C_4F_8$	
$C_4F_8^-$*	83.4	56.3	
$C_4F_7^-$*	1.5		
$C_4F_6^-$*	0.4		
$C_3F_5^-$*[a]	0.9	0.6	
$C_3F_3^-$	0.4		
$C_2F_3^-$	0.2	0.4	
CF_3^-	0.6	1.1	
F^-	12.7	41.6	

[a]Long-lived metastable in the case of $2\text{-}C_4F_8$

C. Decomposition of Gas Dielectrics

Analyses of breakdown products from cyclic C_4F_8 using gas chromatograph/mass spectrometer (GC/MS) techniques reveal that only the product C_2F_4 is produced. These experiments were done for energy inputs of ∿5 and 20 joules per breakdown with the number of breakdowns ranging from 750 to 3000. Preliminary studies indicated that at higher energy inputs and higher concentrations of C_2F_4 the reaction[11-13] $C_2F_4 + C_2F_4 \rightarrow c\text{-}C_4F_8$ may be a likely process. A great deal more work is required since it is known that even at room temperatures this dimerization process is possible. This means that proper control of the time between breakdown and analysis is essential.

Certain mixtures of SF_6 with perfluorocarbons have been found to inhibit carbon formation on electrode surfaces. Table 10 shows the observations of solid deposits for varying concentrations of SF_6. Analyses of gaseous products are currently in progress in order to correlate the disappearance of solid residue with production of carbon-containing gaseous products.

Table 10. Observations of solid deposits for varying amounts of SF_6 for $SF_6/2\text{-}C_4F_6$ mixtures at total pressures of 1000 torr

$2\text{-}C_4F_6$ (%)	SF_6 (%)	Electrode deposit
100	0	black (C, F)
80	20	black - very little on chamber walls
60	40	small amount of black around spark point surrounded by white-yellow deposit
40	60	trace of black, trace of white-yellow
20	80	no black - trace of white-yellow deposit

D. Linking A to C (From Initial Decomposition to Final Products)

A complete picture of the processes which result in the formation of final decomposition products of sparked dielectric gases requires the experimental identification of short-lived products (ions and/or radicals) which link the initial products to the final stable products. These precursors may be detected and identified by attaching a quadrupole mass spectrometer to a discharge cell separated by a pinhole orifice large enough to transmit ions and radicals of sufficient intensity, but small enough to maintain a pressure differential corresponding to $P \sim 10^{-7}$ torr in the mass spectrometer. This atmospheric pressure quadrupole mass spectrometer is currently being built. It can be applied to the detection of intermediate products from corona, continuous arcing, and high voltage stress as well as from high voltage breakdowns. By discovering the reaction pathways that lead from initial decomposition to final stable products, there exists the potential for designing and tailoring a gas insulating system for such purposes as inhibiting toxic products, carbon deposits, or corrosive products.

E. Toxicity Tests

Inhalation tests of 2-C_4F_8 on mice have been performed by Dr. H. Witschi of the ORNL Biology Division. A complete report of these tests is attached as Appendix D. No ill effects were observed for 8-hr exposures at a concentration of 1000 ppm in air; however, all of the mice died following the 24-hr exposure tests at the same concentration of 2-C_4F_8 in air.

VII. APPLIED STUDIES

Small scale, practical conditions testing of the gases SF_6, c-C_4F_8 (perfluorocyclobutane), 2-C_4F_8 (perfluorobutene-2), and 2-C_4F_6 (perfluoro-2-butyne), and their binary mixtures with N_2 have continued in cylindrical geometry. The apparatus has been described in detail in an earlier report.[4] In this period, tests of the binary mixtures have been completed for the remaining cases of three different smooth, uncontaminated inndr electrodes of stainless steel, with the exception of a few points for 2-C_4F_6/N_2 at the highest voltages. Also, tests have been made for the effects of inner electrode surface roughness, effects of inner electrode material composition, and effects of interelectrode particle contamination. All tests were made at 1-atm total pressure and ambient temperature ($\sim$21°C).

The new 300-kV Delta Ray power supply for the applied studies has been received and operated. A new chamber has been under construction to replace the one now in use and to increase pressure capability from 1 to 10 atm. This chamber is near completion and, after careful testing, will be installed with the new power supply.

A. Breakdown Tests with Smooth Cylinders

The 1-atm tests of the four electron attaching gases and their binary mixtures with N_2 are practically complete, except for the highest voltages with 2-C_4F_6/N_2 mixtures. Tests for the other three gases have been previously reported,[4,5] and those for 2-C_4F_6/N_2 are presented in FIg. 14. The error bars indicate combined systematic and random errors, the latter ($\leq$3%) being standard deviation divided by mean of at

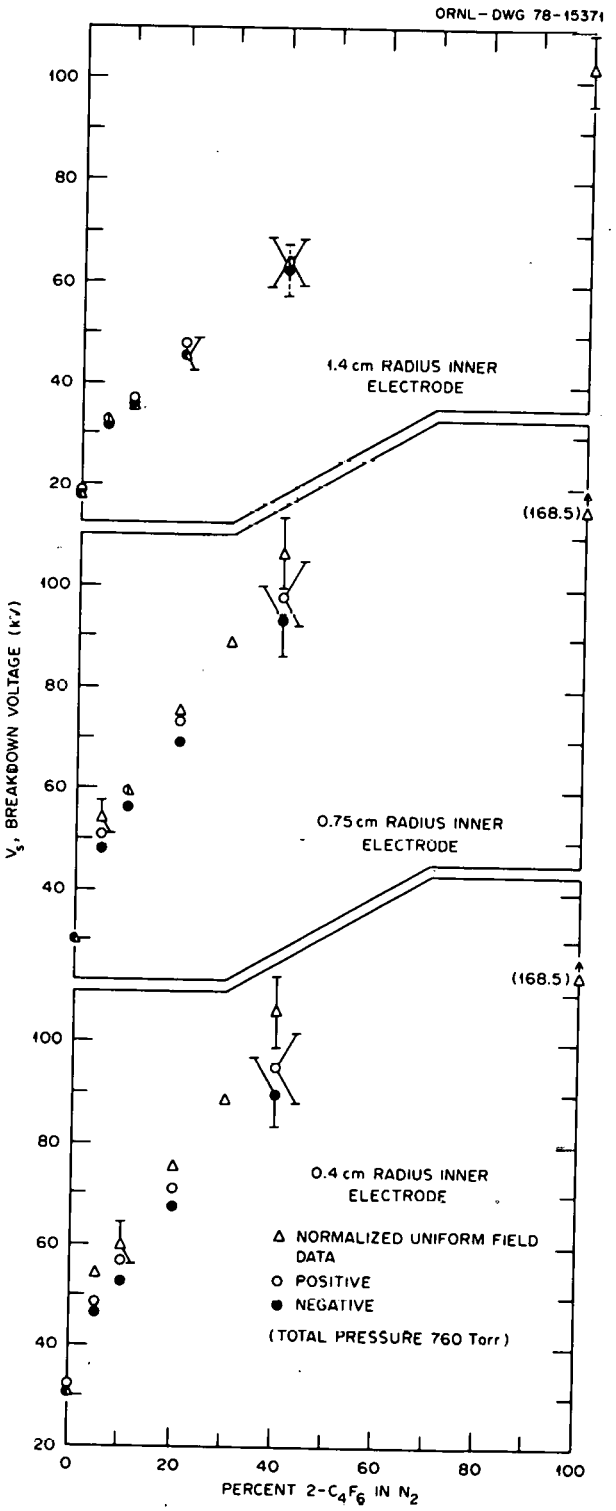

Fig. 14. Breakdown voltages in three cylindrical geometries for 2-C_4F_6 (hexafluoro-2-butyne)/N_2 mixtures at 1 atm and ~21°C. Mixtures are identified by the percentage of 2-C_4F_6 by pressure. The uniform field breakdown curve has been normalized to each point for pure N_2 with negative polarity.

least 10 measurements. Based on experience with other fluorocarbon/N_2 mixtures in cylindrical geometry as well as with 2-C_4F_6/N_2 mixtures in uniform fields, it is expected that the experimental points in Fig. 14 for 2-C_4F_6/N_2 > 40% will continue to follow a straight line fairly closely when they are taken in the future. Therefore, 2-C_4F_6/N_2 mixtures remain superior to SF_6/N_2 in cylindrical geometry, and the former do not show the saturation characteristic of the latter.

A typical comparison of the four (attaching gas)/N_2 mixtures for smooth, uncontaminated stainless steel electrodes is given in Fig. 15 for the inner electrode radius of 0.4 cm. (Similar results were obtained for the other two radii). As SF_6 is substituted for N_2, the breakdown voltage rises at first, but then further substitution provides relatively little improvement even though the strength of SF_6 is generally taken to be approximately 2.5 times that of N_2; this is the saturation effect. As each fluorocarbon is increasingly substituted for N_2, however, breakdown strength improves in an approximately linear mode. This difference has already been attributed to the fact that electron attachment by SF_6 is quite strong but limited to a narrow (low) energy range, while the other attaching gases capture electrons over a wider energy range.[15] If the results for the other two inner radii are also examined, one finds that for the c-C_4F_8/N_2 mixtures the breakdown strength (vs percentage in N_2) crosses that for SF_6/N_2 mixtures at values of 66%, 42%, and 28% for respective inner radii of 1.4 cm, 0.75 cm, and 0.4 cm, corresponding to increasing field inhomogeneity in that order. The 2-C_4F_8/N_2 mixtures breakdown strength (vs percentage in N_2) crosses that for SF_6 mixtures at values of 51%, 17%, and 0% for respective inner radii of 1.4 cm, 0.75 cm, and 0.4 cm, again

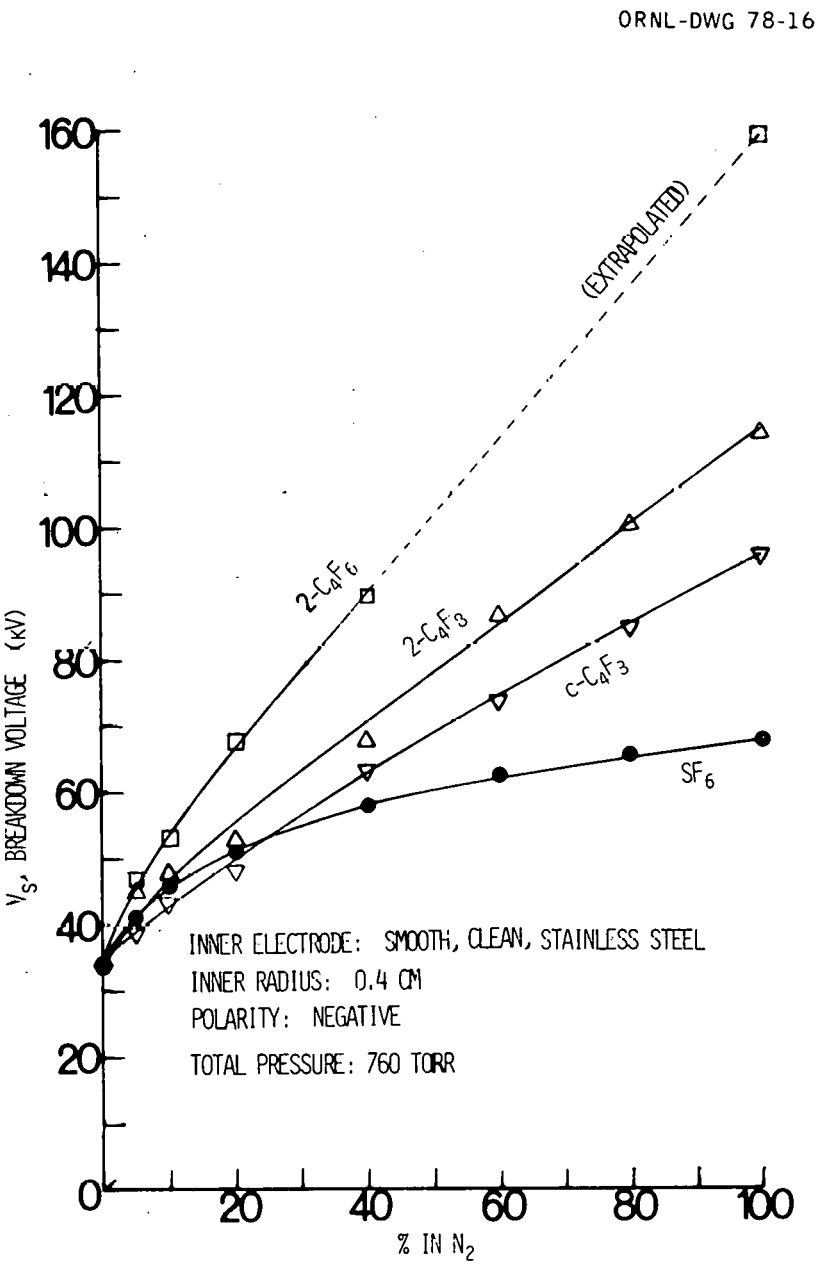

Fig. 15. Breakdown voltages of all attaching gas/N_2 binary mixtures studied, with negative polarity on the 0.4-cm-radius inner cylindrical electrode at 1 atm and ∿21°C. Mixtures are identified by the percentage of attaching gas by pressure. (The 2-C_4F_6/N_2 curve has been extrapolated for the percentage of 2-C_4F_6 > 40%.)

corresponding to increasing field inhomogeneity in that order. Therefore, both c-C_4F_8 and 2-C_4F_8 surpass SF_6 as a substitute for N_2 more quickly as the field is made more nonuniform, indicating a better tolerance to nonuniform fields for the fluorocarbon/N_2 mixtures.

B. Breakdown Tests with Rough Cylinders

The effects of inner electrode surface roughness are shown in Figs. 16 through 19 for two degrees of roughness on the 0.75-cm-radius inner stainless steel electrode, for comparison with the case of the smooth electrode. The error bars indicate combined systematic and random errors, the latter (≤3%) being standard deviation divided by mean for at least 10 breakdowns. For these tests two 0.75-cm-radius electrodes were grooved over a 2-in. length in the central interelectrode region; one had spiralling grooves of 0.004-in. depth, and the other had spiralling grooves of 0.020-in. depth. In both cases there were 28 threads per inch of triangular cross section. The results show that each fluorocarbon is still superior to SF_6 in the face of roughness. Comparisons between the smooth electrode case and each of the rough cases indicate that a mixture of approximately 5% attaching gas/ 95% N_2 is least sensitive to roughness and may, in fact, be almost completely tolerant of roughness. Since roughness gives a much greater degree of field nonuniformity than does the curvature of an electrode, the ionization cross sections could play a role in roughness effects, though they are insignificant in previous studies of less nonuniform fields (see Sect. II and Appendix B).

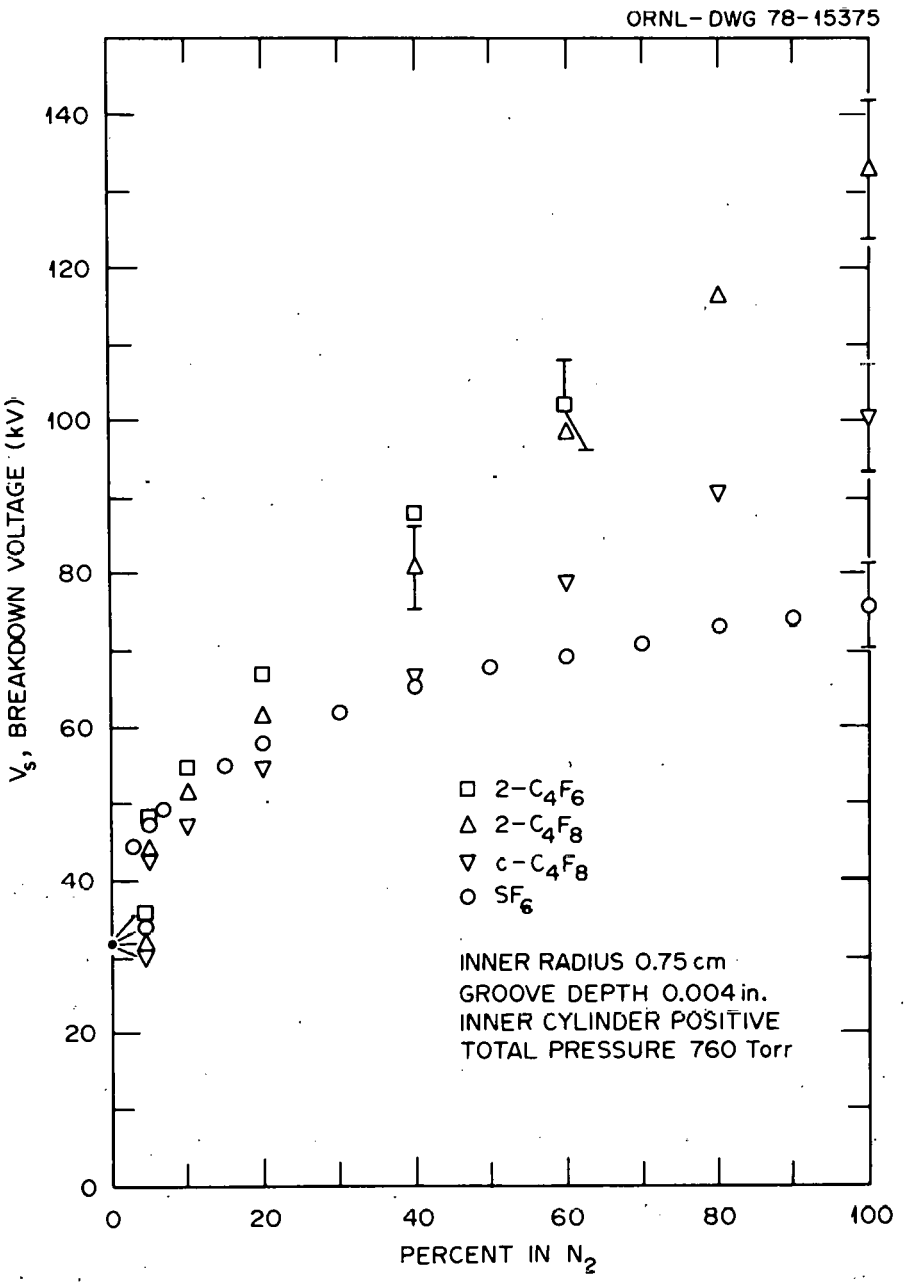

Fig. 16. Breakdown voltages for the four attaching gas/N_2 binary mixtures for inner electrode roughness of 0.004 in. and positive polarity at 1 atm and ∿21°C. Mixtures are identified by the percentage of attaching gas by pressure.

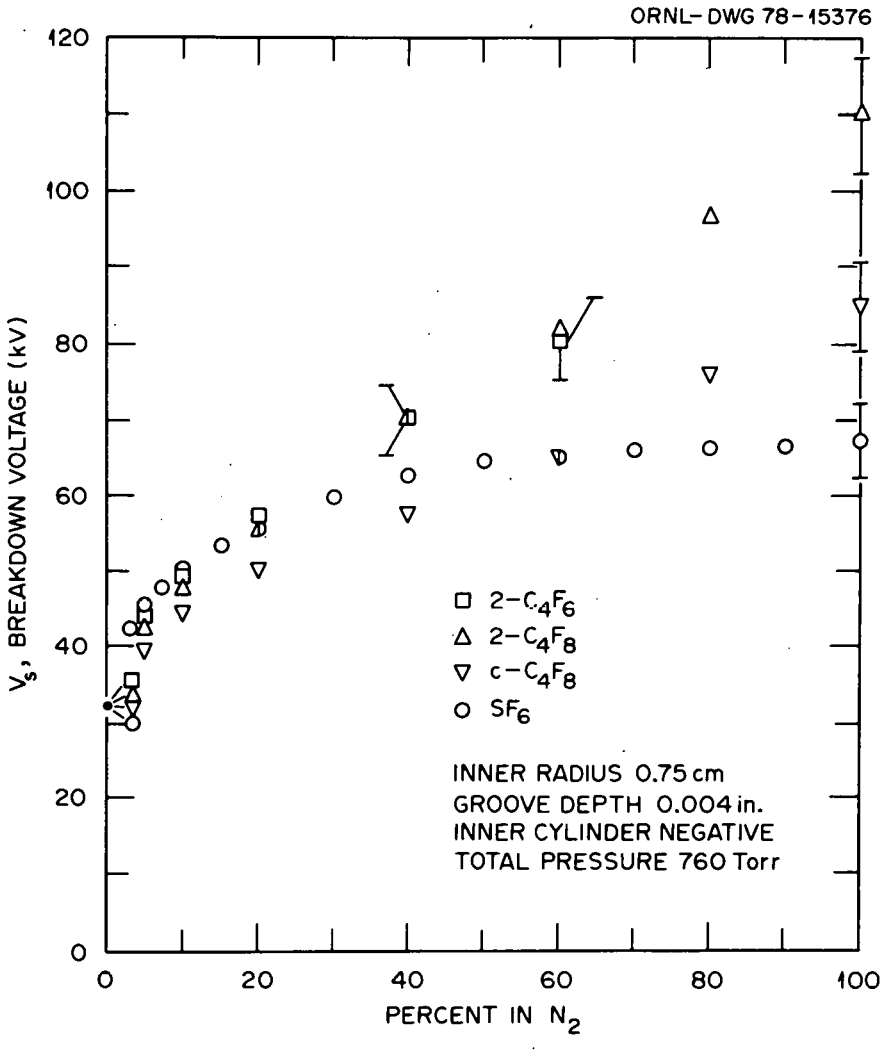

Fig. 17. Breakdown voltages for the four attaching gas/N_2 binary mixtures for inner electrode roughness of 0.004 in. and negative polarity at 1 atm and ∿21°C. Mixtures are identified by the percentage of attaching gas by pressure.

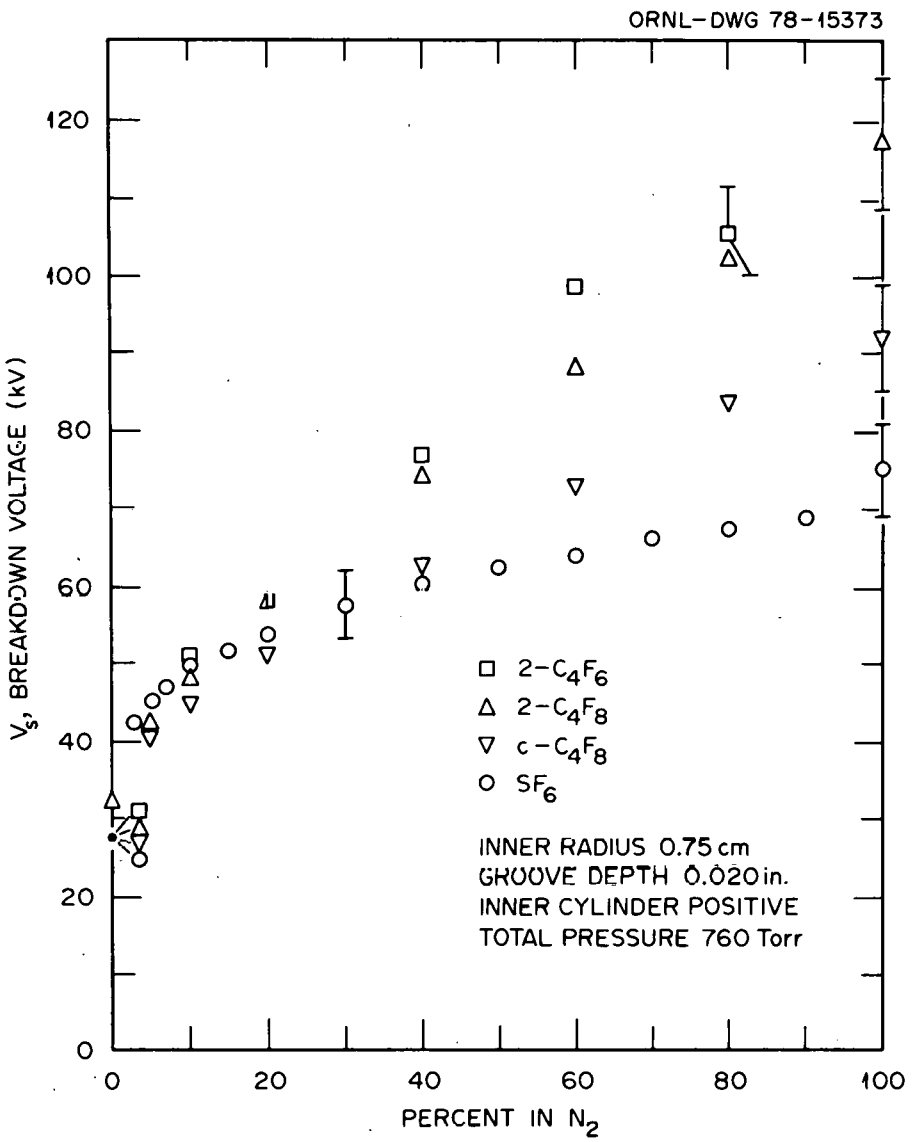

Fig. 18. Breakdown voltages for the four attaching gas/N_2 binary mixtures for inner electrode roughness of 0.020 in. and positive polarity at 1 atm and ∿21°C. Mixtures are identified by the percentage of attaching gas by pressure.

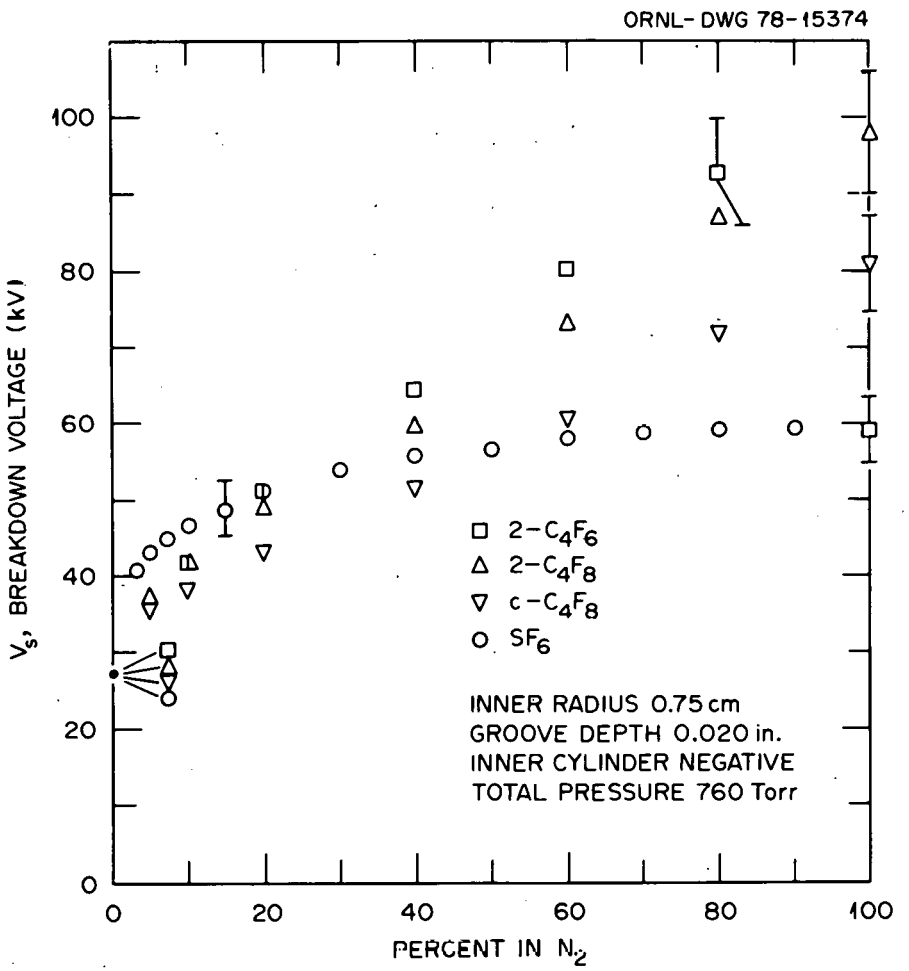

Fig. 19. Breakdown voltages for the four attaching gas/N_2 binary mixtures for inner electrode roughness of 0.020 in. and negative polarity at 1 atm and ~21°C. Mixtures are identified by the percentage of attaching gas by pressure.

C. Breakdown Tests with Cylinders of Different Material Composition

The effects of inner electrode material composition have been sought by performing breakdown measurements for all four (attaching gas)/N_2 mixtures with each of three different 1.4-cm-radius electrodes: one of stainless steel, one of aluminum, and one of copper. The results, shown in Table 11, indicate no great effect of material composition. The variations with material can perhaps be explained by the combined systematic and random error, and any material effects seem to be too slight to be of importance in practical systems.

D. Breakdown Tests with Cylinders and Particle Contamination

The effects of contamination by particles were also studied this period. Since it has been found that conducting particles of long slender shape are most troublesome, several particles of that description were placed in the central interelectrode region with the smooth, 0.75-cm-radius stainless steel inner electrode. Several types of particles were tried, including wires of steel, aluminum, and copper. We found any diameter desired could be obtained by acid etching. To prevent particles from escaping at the open cylinder ends, we tried two methods: tethering particles on a 0.007-in.-diam nylon line, and blocking the open cylinder ends. A complete set of data was taken using free copper wire particles 0.125 x 0.015-in. diam, with the ends of the *small* diameter portion of the outer cylinder blocked by Lexan discs with holes for the inner electrode. The original Plexiglas discs at the *large* diameter portion of the outer cylinder remained to accurately fix the relative position of the two electrodes.

The copper wire particles exhibited the bouncing and hovering modes

Table 11. Observed percentage of variation of breakdown voltage with other materials, compared to stainless steel, for 1.4-cm-radius electrodes. (Random error: ±3%; systematic error ±5%)

Gas	Electrode	Polarity	Percentage in N_2							
			0	5	10	20	40	60	80	100
SF_6	Al	+	-6.6	-6.2	-5.3	-4.0	-3.6	-3.1	-3.0	-1.9
SF_6	Al	-	-7.2	-7.1	-4.9	-5.9	-4.2	-4.2	-3.3	-4.3
SF_6	Cu	+	-5.9	-6.2	-5.2	-4.1	-3.5	-2.8	-2.8	-2.1
SF_6	Cu	-	-9.4	-7.4	-5.2	-5.4	-3.9	-3.3	-2.9	-3.0
$c\text{-}C_4F_8$	Al	+	-6.6	+7.3	+8.4	+7.4	+4.3	+7.5	+9.0	+6.1
$c\text{-}C_4F_8$	Al	-	-7.2	+4.8	+7.2	+4.7	+1.3	+12.0	+8.1	-0.6
$c\text{-}C_4F_8$	Cu	+	-5.9	+7.9	+10.0	+9.7	+8.4	+14.1	+16.2	+12.9
$c\text{-}C_4F_8$	Cu	-	-9.4	+8.2	+10.2	+9.3	+6.4	+18.5	+15.9	+9.1
$2\text{-}C_4F_8$	Al	+	-6.6	+3.2	+6.3	+8.5	+22.9	+16.6	+10.8	+7.4
$2\text{-}C_4F_8$	Al	-	-7.2	+0.6	+4.6	+7.0	+14.3	+18.2	+16.4	+12.5
$2\text{-}C_4F_8$	Cu	+	-5.9	+2.6	+5.9	+4.9	+19.1	+10.9	+3.1	-1.8
$2\text{-}C_4F_8$	Cu	-	-9.4	+2.5	+6.0	+6.5	+11.7	+14.1	+9.1	+3.7
$2\text{-}C_4F_6$	Al	+	-6.6	-7.4	-3.1	-9.0	-2.2			
$2\text{-}C_4F_6$	Al	-	-7.2	-8.3	-6.6	-9.6	-11.0			
$2\text{-}C_4F_6$	Cu	+	-5.9	-6.0	-1.6	-2.4	-0.2			
$2\text{-}C_4F_6$	Cu	-	-9.4	-9.1	-3.4	-4.9	-9.2			

reported by others. As the voltage was raised slowly from zero the particles would abruptly leave the bottom inside surface of the outer cylinder and bounce between the electrodes. If the voltage was raised further and breakdown did not occur first, the particle behavior would eventually change to a hovering motion barely off of the negative electrode and perpendicular to its surface. This bouncing began at 17.0 ± 1.5 kV as voltage was raised from zero and ceased at 7.0 ± 1.5 kV as the voltage was lowered, independent of the gas. Hovering inception and breakdown voltages were dependent on the gas. The particles were watched closely during tests to allow rejection of any breakdown data due to sparks caused by two or more aligned particles or by particles clinging to the insulator discs. If a particle stuck to an insulator no more data were taken until it was freed by the other (bouncing) particles.

The breakdown voltages under this particle contamination are shown in Figs. 20 and 21 for each of the four mixtures studied this period. The error bars indicate combined systematic and random errors; the latter (≤5%) was defined as standard deviation divided by the mean for at least five measurements. Although this particle contamination lowered the breakdown voltages of all mixtures significantly, the mixtures containing fluorocarbons remained superior to those containing SF_6 by approximately the same ratios as obtained without particle contamination.

Similar studies in cylindrical geometry are under way for argon mixtures with fluorocarbons and with SF_6, as well as for CF_4 mixtures with fluorocarbons and with SF_6.

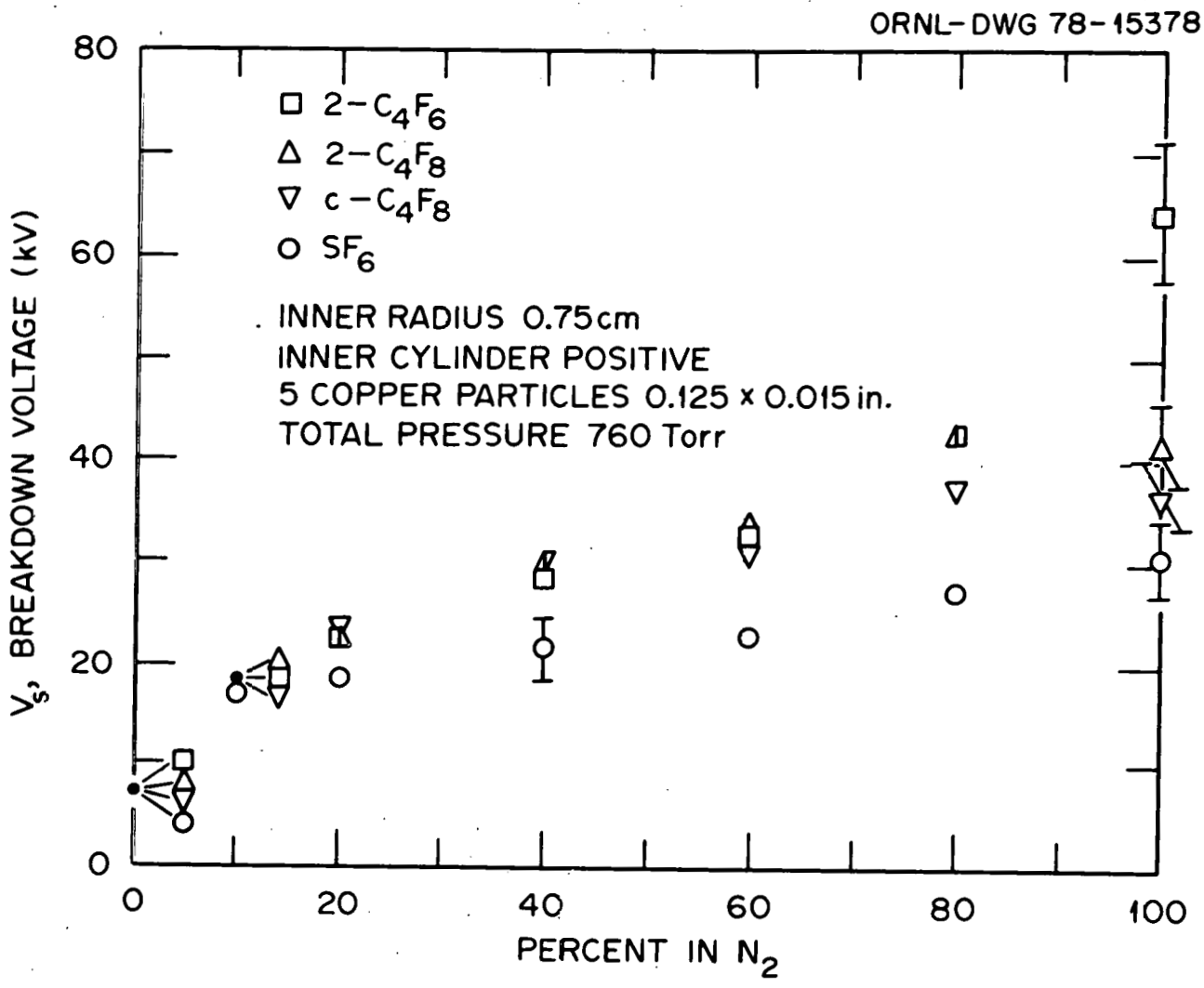

Fig. 20. Breakdown voltages for the four attaching gas/N_2 binary mixtures with contaminating free wire particles at positive polarity, 1 atm, and ∿21°C. Mixtures are identified by the percentage of attaching gas by pressure.

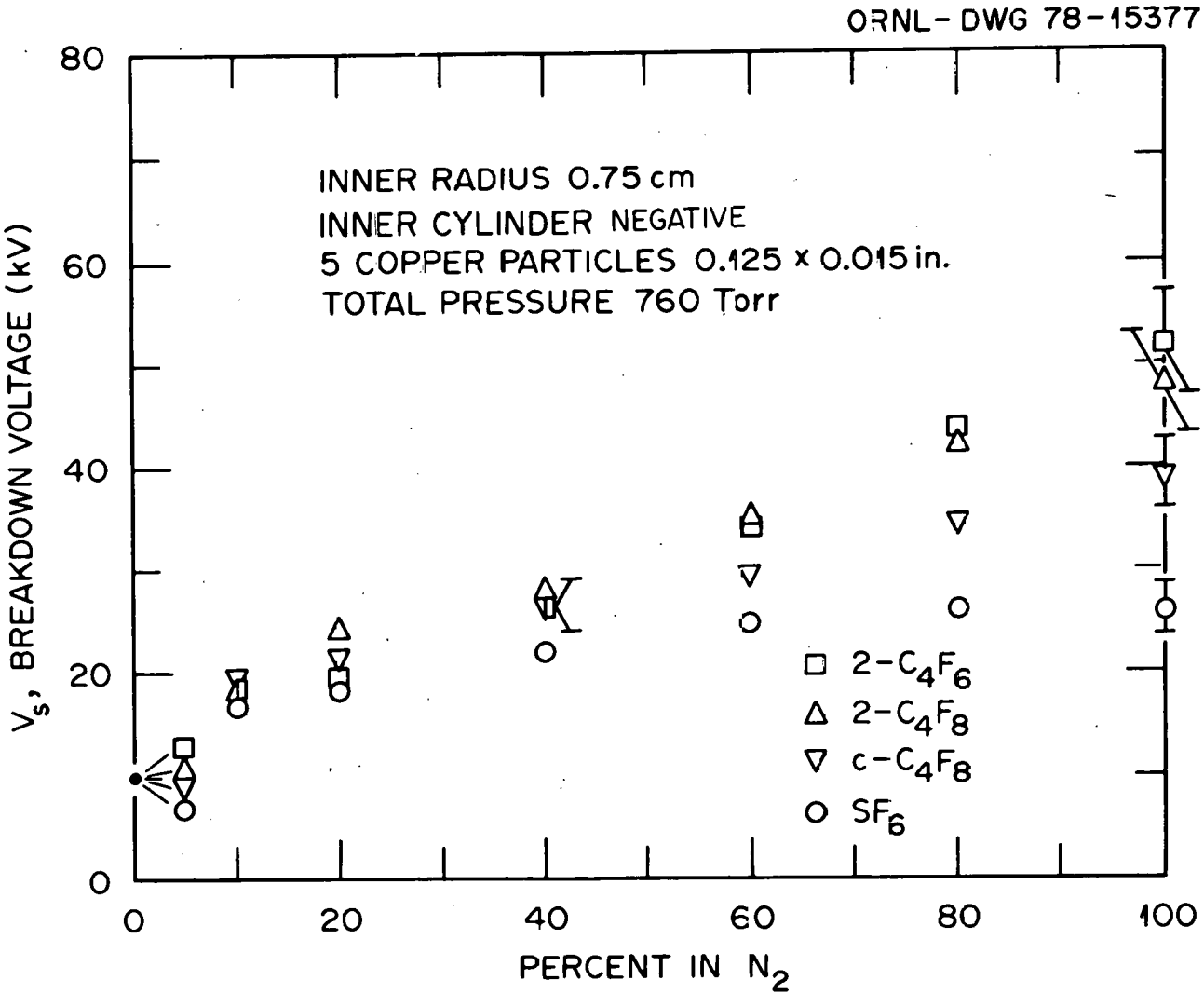

Fig. 21. Breakdown voltages for the four attaching gas/N_2 binary mixtures with contaminating free wire particles at negative polarity, 1 atm, and ~21°C. Mixtures are identified by the percentage of attaching gas by pressure.

VIII. RESEARCH ON LIQUID DIELECTRICS

The behavior of insulating dielectric liquids under electric stress is of considerable engineering importance because these liquids are commonly used in transformers, capacitors, and other power system apparatus. Although such liquids have been under investigation for many years, knowledge of their behavior has been gained largely by empirical means without the benefit of systematic studies based on well-developed theories. Therefore, a study of liquid dielectrics utilizing fundamental physico-chemical knowledge and highly refined experimental techniques has begun during this period as a natural extension of work already in progress at ORNL on gaseous dielectrics.

In reviewing the literature on liquid dielectrics, it became evident that although a considerable degree of understanding has been achieved for solids under electrical stress, the situation is far from satisfactory for liquid dielectrics. This stems principally from the difficulties encountered in observing the behavior just before, during, and after electric breakdown and the failure of many investigators to exercise precise scientific control of their experiments. Observation of the breakdown phenomenon in liquids is difficult because of its ultrafast transient nature, but recently laser schlieren techniques have provided photographic results which may lead to a better understanding of the process. (It is anticipated that the image converter camera we acquired will provide valuable information in this regard.) Also, electromagnetic radiation which is produced during breakdown can interfere with the measurements, but this can be overcome with proper shielding.

The most pronounced effect on the dielectric strength of liquids

is the presence of impurities. For example, bubbles of gas, formed between the electrodes either by decomposition of the liquid or from insufficient degassing of the liquid and electrodes, permit breakdown since they have a breakdown strength lower than that of the liquid itself. Also, globules of water, caused by moisture condensation or insufficient purification, become unstable in the electric field and enable a low-resistance bridge to be set up between the electrodes. Conducting particles which have not been removed by the purification system can give rise to local enhancement of the electric field which may exceed critical values locally such that total breakdown occurs.

Therefore, reliable data on liquid dielectrics under stress can be obtained only be exercising great care in experimental technique. Hence, an elaborate purification system was designed to attain a high degree of purity of the liquid under test. Figure 22 shows a block diagram of this system.† The Si-Gel trap is heated to 300°C and the activated charcoal trap to 400°C for 48 hr while being evacuated to the 10^{-6} torr scale. The rest of the system is heated to 150°C and pumped to 1×10^{-7} torr for 48 hr. The temperature is then reduced to 50°C, and the vacuum system liquid nitrogen trap is filled, reducing the pressure to 2×10^{-8} torr before introduction of the sample. The sample in flask No. 1 is then passed through the Si-Gel and activated charcoal columns, which are at room temperature, into the freeze-pump-thaw chamber by placing an ice bath around the chamber. The inner cylinder in this chamber is cooled by liquid nitrogen, and the sample is opened to the vacuum system, degassing

†We are grateful to J. G. Carter for the design, building, and testing of this system.

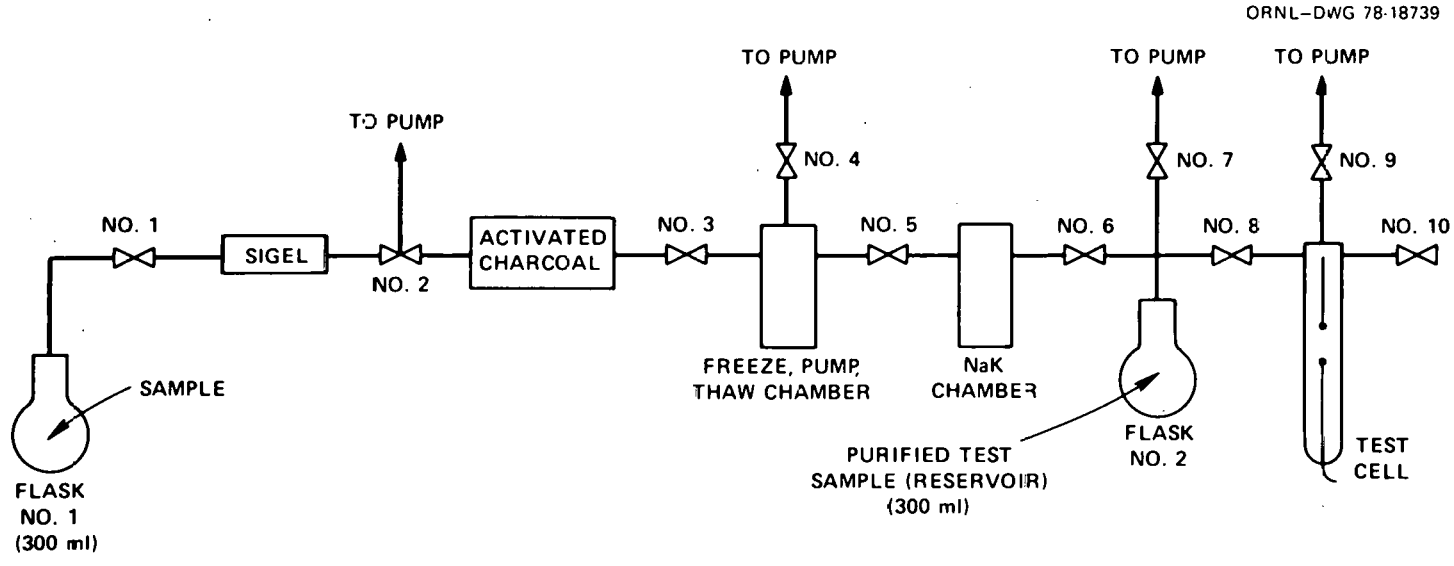

Fig. 22. Purification system for liquid dielectric studies.

the liquid. After 2 hr of this procedure the sample is transferred to the NaK alloy chamber and stirred with 50 ml of the alloy for 24 hr. The final step consists of transferring the sample into the reservoir via the ice bath technique. The appropriate amount is then transferred to the test cell. This entire procedure has been utilized in basic studies and has, through experience, been found to be an effective means of purification of liquids.

Design of the test cell for studying electric breakdown in liquid dielectrics required careful consideration of the experimental goals and constraints. Test cells are usually small (<100 ml) in order to economize in the use of liquids and must permit accurate electrode separation of 200 μm or less. Rigid mechanical control can be obtained using a metal chamber, but photographic observation of breakdown is not possible. future studies of corona would not be feasible if the sides of the chamber are too near the electrodes.

Hence, the test cell in Fig. 23 was designed to allow accurate electrode separation and visual observation. The lower electrode is fixed while the upper electrode is adjustable through a 25-mm range with an accuracy of 0.001 mm. The center portion of the cell is quartz, which allows unrestricted observation of breakdown without filtering of ultraviolet light. The toroid positioned at the lower electrode protruding through the glass cell shields the resulting E-field to prevent breakdown from occurring in air outside the test cell. The liquid volume is typically 30 ml (with the test cell filled to a level 15 mm above the top electrode).

Fabrication of the purification system and the test cell were

ORNL-DWG 78-19764

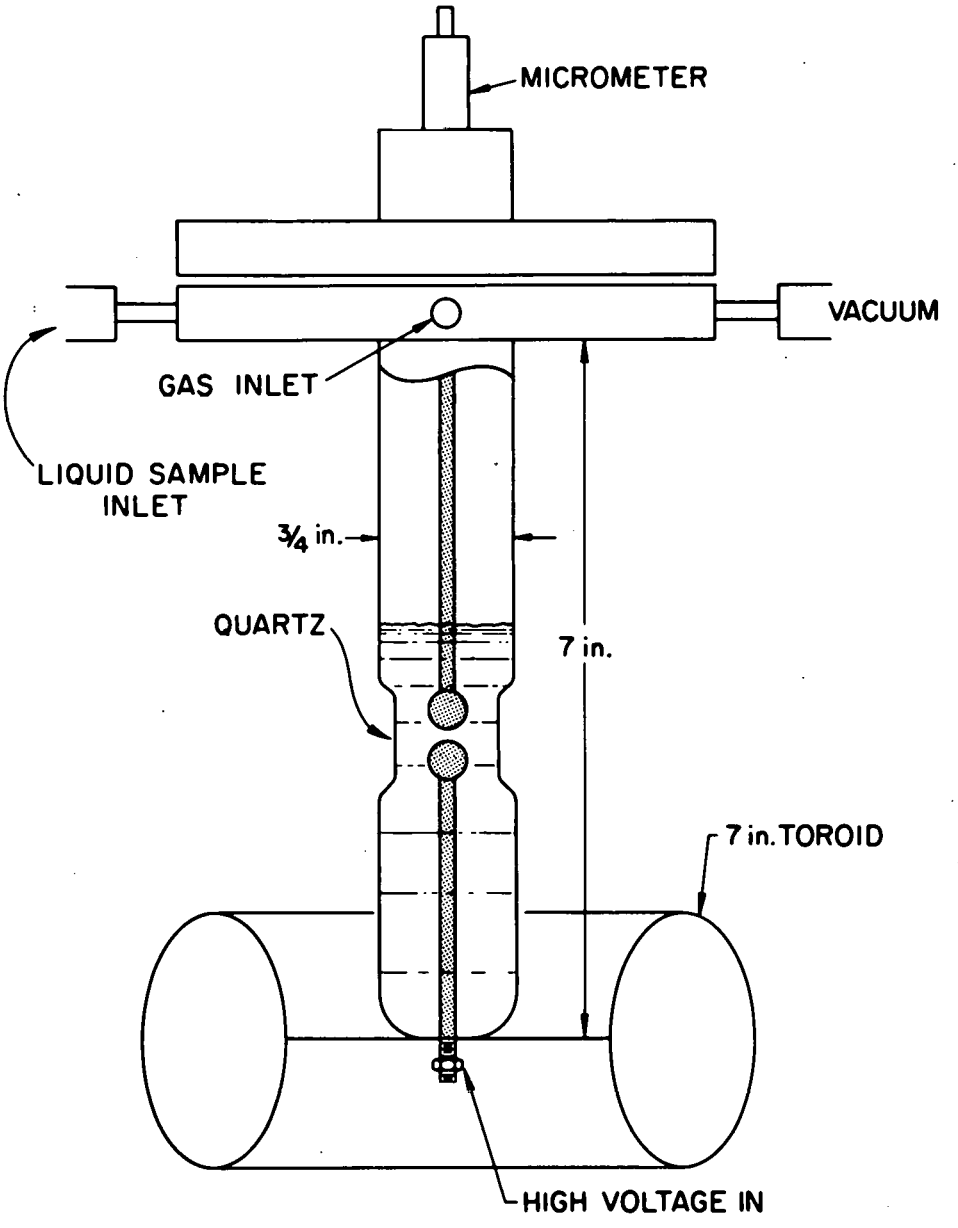

Fig. 23. Liquid breakdown test cell.

completed during this reporting period. A Sorensen 120 kV dc power supply will become available for these studies. An electronic controller (like those on our other apparatuses) is being fabricated to automatically apply voltage to the electrodes.

The entire apparatus is in the final stages of testing and measurements on the dielectric strengths of liquids will commence in the very near future.

IX. APPARATUS

The Imacon 790 image converter camera has been received and tested successfully. It will provide 16 consecutive frames at rates of 10^6 frames per second and 20 x 10^6 frames per second. Events somewhat faster than 10^{-9} sec can be resolved using the streak mode, in which one dimension is collapsed to a line and the other dimension is swept with time. Initial plans for the camera include a return to our earlier diverter studies.[14]

The atmospheric pressure quadrupole mass spectrometer has been ordered from Extranuclear Laboratories, Inc. Delivery is anticipated in January, 1979. It is intended to mass-analyze neutrals and ions of either polarity that leave a gas cell operating at pressures on the order of 1 atm. The apparatus consists of an ultrahigh vacuum system with fast turbomolecular pumps, pinhole orifice, quadrupole mass spectrometer and electronics, and an electron multiplier.

The variable temperature experiment high voltage cable has been irradiated with gamma rays along 1.5 ft at one end, at the ORNL high flux isotope reactor. The resulting crosslinking of the polyethylene should raise the melting point so that temperatures $\geq$ 150°C can be attained. This was accomplished by sealing the cable in an aluminum tube, which was lowered into the reactor pool such that the lower 1.5 ft. reached the radiation zone. A cooling coil has also been installed around the exterior of the high voltage chamber feedthrough. For low-temperature work it was necessary to develop localized heating of the O-ring seal of the high voltage chamber feedthrough, providing a leakproof

seal at -25°C with a pressure corresponding to 5 atm at room temperature.

A 400 kV, 4kJ impulse generator has been ordered from Haefely. A transient waveform digitizer has been ordered from Tektronix to better view the impulse breakdown waveform. A new digital voltmeter has been ordered.

The new-high pressure chamber for practical studies is near completion and will soon be ready for pressure tests. A new Wallace and Tiernan pressure gauge has been received for it.

X. PUBLICATIONS AND CONTACTS

A. Publications

1. L. G. Christophorou (editor), *Gaseous Dielectrics (Proceedings of the International Symposium on Gaseous Dielectrics, Knoxville, Tennessee, Mar. 6-8, 1978)* CONF-780301 (May 1978).
2. D. R. James, L. G. Christophorou, R. Y. Pai, M. O. Pace, R. A. Mathis, I. Sauers, C. C. Chan, "Dielectric Strengths of New Gases and Gas Mixtures," *Gaseous Dielectrics (Proceedings of the International Symposium on Gaseous Dielectrics, Knoxville, Tennessee, Mar. 6-8, 1978)* CONF-780301 (May 1978), pp. 224-257.
3. R. Y. Pai, T. F. Garrity, "Basic Discussion Panel Summary," *Gaseous Dielectrics (Proceedings of the International Symposium on Gaseous Dielectrics, Knoxville, Tennessee, Mar. 6-8, 1978)* CONF-780301 (May 1978), pp. 414-427.
4. M. O. Pace, V. H. Tahiliani, "Applied Discussion Panel Summary," *Gaseous Dielectrics (Proceedings of the International Symposium on Gaseous Dielectrics, Knoxville, Tennessee, Mar. 6-8, 1978)* CONF-780301 (May 1978), pp. 428-446.
5. L. G. Christophorou, "The Use of Basic Physical Data in the Design of Multicomponent Gaseous Insulators," *Gas Discharges (Proceedings of the 5th International Conference on Gas Discharges, September 11-14, 1978, Liverpool, United Kingdom)* IEE Conference Publication Number 165 (1978).
6. M. O. Pace, C. C. Chan, L. G. Christophorou, "Application of Basic Gas Research to Practical Systems," *7th IEEE/PES Conference and Exposition on Overhead and Underground Transmission and Distribution,*

April 1-6, 1979, Atlanta, Georgia (accepted--see Appendix E)

7. A. A. Christodoulides, L. G. Christophorou, R. Y. Pai, C. M. Tung, "Electron Attachment to Perfluorocarbon Compounds: Part I: c-C_4F_6 2-C_4F_6, 1,3-C_4F_6, c-C_4F_8, and 2-C_4F_8" (accepted for publication in the *Journal of Chemical Physics.*
8. R. Y. Pai, L. G. Christophorou, A. A. Christodoulides, "Electron Attachment to Perfluorocarbon Compounds: Part II: c-C_5F_8, c-C_6F_{10}, c-C_6F_{12}, C_7F_8, and C_8F_{16}- Relevance to Gaseous Dielectrics" (accepted for publication in the *Journal of Chemical Physics.*
9. L. G. Christophorou, D. R. James, R. A. Mathis, "On the Role of the Electron Impact Ionization Cross Section in the Breakdown Strength of Dielectric Gases" (submitted to *Journal of Physics D: Applied Physics;* see Appendix B).
10. A. A. Christodoulides, L. G. Christophorou, "Electron Attachment to c-C_7F_{14} and 1-C_7F_{14}" (submitted to *Chemical Physics Letters* see Appendix A).

B. Contacts

In May, M. O. Pace attended the IEEE Power Engineering Society Switchgear Committee Meeting in New Orleans.

Extranuclear Laboratories, Inc. of Pittsburgh was visited in June by I. Sauers, to view a demonstration of an atmospheric pressure quadrupole mass spectrometer. In September, L. G. Christophorou visited the Electrical Engineering Departments at the Universities of Liverpool and Strathclyde and the Physics Department at the University of Manchester, all in the United Kingdom.

Those visiting us in this period included: R. J. Van Brunt, R. E. Webner, and M. Masakian, of the National Bureau of Standards; A. Pedersen, of the Technical University of Denmark; R. Koerwer, M. Reddi, and H. G. Lorsch, of the Franklin Institute; F. V. Struisa, J. Barron, W. J. Cole, and Mel Singer, of the New York State Energy Authority; R. S. Berry of the University of Chicago; S. Rice of the University of Ontario; William McElroy , Chancellor, University of California at San Diego and member of ORNL Advisory Committee; P. Markovitch of the Boris Kidric Institute of Nuclear Sciences, Belgrade, Yugoslavia; K. Kite of Tektronix, Inc.; E. Larsen of Biomation; and J. Owren of Marco Scientific, Inc.

Also in this period a request to us from Dr. Floyd Culler, Director of E.P.R.I., was honored, for a wide source of information on SF_6 and its use. Particle contamination experiments were discussed with Dr. Chat Cooke of the Massachusetts Institute of Technology. Discussions were also held with J. P. Vora of the Department of Energy, Columbia Organic Chemicals Co., Armegeddon Chemical Co., Linde Division of Union Carbide and Air Products and Chemicals Inc.

At ORNL, John Million (Gaseous Diffusion Plant) and Bill Rainey (Y-12) aided in gas analysis. Gerald Goldberg (High Flux Isotope Reactor) irradiated the polyethylene cable for the high temperature apparatus. J. Bair (accelerator group) discussed gaseous dielectrics. The interaction with H.C. Schweinler, especially on electric field-induced electron detachment, is gratefully acknowledged. Thanks are also due to V. E. Anderson for computational help.

XI. REFERENCES

1. L. G. Christophorou, *Atomic and Molecular Radiation Physics*, chap. 4, Wiley-Interscience, New York, 1971.
2. L. G. Christophorou and A. A. Christidoulides, *J. Phys. B: Atom. Molec. Phys.* 2, 71 (1969).
3. L. G. Christophorou, *Int. J. Rad. Phys. Chem.* 7, 205 (1975).
4. L. G. Christophorou, D. R. James, R. Y. Pai, R. A. Mathis, M. O. Pace, D. W. Bouldin, A. A. Christodoulides, and C. C. Chan, *High Voltage Research (Breakdown Strengths of Gaseous and Liquid Insulators)* ORNL/TM-6113 (November 1977).
5. L. G. Christophorou, D. R. James, R. Y. Pai, R. A. Mathis, I. Sauers, M. O. Pace, D. W. Bouldin, A. A. Christodoulides, and C. C. Chan, *High Voltage Research (Breakdown Strengths of Gaseous and Liquid Insulators)* ORNL/TM-6384 (June 1978).
6. L. G. Christophorou, "Elementary Electron-Molecule Interactions and Negative Ion Resonances at Subexcitation Energies and Their Significance in Gaseous Dielectrics," *Proceedings of the XIIIth International Conference on Phenomena in Ionized Gases, Berlin, GDR, Sept. 11-17, 1977*, Vol. II (1978) p. 51-72.
7. H.S.W. Massey, *Negative Ions, Third Edition*, Cambridge University Press, Cambridge, 1976.
8. L. G. Christophorou, "Interactions of O_2 with Slow Electrons," *Int. J. Rad. Phys. Chem.* (in press).
9. G. Camilli, T. W. Liao, and R. E. Plump, *Trans. AIEE* 74 Pt. I, 637 (1955); *Trans. AIEE* 77 Pt. 3, 1659 (1958).

10. I. Sauers, L. G. Christophorou, and J. G. Carter, *Book of Abstracts, 31st Annual Gaseous Electronics Conference, Buffalo, New York,* p. 130, Paper MA-11 (October 1978).

11. J. H. Simons, *Fluorine Chemistry, Vol. I,* p. 476, Academic Press Inc., New York, 1950.

12. William Brahen and Allen L. Mossman, *Matheson Gas Data Book, Fifth Edition,* p. 536, Matheson Gas Products, East Rutherford, New Jersey, 1971.

13. A. M. Lovelace, D. A. Rausch and William Postelnek, *Aliphatic Fluorine Compounds,* p. 43, Reinhold Publishing Corp., New York, 1958.

14. L. G. Christophorou, D. R. James, R. Y. Pai, M. O. Pace, R. A. Mathis, and D. W. Bouldin, *High Voltage Research (Breakdown Strengths of Gaseous and Liquid Insulators)* ORNL/TM-5917 (June 1977).

15. M. O. Pace, L. G. Christophorou, D. R. James, R. Y. Pai, R. A. Mathis, and D. W. Bouldin, "Improved Unitary and Multicomponent Gaseous Insulators," *IEEE. Trans. Elect. Insul.* Vol. EI-13, 31 (1978).

APPENDIX A

Paper Submitted to Chemical Physics Letters

ELECTRON ATTACHMENT TO c-C_7F_{14} and 1-C_7F_{14}*

A.A. CHRISTODOULIDES† and L.G. CHRISTOPHOROU‡

Atomic, Molecular and High Voltage Physics Group, Health and Safety Research Division, Oak Ridge National Laboratory, Oak Ridge, Tennessee 37830, U.S.A.

The results of a swarm study on the attachment of slow ($\lesssim$3 eV) electrons to c-C_7F_{14} and 1-C_7F_{14} are presented and discussed. For both molecules the attachment cross sections show resonance maxima at 0.07 and 0.25 eV, and they are much larger for the cyclic isomer. The thermal values of the electron attachment rate are 18.3 and 1.33 x 10^8 sec^{-1} $torr^{-1}$ for c-C_7F_{14} and 1-C_7F_{14}, respectively.

1. Introduction

The study of the electron attaching properties of halocarbon molecules is both of basic and applied significance. Knowledge of the rates and cross sections for production of parent and fragment negative ions, of the autodetachment lifetimes of metastable parent and fragment negative ions and of their energy dependences is necessary for the development of an understanding of the formation and fragmentation of molecular negative ions in impacts with low-energy electrons [1,2]. Certain halocarbons are of special significance to the environment [2] and also to other applied areas such as gaseous dielectrics (e.g., see refs. 3-5).

In this paper we report and briefly discuss the results of a swarm study on electron attachment to c-C_7F_{14} (perfluoromethylcyclohexane) and 1-C_7F_{14} (perfluoro-1-heptene). Although c-C_7F_{14} has been the subject of earlier studies [6-14] (mostly at thermal energies), to our knowledge no study of 1-C_7F_{14} has been made. Recent work on electron attachment to other perfluorocarbon molecules can be found in refs. 15 and 16.

---

*Research sponsored by the Division of Electric Energy Systems of the U.S. Department of Energy under contract W-7405-eng-26 with Union Carbide Corporation.

†Visiting Scientist; permanent address, Department of Physics, University of Ioannina, Ioannina, Greece.

‡Also Department of Physics, University of Tennessee, Knoxville, Tennessee 37916.

2. Experimental

The experimental and analytical methods used in the present study have been described previously (see, for example, refs. 1, 15 and 17). The purity of c-C_7F_{14} and 1-C_7F_{14} was >97+%, and the measurements were performed at ~298°K.

3. Results and Discussion

The attachment rates, αw, (α is the electron attachment coefficient, and w is the electron swarm drift velocity) [1] for c-C_7F_{14} and 1-C_7F_{14} have been measured as a function of the pressure-reduced electric field, E/P_{298}, in mixtures with the "carrier" gases [1] N_2 and Ar at total pressures 500, 1000, 1500 and 2000 torr and 500, 1000 and 1500 torr, respectively. The perfluorocarbon pressures ranged from 5.4 to 19 x 10^{-5} torr ror c-C_7F_{14} and from 30.7 to 98.8 x 10^{-5} torr for 1-C_7F_{14}. Twenty independent measurements of the attachment rate as a function of E/P_{298} have been made for c-C_7F_{14} and 1-C_7F_{14} in mixtures with N_2. The average of these is listed in table 1 and is plotted in fig. 1 (solid points). Similarly, nine independent measurements of $\alpha w(E/P)$ have been made for 1-C_7F_{14} and twelve for c-C_7F_{14} using Ar as the carrier gas. The average of these is listed in table 2 and is plotted in fig. 1 (open points). In fig. 1 αw is plotted as a function of the mean electron energy $\langle\varepsilon\rangle$; the relationship between $\langle\varepsilon\rangle$ and E/P_{298} is given in tables 1 and 2 for N_2 and Ar respectively (see refs. 1 and 15). A slight increase in αw with increasing total pressure was noticed for each molecule in both carrier gases, but it was not sufficiently outside of the experimental error (see tables 1 and 2) to be considered significant. For each carrier gas, at each E/P the average value of αw for each total pressure is within a standard deviation of the mean value of αw using all data (i.e., for all attaching and all carrier-gas pressures) for that particular E/P.

The $\alpha w(\langle\varepsilon\rangle)$ functions show a characteristic maximum at 0.17 eV for c-C_7F_{14} and at 0.25 eV for 1-C_7F_{14}. They are much larger for the cyclic isomer.

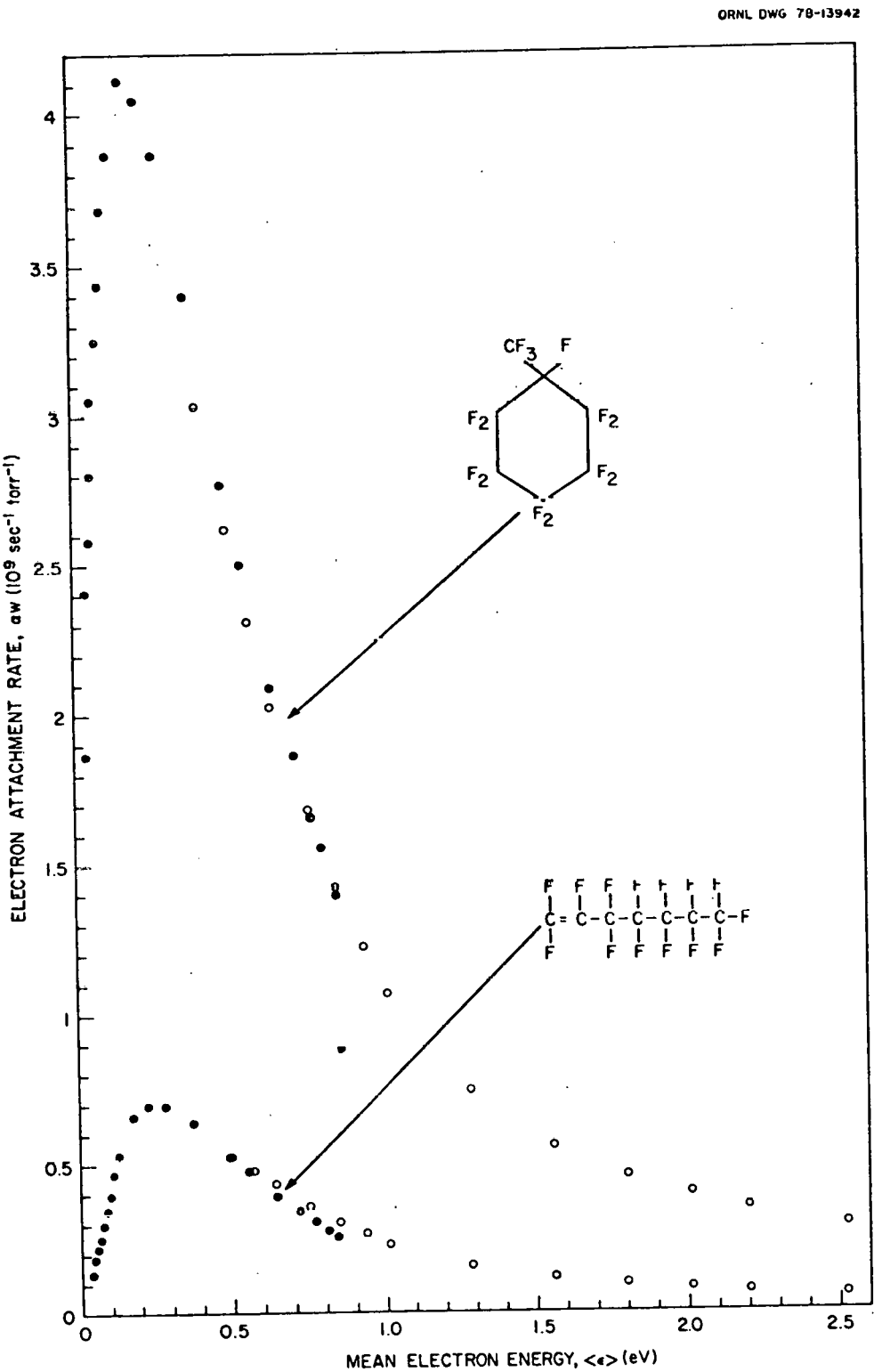

Fig. 1. Electron attachment rate as a function of mean electron energy for c-C_7F_{14} and 1-C_7F_{14}. (●) Data taken using N_2 as the carrier gas; (○) data taken using Ar as the carrier gas (see tables 1 and 2 for error estimates).

Table 1

Electron attachment rates for $1\text{-}C_7F_{14}$ and $c\text{-}C_7F_{14}$ in N_2 [a]

E/P_{298} (volt cm^{-1} $torr^{-1}$)	$\langle\varepsilon\rangle$ (eV)	$1\text{-}C_7F_{14}$ [b]		$c\text{-}C_7F_{14}$ [c]	
		αw (10^8 sec^{-1} $torr^{-1}$)	s.d./(αw) [d] (%)	αw (10^9 sec^{-1} $torr^{-1}$)	s.d./(αw) [d] (%)
0.007		1.07	6.9	1.47	5.1
0.01	0.041	1.38	7.5	1.86	4.6
0.02	0.046	1.87	6.0	2.41	3.1
0.03	0.054	2.13	6.5	2.58	3.6
0.04	0.064	2.49	6.7	2.80	3.6
0.05	0.075	2.97	7.0	3.05	2.4
0.06	0.087	3.43	7.2	3.25	3.7
0.07	0.099	3.92	7.4	3.44	3.8
0.08	0.109	4.67		3.69	
0.10	0.131	5.29	7.0	3.87	3.5
0.15	0.181	6.61	6.3	4.12	3.2
0.20	0.230	6.95	6.1	4.05	2.9
0.25	0.285	6.95	6.0	3.87	2.6
0.35	0.376	6.34	5.4	3.40	2.6
0.50	0.490	5.24	5.1	2.77	2.2
0.60	0.550	4.74	5.1	2.50	2.2
0.80	0.646	3.90	5.2	2.09	2.1
1.00	0.715	3.40		1.86	
1.20	0.764	3.02		1.65	
1.40	0.803	2.74		1.54	

a) The pressures of N_2 employed are: 500, 1000, 1500 and 2000 torr.
b) Average of twenty independent runs with $1\text{-}C_7F_{14}$ pressures in the range 30.7 to 98.8 x 10^{-5} torr.
c) Average of twenty independent runs with $c\text{-}C_7F_{14}$ pressures in the range 5.4 to 19 x 10^{-5} torr.
d) Standard deviation divided by αw.

Table 2

Electron attachment rates for $1\text{-}C_7F_{14}$ and $c\text{-}C_7F_{14}$ in Ar [a]

E/P_{298} (volt cm^{-1} $torr^{-1}$)	$\langle\varepsilon\rangle$ (eV)	$1\text{-}C_7F_{14}$ [b]		$c\text{-}C_7F_{14}$ [c]	
		αw (10^8 sec^{-1} $torr^{-1}$)	s.d./(αw) [d] (%)	αw (10^9 sec^{-1} $torr^{-1}$)	s.d./(αw) [d] (%)
0.006	0.409	5.36	8.6	3.03	3.8
0.010	0.498	5.24	7.5	2.62	5.0
0.015	0.570	4.80	6.0	2.31	4.3
0.02	0.641	4.31	4.9	2.02	4.3
0.03	0.752	3.60	4.5	1.69	3.8
0.04	0.848	3.05	3.9	1.42	4.0
0.05	0.935	2.63	3.8	1.22	3.8
0.06	1.012	2.29	3.8	1.07	3.5
0.10	1.285	1.57	3.5	0.74	3.7
0.15	1.559	1.14	3.6	0.56	3.5
0.20	1.795	0.92	3.5	0.46	4.0
0.25	2.008	0.79	3.6	0.40	3.4
0.30	2.197	0.69	3.6	0.35	3.5
0.40	2.526	0.55	3.8	0.29	3.5
0.50	2.808	0.50	-	0.26	-

a) The pressures of Ar employed are: 500, 1000 and 1500 torr.
b) Average of nine independent runs with $1\text{-}C_7F_{14}$ pressures ranging from 35.3 to 52.1 x 10^{-5} torr.
c) Average of twelve independent runs with $c\text{-}C_7F_{14}$ pressures in the range 9.7 to 17.1 x 10^{-5} torr.
d) Standard deviation divided by αw.

The data on $\alpha w(<\varepsilon>)$, taken using N_2 as the carrier gas (table 1; fig. 1), were unfolded by application of the swarm unfolding technique [18]. The $\sigma_a(\varepsilon)$ obtained are listed in table 3 and are plotted in fig. 2. Two resonance maxima are seen which for both molecules occur at $\sim$0.07 and $\sim$0.25 eV. Although the positions of the cross section maxima are the same for the two isomers, the magnitude and the energy dependence of $\sigma_a(\varepsilon)$ are substantially different.

Earlier electron beam studies [11] on c-C_7F_{14} have shown that the most abundant negative ion is the long-lived metastable parent ion c-$C_7F_{14}^{-*}$ formed at thermal and epithermal energies with maximum intensity at $\sim$0.07 eV, in agreement with the present work. Other (weaker) ions such as $C_7F_{13}^-$, $C_6F_{11}^-$ and $C_5F_9^-$ were detected [11] at higher energies ($\sim$0.3 eV). Based on this work and also on recent work on other fluorocarbon compounds [4,5], the 0.07 eV resonance in fig. 2 should be mostly due to the parent c-$C_7F_{14}^{-*}$ ion and the 0.25 eV resonance due mostly to fragment ions. Other beam studies [10,13] found the auto-detachment lifetime τ_a of c-$C_7F_{14}^{-*}$ at $\sim$0.0 eV to be 793 μsec [10] and 757 μsec [13]. Although no similar work has been reported for 1-C_7F_{14}, on the basis of the work on c-C_7F_{14} and other fluorocarbons (refs. 1, 4, 5, 10, 15, 16 and 19), the 1-$C_7F_{14}^{-*}$ ion is expected to form at $\sim$0.07 eV and to be long-lived ($\tau_a > 10^{-6}$ sec); fragment negative ions would predominate at higher energies.

The results of earlier studies [8,9,12,14] on the value of the thermal (T = 298°K) attachment rate for c-C_7F_{14} are compared in table 4 with the present value of 18.3×10^8 sec^{-1} $torr^{-1}$. The thermal value of the attachment rate for 1-C_7F_{14} is 1.33×10^8 sec^{-1} $torr^{-1}$ (i.e., $\sim$14 times smaller than for c-C_7F_{14}).

The higher values of the attachment cross section for the cyclic perfluorocarbon are consistent with the conclusion we reached recently [15,16] that the cyclic structure increases the attachment cross section. They are also consistent with the higher dielectric strength of c-C_7F_{14} relative to 1-C_7F_{14} (refs. 3-5). Christophorou et al. [4] reported the relative DC breakdown voltage of c-C_7F_{14}, 1-C_7F_{14} and SF_6 to be 2.2, 1.2 and 1.0, respectively.

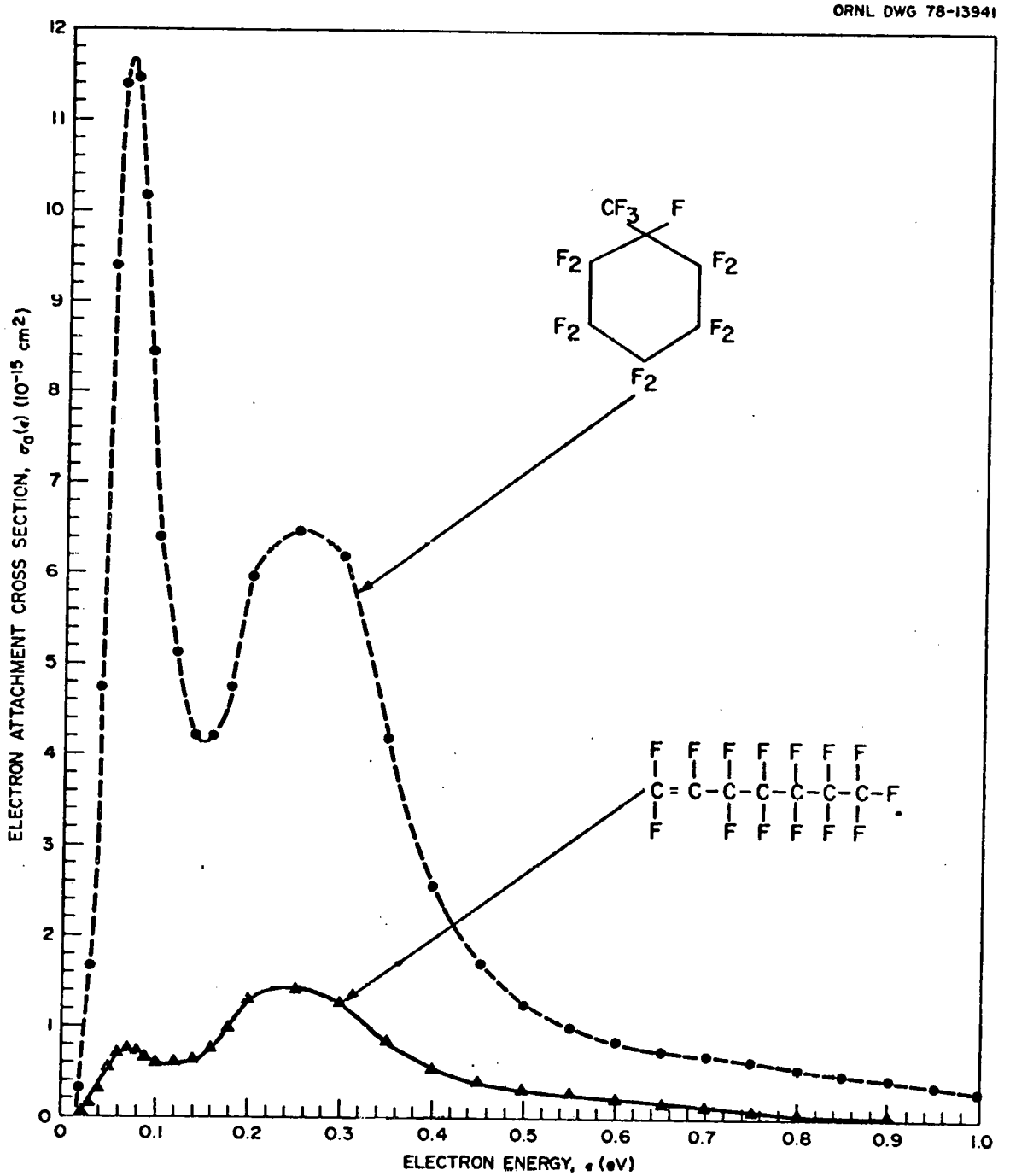

Fig. 2. Swarm-unfolded electron attachment cross sections as a function of electron energy for c-C_7F_{14} (●) and l-C_7F_{14} (▲).

Table 3

Electron attachment cross sections, $\sigma_a(\varepsilon)$, for $1\text{-}C_7F_{14}$ and $c\text{-}C_7F_{14}$

ε(eV)	$\sigma_a(\varepsilon)$ (10^{-16} cm^2)	
	$1\text{-}C_7F_{14}$	$c\text{-}C_7F_{14}$
0.02	0.31	3.3
0.03	1.26	16.6
0.04	3.02	47.3
0.05	5.75	93.9
0.06	7.01	113.9
0.07	7.44	114.7
0.08	7.17	101.7
0.10	5.90	63.9
0.12	6.09	51.4
0.14	6.30	42.2
0.16	7.61	42.0
0.18	9.93	47.6
0.20	12.93	59.7
0.25	14.02	64.6
0.30	12.60	62.0
0.35	8.31	42.0
0.40	5.45	25.7
0.45	4.02	16.9
0.50	3.29	12.4
0.55	2.79	10.1
0.60	2.19	8.47
0.65	1.67	7.46
0.70	1.30	7.00
0.75	0.90	6.33
0.80	0.58	5.66
0.85	0.35	4.91
0.90	0.21	4.39
0.95	0.12	3.78
1.0	0.05	2.79
1.1	0.012	1.54
1.2	0.001	0.47
1.3		0.07

Table 4

Values of the thermal attachment rate, positions, ε_{max}, of the maxima in the attachment cross section $\sigma_a(\varepsilon)$ and values of $\sigma_a(\varepsilon)$ at ε_{max} for $1\text{-}C_7F_{14}$ and $c\text{-}C_7F_{14}$

Molecule	Structural Formula	Thermal Attachment Rate [a] (10^8 sec^{-1} torr^{-1})	ε_{max} (eV)	$\sigma_a(\varepsilon_{max})$ (10^{-15} cm^2)
Perfluoro-1-heptene ($1\text{-}C_7F_{14}$)	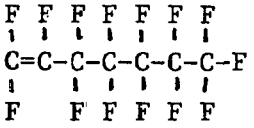	1.33	0.07; 0.25	0.75; 1.4
Perfluoromethyl-cyclohexane ($c\text{-}C_7F_{14}$)	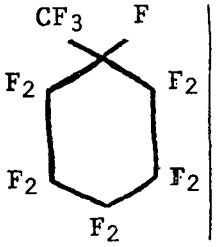	18.3 13 [14] 16.9 [12] 26 [9] 31.9 [8]	0.07; 0.25 0.15 [7]	11.5 6.5 7.5 [7]

[a] Determined by integrating the $\sigma_a(\varepsilon)$ obtained in this work (table 3) over a maxwellian function (T = 298°K) (ref. 19).

REFERENCES

[1] L.G. Christophorou, Atomic and molecular radiation physics (Wiley-Interscience, New York, 1971).

[2] J.P. Johnson, L.G. Christophorou and J.G. Carter, J. Chem. Phys. 67 (1977) 2196.

[3] L.G. Christophorou, Proceedings of the XIIIth International Conference on Ionization Phenomena in Gases, Invited lectures, Berlin (G.D.R.) (1977) p. 51.

[4] L.G. Christophorou, D.R. James, R.Y. Pai, R.A. Mathis, M.O. Pace, D.W. Bouldin, A.A. Christodoulides and C.C. Chan, High Voltage Research (Breakdown Strengths of Gaseous and Liquid Insulators) ORNL/TM-6113 (1977).

[5] L.G. Christophorou, D.R. James, R.Y. Pai, R.A. Mathis, I. Sauers, M.O. Pace D.W. Bouldin, A.A. Christodoulides and C.C. Chan, High Voltage Research (Breakdown Strengths of Gaseous and Liquid Insulators) ORNL/TM-6384 (1978).

[6] L.H. James and G. Carter, J. Electronics and Control 13 (1962) 213.

[7] R.K. Asundi and J.D. Craggs, Proc. Phys. Soc. (London) 83 (1964) 611.

[8] B.H. Mahan and C.E. Young, J. Chem. Phys. 44 (1966) 2192.

[9] C. Chen, R.D. George and W.E. Wentworth, J.Chem. Phys. 49 (1968) 1973.

[10] W.T. Naff, C.D. Cooper and R.N. Compton, J. Chem. Phys.49 (1968) 2784.

[11] C. Lifshitz, A.M. Peers, R. Grajower and M. Weiss, J. Chem. Phys. 53 (1970) 4605.

[12] K.G. Mothes, E. Schultes and R.N. Schindler, J. Phys. Chem. 76 (1972) 3758.

[13] J.C.J. Thynne, Dynamic mass spectroscopy, Vol. 3, Chap. 2 (Heyden & Son Ltd., London, 1972) pp. 67-97.

[14] F.J. Davis, R.N. Compton and D.R. Nelson, J. Chem. Phys. 59 (1973) 2324.

[15] A.A. Christodoulides, L.G. Christophorou, R.Y. Pai and C.M. Tung, Electron attachment to perfluorocarbon compounds: Part I: c-C_4F_6, 2-C_4F_6, 1,3-C_4F_6, c-C_4F_8, 2-C_4F_8, J. Chem. Phys. (submitted for publication).

[16] R.Y. Pai, L.G. Christophorou and A.A. Christodoulides, Electron attachment to perfluorocarbon compounds: Part II: c-C_5F_8, c-C_6F_{10}, c-C_6F_{12}, C_7F_8 and C_8F_{16} - relevance to gaseous dielectrics, J. Chem. Phys. (submitted for publication).

[17] L.G. Christophorou, Chem. Rev. 76 (1976) 409.

[18] L.G. Christophorou, D.L. McCorkle and V.E. Anderson, J. Phys. B 4 (1971) 1163.

[19] L.G. Christophorou, The lifetimes of metastable negative ions, in: Advances in electronics and electron physics, Vol. 46, ed. E. Marton (Academic Press, Inc., New York, 1978) pp. 55-129.

APPENDIX B

Paper Submitted to the Journal of Physics D: Applied Physics

On the Role of the Electron Impact Ionization Cross Section in the Breakdown Strength of Dielectric Gases*

L. G. CHRISTOPHOROU†, D. R. JAMES and R. A. MATHIS

Atomic, Molecular and High Voltage Physics Group,
Health and Safety Research Division,
Oak Ridge National Laboratory, Oak Ridge, Tennessee, 37830, U.S.A

Abstract. In this paper we discuss the role of the electron impact ionization cross section, $\sigma_i(\varepsilon)$, as a function of electron energy, ε, in the breakdown strength, V_s, of gases/mixtures. Four gases (Ne, Ar, N_2 and SF_6) were chosen for which the $\sigma_i(\varepsilon)$ and the total electron scattering cross section, $\sigma_{sc}(\varepsilon)$, at low energies are known. Direct current breakdown strengths on Ne, Ar, Ne + SF_6, Ar + SF_6, N_2 + Ne + SF_6, and N_2 + Ar + SF_6 were made and are reported, using sphere on sphere-sphere and square rod-plane electrode geometries. On the basis of these measurements and the data on $\sigma_{sc}(\varepsilon)$ and $\sigma_i(\varepsilon)$ it was concluded that the magnitude of $\sigma_{sc}(\varepsilon)$ at subionization ($\varepsilon < I$) and especially at subexcitation ($\varepsilon <$ energy of lowest excited electronic state) energies is much more significant in effecting high values of V_s than $\sigma_i(\varepsilon)$. The effect of perfluorination and static polarizability on $\sigma_i(\varepsilon)$ is also discussed.

---

*Research sponsored by the Division of Electric Energy Systems, U.S. Department of Energy under contract W-7405-eng-26 with Union Carbide Corporation.

†Also Department of Physics, University of Tennessee, Knoxville, Tennessee 37916.

1. Introduction

We have indicated earlier (Christophorou 1977, Christophorou *et al* 1977a, 1978, James *et al* 1978) that in designing a gas dielectric the quantity[1]

$$\int_0^\infty \sigma_a(\varepsilon) f(\varepsilon, E/P) d\varepsilon \qquad (1)$$

should be maximized, and the quantity[1]

$$\int_I^\infty \sigma_i(\varepsilon) f(\varepsilon, E/P) d\varepsilon \qquad (2)$$

should be minimized. In (1) and (2) $\sigma_a(\varepsilon)$ and $\sigma_i(\varepsilon)$ are, respectively, the electron attachment and the electron impact ionization cross sections as functions of the electron energy ε, $f(\varepsilon, E/P)$ is the electron energy distribution as a function of ε and the pressure-reduced electric field E/P, and I is the ionization threshold energy. We have also emphasized in our earlier reports (e.g., Christophorou *et al* 1976, 1977a,b, 1978, James *et al* 1978, Pace *et al* 1978) the dominant role of $\sigma_a(\varepsilon)$ and the importance of the electron scattering processes which strongly influence $f(\varepsilon, E/P)$. In this paper we assess and discuss the role of $\sigma_i(\varepsilon)$ in the breakdown voltage, V_s, for gases/mixtures, on the basis of experimental data on $\sigma_{sc}(\varepsilon)$, $\sigma_i(\varepsilon)$ and V_s. From the dielectric point of view the portion of $\sigma_i(\varepsilon)$ close to I is the most significant.

For multicomponent mixtures the role of the Penning ionization process ($A^* + B \longrightarrow B^+ + e + A$) must be assessed also.

---

[1] Usually, the velocity weighted forms of (1) and (2) are used [i.e., $\int_0^\infty \sigma_a(\varepsilon)\varepsilon^{\frac{1}{2}} f(\varepsilon, E/P)d\varepsilon$ and $\int_I^\infty \sigma_i(\varepsilon)\varepsilon^{\frac{1}{2}} f(\varepsilon, E/P)d\varepsilon$], which are proportional, respectively, to the attachment and ionization coefficients. Expressions (1) and (2) may be referred to, respectively, as the energy distribution weighted effective attachment and ionization.

2. The electron impact ionization cross section

A. Direct and indirect ionization

In the vicinity of I (say, 0 to 10 eV above I) ionization proceeds directly,

$$e + XY \longrightarrow XY^+ + 2e \text{ (or } X + Y^+ + 2e) \qquad (3)$$

or indirectly,

$$e + XY \longrightarrow XY^{**} \text{ (superexcitation)} + e' \begin{cases} \rightarrow XY^+ + e \text{ (or } X + Y^+ + e) & (4a) \\ \rightarrow \text{"Dissociation"} + e & (4b) \\ \rightarrow \text{Electronic relaxation} & (4c) \end{cases}$$

Superexcitation (i.e., excitation of an electronic state of a neutral molecule AX above I) plays an important role for many molecules (e.g., see Christophorou 1971, Donohue *et al* 1977). The competition between (3) and (4) is a function of (ε - I); as (ε - I) increases, (3) dominates over (4). The competition between indirect ionization (4a) and "dissociation" (4b) giving neutral fragments should depend on (ε - I), the state of excitation, and the vibrational distribution of internal energy and it could be beneficial in that it could reduce σ_i. Close to I the parent positive ions are the most abundant but as (ε - I) increases, so does the yield of fragment positive ions.

B. Electron impact ionization cross section close to threshold and its dependence on the static polarizability.

The single ionization cross section by electron impact, $\sigma_i(\varepsilon)$, increases more or less linearly with energy ε - I above I, maximizes at some energy (usually around $\sim$100 eV) above I (see Christophorou 1971) and decreases with ε, at large ε, as predicted by the Born approximation viz. as $\ell n\varepsilon/\varepsilon$. Figure 1 shows examples of the variation of the total ionization cross section, σ_T, with electron energy. Close to I double and multiple ionization is negligible (or not energetically possible) and for this reason we shall refer to $\sigma_T(\varepsilon)$ as $\sigma_i(\varepsilon)$.

In figure 2 $\sigma_i(\varepsilon)$ are plotted for a number of gases and are seen to vary greatly in the indicated energy range. A plot of σ_i vs $(\varepsilon - I)$ (figure 3) shows a similar variation. If the values of σ_i for various species at a particular value of $(\varepsilon - I)$ (say, 5 or 10 eV; figure 3) are plotted as a function of the species' static polarizability, α, σ_i increases with α, although the data show a considerable spread. In the inset of figure 4 the slopes, $\Delta\sigma_i/\Delta(\varepsilon - I)$, of the σ_i vs $(\varepsilon - I)$ plots for $(\varepsilon - I) \lesssim 2$ eV are plotted as a function of α. A general increase of $\Delta\sigma_i/\Delta(\varepsilon - I)$ with α is evident. This is consistent with earlier data by Beran and Kevan (1969a) some of which are shown in figure 4. For large values of ε the Born approximation is valid and one would expect σ_i to be proportional to α since both σ_i and α are roughly proportional to the square of the transition moment matrix element. Indeed a linear relationship between σ_i and α, as seen in figure 4, has been noted between $\sigma_i(\varepsilon = 75$ eV) and α earlier (Beran and Kevan 1969a, Lampe *et al* 1957). At 75 eV the Born approximation is probably valid and direct ionization dominates over indirect for molecules. Beran and Kevan (1969a) noted that the correlation between σ_i and α holds better within given classes of molecules.

It is seen from figure 4 that for a given value of α, perfluorination of a hydrocarbon molecule reduces $\sigma_i(\varepsilon)$ and that this reduction is larger the lower the ε. This observation seems to be of quite general validity, as can be seen from the data in table 1.

C. Effect of perfluorination on the magnitude of $\sigma_i(\varepsilon)$ and I

It can be seen from table 2 that the I of perfluorinated hydrocarbons is, as a rule, higher than for their nonfluorinated analogues. Quite generally, when an F atom is substituted for an H atom, $\sigma_i(\varepsilon)$ decreases. The other halogen atoms (Cl, Br, I) do not behave in this manner; for these, $\sigma_i(\varepsilon)$ increases with increasing number of halogens and atomic number (i.e., in the order Cl < Br < I; see table 1 and Beran and Kevan 1969a). This behavior indeed reflects the unique properties of the ground state F atom [the electronegativity (4.0) and I (17.42 eV) of fluorine are very high] allowing for strong C-F bonds and

Table 1. Ionization cross sections, σ_i, at three (20, 35 and 70 eV) electron energies for hydrocarbons showing the effect of fluorine and other halogen atoms on σ_i [a]

Molecule	σ_i (10^{-16} cm^2)		
	ε = 20 eV	ε = 35 eV	ε = 70 eV
CH_4	1.62	3.65	4.67
CH_3F	1.27	3.03	4.46
CH_2F_2	0.94	2.75	4.56
CHF_3	0.55	2.41	4.47
CF_4	0.26	2.22	4.68
C_2H_6	3.32	6.45	8.51
C_2F_6	0.61	3.89	7.79
C_3H_8	4.79	8.91	11.5
C_3F_8	1.07	5.52	10.5
C_4H_{10}	6.45	11.4	15.3
C_4F_{10}	1.62	7.25	13.5
C_3H_6			10.2
C_3F_6			9.16
2-C_4H_8			13.9
2-C_4F_8			12.2
C_2H_4			6.93
C_2F_4			6.16
CH_3F			4.46
CH_3Cl			8.68
CH_3Br			10.1
CF_4	0.26	2.22	4.68
CF_3Cl	2.02	5.15	7.79
CF_3Br			9.07
CF_3I			10.9
CF_4	0.26	2.22	4.68
CF_2Cl_2	4.2	8.52	11.2
CF_2Br_2			14.2
$CFCl_3$	6.26	11.7	14.6

[a] From Beran and Kevan (1969 a)

Table 2. First ionization potential, I of hydrocarbons showing the effect of F substitution on the value of I [a]

Compound	I(eV)
CH_4	12.7
CH_3F	12.54
CH_2F_2	12.71
CHF_3	13.83
CF_4	≤15.0
C_3H_8	11.07
C_3F_8	13.38
2-C_4H_8	9.13
2-C_4F_8	11.25
c-C_3H_6	9.97
c-C_3F_6	11.3
C_5H_{10} (cyclopentane)	10.5
C_5F_{10}	11.7
C_6H_{12} (cyclohexane)	9.83
C_6F_{12}	13.2
C_6H_6 (benzene)	9.24
C_6F_6	9.93
$C_{12}H_{10}$ (biphenyl)	8.23
$C_{12}H_{10}$	10.00
C_2H_4	10.51
$C_2H_2F_2$	10.31
C_2HF_3	10.14
C_2F_4	10.12
C_2H_2	11.4
C_2F_2	11.4

[a] Data on I are from Christophorou (1971) and Rosenstock *et al* (1977).

tightly bound electrons.

It is thus seen that perfluorocarbon molecules can possess basic properties which are highly desirable for a gas dielectric. Besides strong C-F bonds, high I and low $\sigma_i(\varepsilon)$, they can have large $\sigma_a(\varepsilon)$ (e.g., Christodoulides *et al* 1978, Pai *et al* 1978), lead predominantly to parent negative ions in impacts with low-energy electrons (Christophorou 1978), have large electron affinities (Christophorou 1978), and possess many negative ion states at $\varepsilon < I$ (Christophorou 1977, 1978; Christodoulides *et al* 1978, Pai *et al* 1978).

3. Electron impact ionization and electron scattering cross sections for Ne, Ar, N_2 and SF_6

To assess the role of $\sigma_i(\varepsilon)$ relative to the electron scattering cross section $\sigma_{sc}(\varepsilon)$--and thus the relative significance of (1) and (2)--we have chosen four gases for which $\sigma_i(\varepsilon)$ and $\sigma_{sc}(\varepsilon)$ are known. These are shown in figure 5A, B and are explained in the figure caption where the sources of the original data are given.

4. DC breakdown strength measurements

Measurements have been made of the DC breakdown strengths of Ar, Ne, Ar + SF_6, Ne + SF_6, N_2 + Ar + SF_6 and N_2 + Ne + SF_6. These data are presented in table 3 and figures 6 to 11. We employed sphere on sphere to sphere electrodes (a 1/8 in. diameter stainless steel sphere attached to the top of a 1 1/2 in. diameter sphere as the negative voltage electrode and a second 1 1/2 in. diameter sphere as the ground electrode) in this work to achieve a nonuniform electric field. Figure 6 shows the breakdown voltages, V_s, as a function of Pd (the product

Table 3. V_s for SF_6, Ar, Ne, N_2 + Ar, N_2 + Ne, SF_6 + Ar, SF_6 + Ne, SF_6 + Ar + N_2, and SF_6 + Ne + N_2 (P_{total} = 2000 torr; sphere on sphere-sphere electrode geometry)

Gas/Mixture	Electrode Separation (inches)				
	0.125	0.225	0.325	0.425	0.525
	V_s (kV)				
SF_6(100%)	41.40	60.31	77.21	92.61	
Ar(100%)	5.38	7.73	9.70	11.41	14.09
Ne(100%)	0.93	1.32	1.55	1.95	2.46
N_2(20%) + Ar(80%)	10.79	15.76	20.14	23.42	26.06
N_2(20%) + Ne(80%)	7.42	10.68	13.50	15.86	17.77
SF_6(20%) + Ar(80%)	20.38	29.00	35.91	43.48	54.29
SF_6(20%) + Ne(80%)	13.56	21.04	28.37	35.49	48.40
SF_6(20%) + Ar(40%) + N_2(40%)	27.76	40.29	50.40	59.11	79.19
SF_6(20%) + Ne(40%) + N_2(40%)	24.43	35.70	44.97	52.77	74.17

of the gas pressure P) and the electrode separation distance, d, at a constant pressure of 2000 torr for pure Ne and Ar as well as for 80% Ne + 20% SF_6 and 80% Ar + 20% SF_6 mixtures. The superiority of Ar over Ne as a single gas and as a buffer gas is clearly seen.

Figures 7 and 8 show, respectively, V_s vs Pd for 40% Ar + 40% N_2 + 20% SF_6 and 100% SF_6, and 40% Ne + 40% N_2 + 20% SF_6 and 100% SF_6. The range of pressures used (see figures) was from 500 to 3500 torr. At a given Pd, the breakdown voltage varies according to pressure. In general, the lower pressure will have the lower V_s at a constant Pd. This effect occurs because the low P will have a correspondingly larger d which makes the electric field for this electrode configuration more nonuniform, and hence the breakdown voltage will be lower. The slight curvature of V_s versus Pd for a constant pressure is also due to the changing electric field as the electrode separation varies. Comparing the two mixtures (figures 7 and 8, respectively) we see that both are substantially lower in breakdown voltage than pure SF_6 and that the Ar mixture is approximately 7 to 14% higher in breakdown voltage than the Ne mixture.

Figures 9 to 11 give the breakdown voltage for the 40% Ar + 40% N_2 + 20% SF_6, 40% Ne + 40% N_2 + 20% SF_6 mixtures and for pure SF_6 as a function of the total pressure for fixed electrode gap separations of 0.125, 0.225, 0.325 in., respectively. For a fixed d, the nonuniformity in the electric field remains the same as the total pressure is increased. Generally, the data vary linearly with pressure up to 3000 torr. For the Ar mixture, beyond this pressure, the V_s falls off approximately 5 to 10% below the value one obtains from an extrapolated line through the rest of the data points. Considerably more scatter in the data occurs at the higher pressures (up to 1.5%) than at the lower pressures (scatter $\lesssim$0.5%) which is an indication of a higher overall

uncertainty in the data at 3500 torr. Hence the fall off at 3500 torr is probably contained within the experimental error at that pressure.

5. DC Breakdown Strength Measurements in Highly Nonuniform Fields

To explore further the possible effects of field inhomogeneity on the relative breakdown strengths of the gases/mixtures under study, we measured V_S using square rod-plane stainless steel electrodes. The square rod was the negative high voltage electrode and had the dimensions 5 x 5 x 62.6 mm; the plane electrode was a 14-cm diameter stainless steel disc with rounded edges. With this electrode geometry we measured both V_S and corona onset voltages.[1] Both of these sets of data are presented in figure 12 for P = 500 torr. It is seen that with the square rod-plane geometry or with the sphere on sphere-sphere geometry, the Ar mixtures are superior to the Ne mixtures. The V_S values for the mixture 40% Ar + 40% N_2 + 20% SF_6 are 14% higher than for the 40% Ne + 40% N_2 + 20% SF_6 mixture, as has been the case with the sphere on sphere-sphere geometry results.

Measurements of breakdown and corona onset voltages on the same tertiary mixtures as in figure 12, but at P_{total} = 3500 torr, have been made and the results are shown in figure 13. It is seen that the breakdown voltage for the Ne tertiary mixtures is now somewhat higher than for the corresponding Ar mixtures; this also seems to be the case for the corona onset voltage for the 40% Ne + 40% N_2 + 20% SF_6 mixture. This is a most interesting observation and can be attributed (see Section 6) to the increased field nonuniformity as d decreases when P is increased.

---

[1]Corona onset voltage is taken to be the voltage at that point where there is a sharp increase in average corona current. The corona current spikes measured in the ground electrode circuit were averaged with an r-c filter.

6. Discussion and Conclusions

The breakdown data in sections 4 and 5 show that Ar as a unitary dielectric gas or as a buffer gas is in general superior to Ne in spite of the fact that $I_{Ar} < I_{Ne}$ and $(\sigma_i)_{Ar} >> (\sigma_i)_{Ne}$ (figure 5A). This is attributed to the differences in $\sigma_{sc}(\varepsilon)$ between Ar and Ne shown in figure 5B: Ar is a much more efficient electron slowing-down gas than Ne. This, in turn, means that for a given value of E/P, $f(\varepsilon, E/P)$ is shifted to higher energies for Ne than for Ar. Recent calculations of $f(\varepsilon, E/P)$ for Ne and Ar by McCorkle (D. L. McCorkle, private communication, 1978) for E/P = 0.5 and 1 V cm^{-1} $torr^{-1}$ show this nicely (see figure 14). The uniform field (plane-plane geometry) limiting breakdown value, $(E/P)_{lim}$, of E/P is ∿8.0 and ∿0.63 V cm^{-1} $torr^{-1}$ for Ar and Ne, respectively (see table 4). Thus, in spite of the fact that $I_{Ar} < I_{Ne}$ and $(\sigma_i)_{Ar} >> (\sigma_i)_{Ne}$ the magnitude of (2) is larger for Ne than for Ar because a larger fraction of electrons overlaps $\sigma_i(\varepsilon)$ for Ne than for Ar producing secondary electrons.

The results on the binary mixtures are consistent with the above rationale: when N_2 for which $\sigma_{sc}(\varepsilon)$ is large (see figure 5B) is added to either Ar or Ne, V_s increases substantially. The ratio of V_s values for the Ne + N_2 mixture to the Ar + N_2 mixture is much larger (∿0.68) compared to the ratio (0.17) of the V_s value for pure Ne to pure Ar. This is attributed to the fact that the $\sigma_{sc}(\varepsilon)$ for N_2, although larger than that of Ar below ∿6 eV, is very much larger than that of Ne over the entire range 0 to ∿20 eV (see figure 5B). Similarly the V_s increases dramatically when SF_6 for which $\sigma_{sc}(\varepsilon)$ is also large [the $\sigma_{sc}(\varepsilon)$ for SF_6, although larger than that of Ar below ∿7 eV, is very much larger than that of Ne over the entire subionization energy range; see figure 5B] is added to either Ne or Ar. In this case the increase in V_s is both due to the increase in $\sigma_{sc}(\varepsilon)$ and due to the large $\sigma_a(\varepsilon)$ of SF_6. The ratio of the V_s values for the Ne + SF_6 mixture to the Ar + SF_6 mixture is again large (∿0.78) compared to the ratio (∿0.17) of the V_s value for pure Ne to pure Ar.

Table 4. DC Uniform-field breakdown strength data for pure Ar ard pure Ne (P = 500 torr; T ≈ 20°C; plane-plane electrode geometry).

Gas	Electrode Separation (inches)									$(E/P)_{lim}$
	0.075	0.125	0.175	0.225	0.275	0.325	0.425	0.525	0.625	
	V_s (kV) [a]									(V cm^{-1} torr^{-1})
Ar	1.286	1.811	2.324	2.811	3.271	3.720	4.536	5.292	6.035	8.0 [b,c]
Ne	0.344	0.378	0.422	0.463	0.506	0.550	0.653	0.746	0.859	0.63 [b]

[a] Average of ten independent measurements at each value of the electrode separation.

[b] Determined from the slope of the data points for the first four values of the electrode separation listed in the table.

[c] The breakdown voltages for 100% Ar reflect a greater uncertainty than for any other gas we investigated. For a given electrode separation the V_s was observed to increase with time on the order of 5 to 10% over the course of ~30 minutes. Also when the V_s of a given Ar sample was measured on succeeding days a difference in V_s of as much as 20% was noted.

The results on the V_s for the tertiary mixtures are also consistent with this interpretation: when N_2 [for which $\sigma_{sc}(\varepsilon)$ is large at subexcitation energies; figure 5B] is added to the SF_6 + Ne mixture, the V_s improves much more than when it is added to the SF_6 + Ar mixture.

Since the values of I for SF_6, N_2, Ar and Ne are (Christophorou 1971, 1977) ∿15.6, ∿15.6, 15.76 and 21.56 eV, respectively, it is unlikely that for the Ar binary (Ar + SF_6) and tertiary (Ar + SF_6 + N_2) mixtures a Penning ionization process occurs.[1] Such a process, however, is possible for the Ne binary (Ne + SF_6) and tertiary (Ne + SF_6 + N_2) mixtures (see positions of onsets of the lowest Ne excitations in figure 5A). In view of this possibility the actual relative improvement in V_s when SF_6 or SF_6 + N_2 are added to Ne could be even higher. These findings are consistent also with earlier observations (Christophorou *et al* 1977a,b, 1978, Christophorou, 1977, James *et al* 1978) and demonstrate the significance of efficient electron scattering at subionization and subexcitation energies. They indicate that large electron scattering cross sections in the subionization (ε < I) and subexcitation (ε < energy of lowest excited electronic state) energy range are more important in effecting a high value of V_s than low $\sigma_i(\varepsilon)$.

Finally, the present results and their interpretation are consistent with the $\alpha/N(E/N)$ data for Ar and Ne shown in figure 15. The primary ionization coefficient α over the gas density N, α/N, is related to $\sigma_i(\varepsilon)$ by

$$\frac{\alpha}{N} = (2/m)^{\frac{1}{2}} w^{-1} \int_I^{\infty} f(\varepsilon, E/N)\varepsilon^{\frac{1}{2}} \sigma_i(\varepsilon)d\varepsilon , \qquad (5)$$

where w is the electron drift velocity and m is the electron mass. On the basis of equation (5), the $\sigma_i(\varepsilon)$ data in figures 1 and 5, and the $\alpha/N(E/N)$ data in figure 15 for Ar and Ne it is clear that for any given value of E/P_{298} to ∿52 V cm^{-1} $torr^{-1}$, the $f(\varepsilon, E/N)$ is shifted to higher energies much more for

---

[1]Adding N_2 into Ar does not increase the total ionization produced when α-particles are completely stopped in the gas system (see Christophorou, 1971, Chapter 2).

Ne than for Ar and in such a manner as to make the value of the integral in equation (5) larger[1] for Ne than for Ar in spite of the much lower $\sigma_i(\varepsilon)$ for Ne, demonstrating in this way the significance of $\sigma_{sc}(\varepsilon)$. On the basis of figure 15 and equation (5), beyond an E/P_{298} value of $\sim$52 V cm^{-1} torr^{-1}, the value of the integral in equation (5) becomes larger for Ar than for Ne. It would then seem that the data in figure 13 could be characteristic of very high values of E/P which may be possible in the highly nonuniform fields of the square rod-plane electrodes at small electrode separations.

Acknowledgement

We wish to thank Dr. D.L. McCorkle for the computation of the electron energy distribution functions in Ar and Ne and Drs. M. O. Pace and R. Y. Pai for valuable comments.

---

[1]The drift velocity of electrons in Ne to E/P = 1 V cm^{-1} torr^{-1} is larger than in Ar (Christophorou 1971, pp. 237, 239).

References

Beran J A and Kevan L 1969a *J. Phys. Chem.* 73 3866-76
_____ 1969b *J. Phys. Chem.* 73, 3860-66

Christodoulides A A, Christophorou L G, Pai R Y and Tung C M *"Electron Attachment to Perfluorocarbon Compounds: Part I: c-C_4F_6, 2-C_4F_6, 1,3-C_4F_6, c-C_4F_8 and 2-C_4F_8,"* *J. Chem. Phys.* (submitted, 1978)

Christophorou L G 1971 *Atomic and Molecular Radiation Physics* (New York: Wiley Interscience)

Christophorou L G 1977 *Proc. XIIIth International Conf. on Phenomena in Ionized Gases* (Berlin, GDR), Invited Lectures, pp 51-72

Christophorou L G 1978 *"The Lifetimes of Metastable Negative Ions," in Advances in Electronics and Electron Physics, vol. 46, ed. E. Marton,* (New York: Academic Press) pp 55-129

Christophorou L G, James D R, Pai R Y, Pace M O, Mathis R A and Bouldin D W 1976 *Oak Ridge National Laboratory Report* ORNL-TM-5604

Christophorou L G, James D R, Pai R Y, Mathis R A, Pace M O, Bouldin D W, Christodoulides A A and Chan C C 1977a *Oak Ridge National Laboratory Report* ORNL-TM-6113
——— 1977b *Oak Ridge National Laboratory Report* ORNL-TM-5917

Christophorou L G, James D R, Pai R Y, Mathis R A, Sauers I, Pace M O, Bouldin D W, Christodoulides A A and Chan C C 1978 *Oak Ridge National Laboratory Report* ORNL-TM-6384

Donohue D E, Schiavone J A and Freund R S 1977 *J. Chem. Phys.* 67 769-80

Dutton J 1975 *J. Phys. Chem. Ref. Data,* 4 (No.3) 577-856

Engelhardt A G, Phelps A V and Risk C G 1964 *Westinghouse Research Laboratory Sci. Paper,* 64-928-113-P4

Golden D E 1966 *Phys. Rev. Lett.* 17 847-848

Golden D E and Bandel H W 1966 *Phys. Rev.* 149 58-61

James D R, Christophorou L G, Pai R Y, Pace M O, Mathis R A, Sauers I and Chan C C 1978 *Proc. International Symposium on Gaseous Dielectrics* (Knoxville, Tennessee, USA) *Oak Ridge National Laboratory Report* CONF-780301 pp 224-251

Kruithof A A 1940 *Physica* 7 519-540

Lampe F W, Franklin J L and Field F H 1957 *J. Am. Chem. Soc.* 79 6129-32

Landolt H H and Börnstein R 1951 Tables of Chemical Data, *Zahlenwerte und Funktionen Vol. 1, Parv 3,* (Berlin: Springer) pp 510-513

LeFevre R J W 1965 *Advan. Phys. Org. Chem.* 3 1-90, V. Gold, ed. (New York: Academic Press)

Massey H S W and Burhop E H S 1969 *Electronic and Ionic Impact Phenomena Vol. 1, Collisions of Electrons with Atoms* (Oxford University Press) p 26

McCorkle D L 1978 *private communication (Physics Department, The University of Tennessee, Knoxville)*

Moody G J and Thomas J D R 1971 *Dipole Moments in Inorganic Chemistry,* (London: Edward Arnold Publishers, Ltd.) p 21

Pace M O, Christophorou L G, James D R, Pai R Y, Mathis R A and Bouldin D W 1978 *"Improved Unitary and Multicomponent Gaseous Insulators" IEEE Trans. Elect. Insul. Vol.* EI-13, 31-36

Pai R Y, Christophorou L G and Christodoulides A A *"Electron Attachment to Perfluorocarbon Compounds: Part II: c-C_5F_8. c-C_6F_{10}. c-C_6F_{12}, C_7F_8 and C_8F_{16} - Relevance to Gaseous Dielectrics," J. Chem. Phys.* (submitted 1978)

Rapp D and Englander-Golden P 1965 *J. Chem. Phys.* 43 1464-79

Rohr K 1977 *J. Phys.* B: *Atom. Molec. Phys.* 10 1175-79

Rosenstock H M, Draxl K, Steiner B W and Herron J T 1977 *Energetics of Gaseous Ions, J. Phys. Chem. Ref. Data* 6 (Supplement No. 1)

Srivastava S K, Trajmar S, Chutjian A and Williams W 1967 *J. Chem. Phys.* 64 2767-71

Figure Captions

Figure 1. Total ionization cross sections, $\sigma_T(\varepsilon)$, for Ne, Ar, N_2 and SF_6 [original data from Rapp and Englander-Golden (1965)].

Figure 2. Ionization cross section, σ_i, as a function of electron energy, ε, for He, Ne, Ar and a number of molecular systems [Based on the data of Rapp and Englander-Golden (1965)].

Figure 3. σ_i vs $(\varepsilon - I)$ (see text)

Figure 4. σ_i vs static polarizability, α, for the hydrocarbons CH_4, C_2H_6, C_3H_8, C_4H_{10} and C_5H_{12} and the perfluorocarbons CF_4, C_2F_6, C_3F_8 and C_4F_{10} at three (20, 35, and 70 eV) electron energies. The σ_i values are from Beran and Kevan (1969a), the α-values for the alkanes are from Landolt and Börnstein (1951) and the α-values for the perfluorocarbons are from Beran and Kevan (1969b) and were determined (Beran and Kevan 1969b) using the method of LeFevre (1965).

Inset. $\Delta\sigma_i/\Delta(\varepsilon - I)$ vs α. The $\Delta\sigma_i/\Delta(\varepsilon - I)$ were determined for $(\varepsilon - I)$ values $\lesssim 2$ eV using the $\sigma_i(\varepsilon)$ data of Rapp and Englander-Golden (1965) and I-values from Christophorou (1971). The α-values are from Landolt and Börnstein (1951) except for NO($\alpha = 19 \times 10^{-25}$ cm^3) which is from Moody and Thomas (1971).

Figure 5. A. $\sigma_i(\varepsilon)$ for Ar, SF_6, N_2 and Ne [data from Rapp and Englander-Golden (1965)].

B. Electron scattering cross section as a function of electron energy.

N_2: total electron scattering cross section, σ_t, (Golden 1966); momentum transfer cross section, σ_m (Engelhardt *et al* 1964).

SF_6: ⧫ (Srivastava *et al* 1967); ⧫ (Rohr 1977).

Ar: σ_t (Golden and Bandel 1966).

Ne: σ_t (Massey and Burhop 1969).

Figure 6: Breakdown voltages of pure Ne and pure Ar and respective mixtures with SF_6 (P = 2000 torr; sphere on sphere-sphere electrode geometry).

Figure 7. Breakdown voltages, V_s, of 100% SF_6 and the mixture 40% Ar + 40% N_2 + 20% SF_6 at the indicated pressures (sphere on sphere-sphere electrode geometry).

Figure 8. Breakdown voltages, V_s, of 100% SF_6 and the mixture 40% Ne + 40% N_2 + 20% SF_6 at the indicated pressures (sphere on sphere-sphere electrode geometry).

Figure 9. Breakdown voltages, V_s, of pure SF_6, 40% Ar + 40% N_2 + 20% SF_6 and 40% Ne + 40% N_2 + 20% SF_6 as a function of pressure at a fixed gap distance (sphere on sphere-sphere electrode geometry, d = 0.125 in.).

Figure 10. Breakdown voltages, V_s, of pure SF_6, 40% Ar + 40% N_2 + 20% SF_6 and 40% Ne + 40% N_2 + 20% SF_6 as a function of pressure at a fixed gap distance (sphere on sphere-sphere electrode geometry, d = 0.225 in.).

Figure 11. Breakdown voltages, V_s, of pure SF_6, 40% Ar + 40% N_2 + 20% SF_6 and 40% Ne + 40% N_2 + 20% SF_6 as a function of pressure at a fixed gap distance (sphere on sphere-sphere electrode geometry, d = 0.325 in.).

Figure 12. Breakdown voltage or corona onset as a function of electrode separation distance for the mixtures

① 40% Ar + 40% N_2 + 20% SF_6

② 40% Ne + 40% N_2 + 20% SF_6

③ 60% Ar + 20% N_2 + 20% SF_6

④ 60% Ne + 20% N_2 + 20% SF_6

[P = 500 torr; square rod-plane geometry]

Error bars are one standard deviation; where not specifically indicated, error (standard deviation) is approximately the size of the data point.

Figure 13. Corona onset voltage as a function of electrode separation distance using square rod-plane electrode geometry and 3500 torr pressure for

① 40% Ar + 40% N_2 + 20% SF_6

② 40% Ne + 40% N_2 + 20% SF_6

③ 60% Ar + 20% N_2 + 20% SF_6

④ 60% Ne + 20% N_2 + 20% SF_6

The error bars are one standard deviation.

Figure 14. Computed electron energy distribution functions, $f(\varepsilon, E/P)$, for pure Ar and pure Ne at E/P_{298} = 0.5 and 1.0 V cm^{-1} $torr^{-1}$. The broken and solid lines are the results of recent calculations by McCorkle (D. L. McCorkle, private communication, 1978). The data points (□ for E/P = 0.5 V cm^{-1} $torr^{-1}$ and o for E/P = 1.0 V cm^{-1} $torr^{-1}$) and the $f(\varepsilon, E/P)$ for E/P = 2 V cm^{-1} $torr^{-1}$ for Ar are the results of earlier calculations (see Christophorou 1971). To aid the discussion in the text the low-energy part of the electron impact ionization cross section, $(\sigma_i)_{Ar}$, of Ar and, $(\sigma_i)_{Ne}$, of Ne is also shown in the figure.

Figure 15. α/N (in units of cm^2) and α/P_{298} (in units of cm^{-1} $torr^{-1}$) versus E/N (in units of V cm^2) and E/P_{298} (in units of V cm^{-1} $torr^{-1}$). The α/N data are from Kruithof (1940) [see Dutton (1975)].

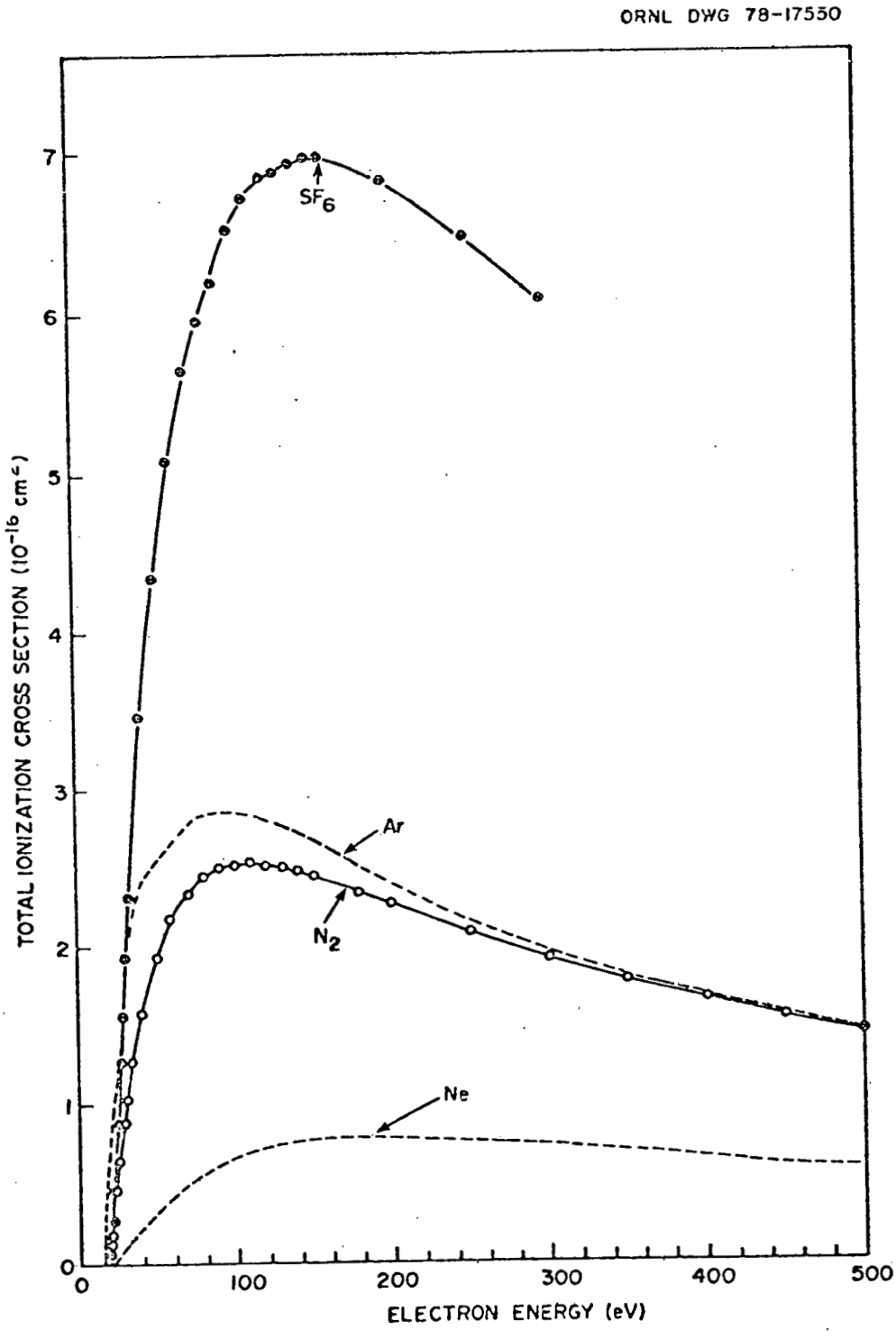
ORNL DWG 78-17550
TOTAL IONIZATION CROSS SECTION (10^{-16} cm^2)
ELECTRON ENERGY (eV)
SF6
Ar
N2
Ne
0
1
2
3
4
5
6
7
0
100
200
300
400
500

Fig. 1

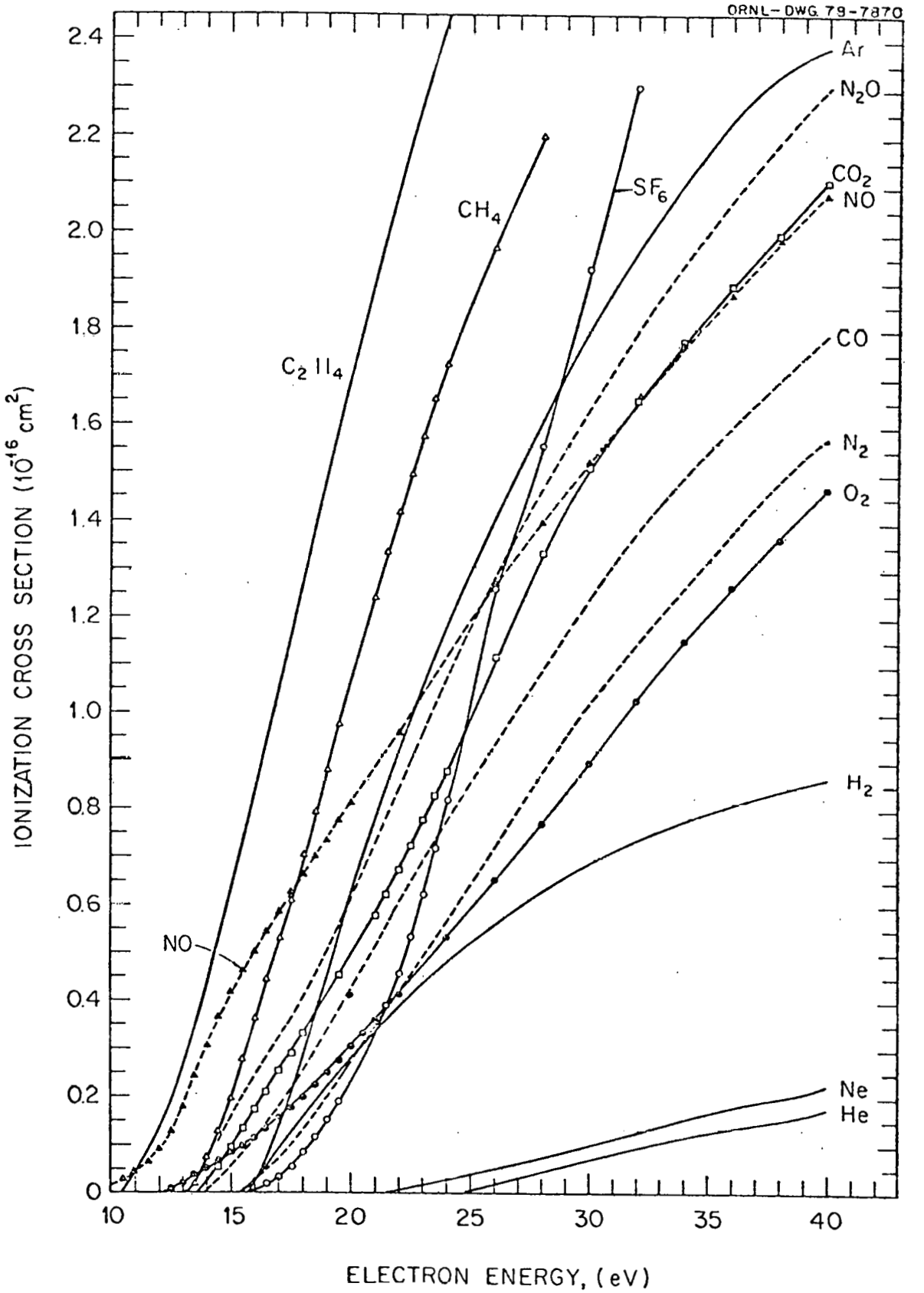
ORNL-DWG 79-7870
IONIZATION CROSS SECTION (10^{-16} cm^2)
ELECTRON ENERGY, (eV)
Ar
N_2O
CO_2
NO
CO
N_2
O_2
H_2
Ne
He
SF_6
CH_4
C_2H_4
NO
0
0.2
0.4
0.6
0.8
1.0
1.2
1.4
1.6
1.8
2.0
2.2
2.4
10
15
20
25
30
35
40

Fig. 2

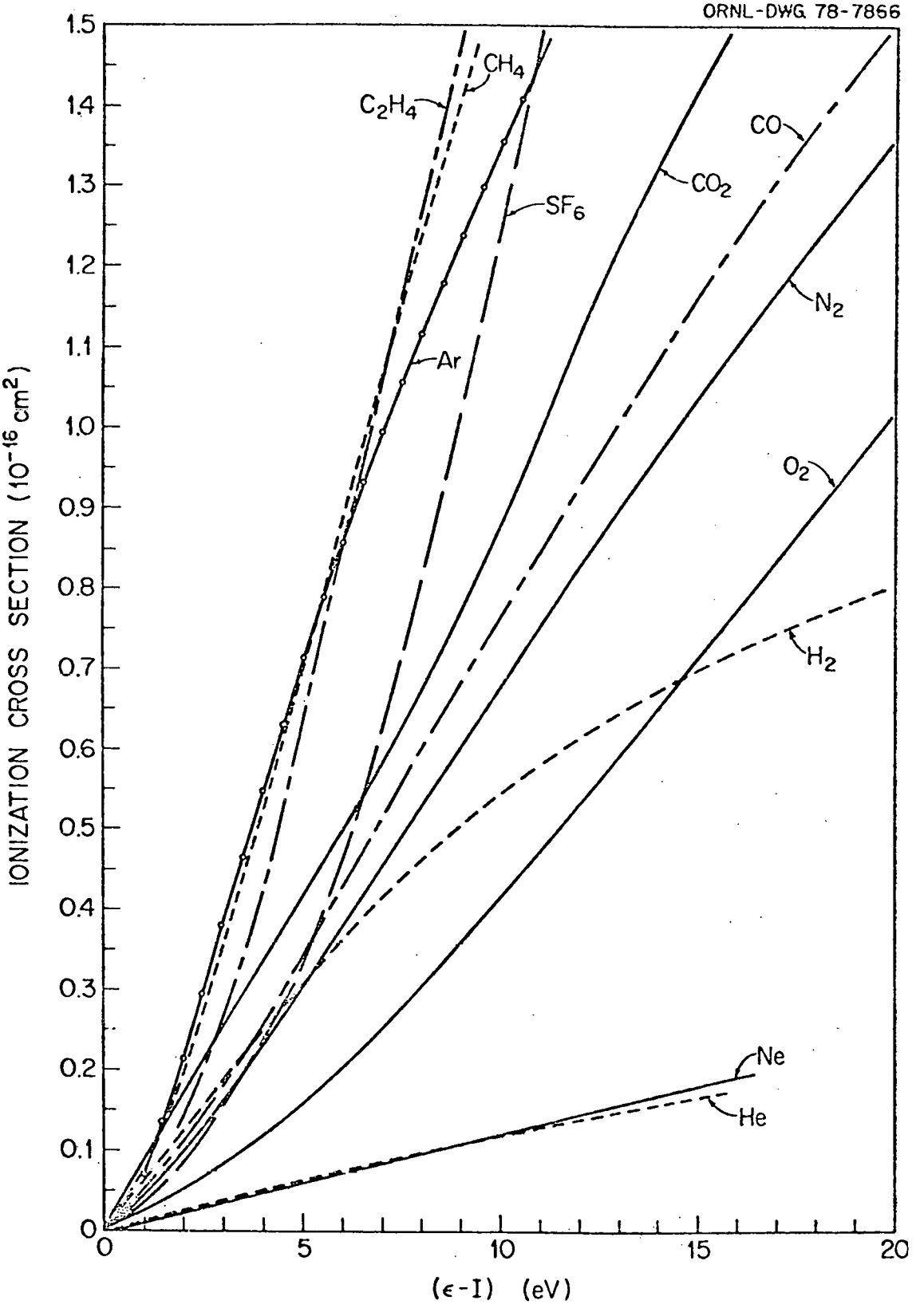
ORNL-DWG 78-7866
IONIZATION CROSS SECTION (10^{-16} cm^2)
(ϵ-I) (eV)
C_2H_4
CH_4
Ar
SF_6
CO_2
CO
N_2
O_2
H_2
Ne
He
0
0.1
0.2
0.3
0.4
0.5
0.6
0.7
0.8
0.9
1.0
1.1
1.2
1.3
1.4
1.5
0
5
10
15
20

Fig. 3

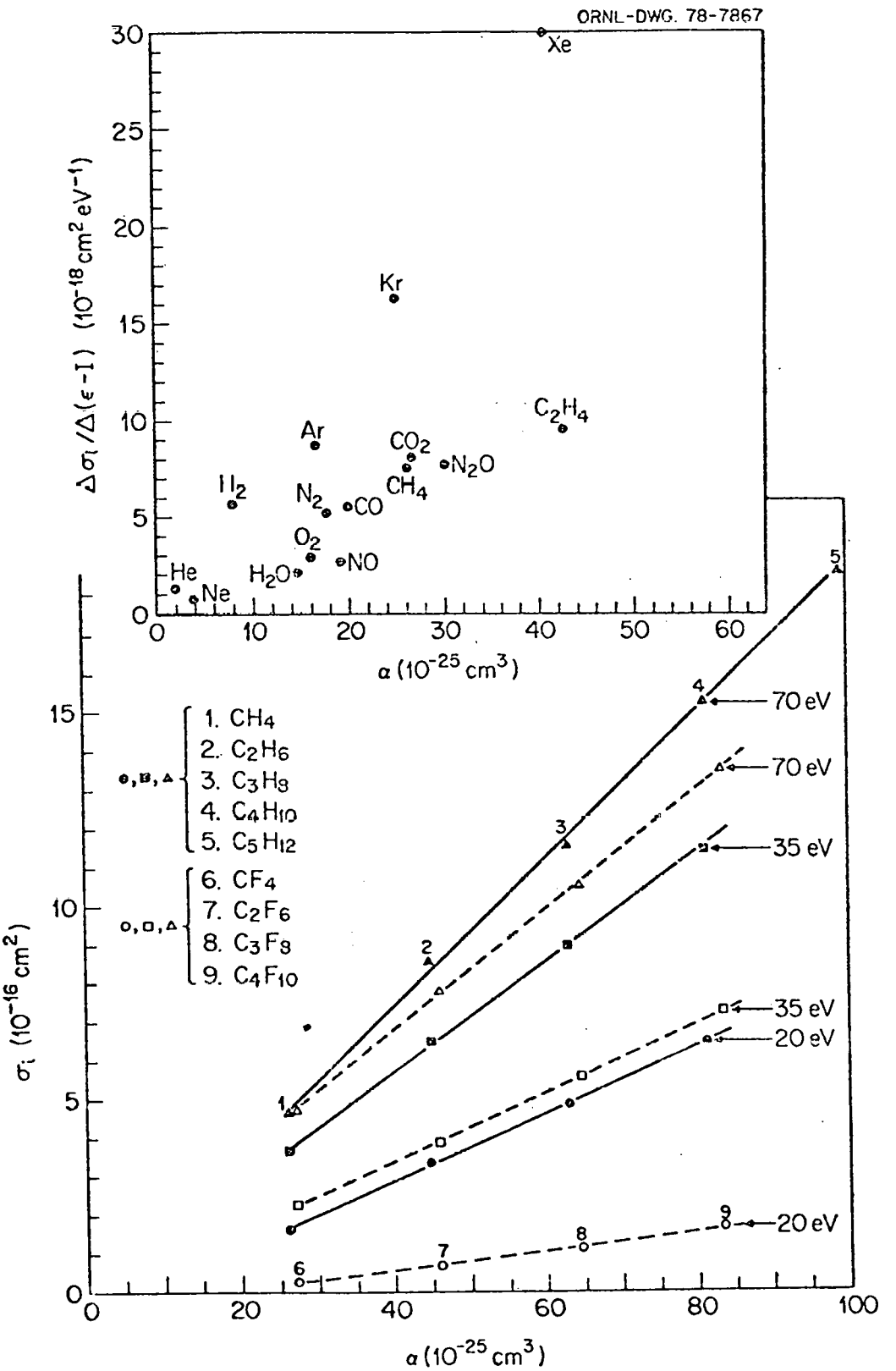
ORNL-DWG. 78-7867
Xe
Kr
C_2H_4
Ar
CO_2
N_2O
H_2
N_2
CO
CH_4
O_2
NO
He
Ne
H_2O
$\Delta\sigma_i/\Delta(\epsilon-I)$ $(10^{-18}\,cm^2\,eV^{-1})$
$\alpha\,(10^{-25}\,cm^3)$
1. CH_4
2. C_2H_6
3. C_3H_8
4. C_4H_{10}
5. C_5H_{12}
6. CF_4
7. C_2F_6
8. C_3F_8
9. C_4F_{10}
70 eV
70 eV
35 eV
35 eV
20 eV
20 eV
σ_i $(10^{-16}\,cm^2)$
$\alpha\,(10^{-25}\,cm^3)$

Fig. 4

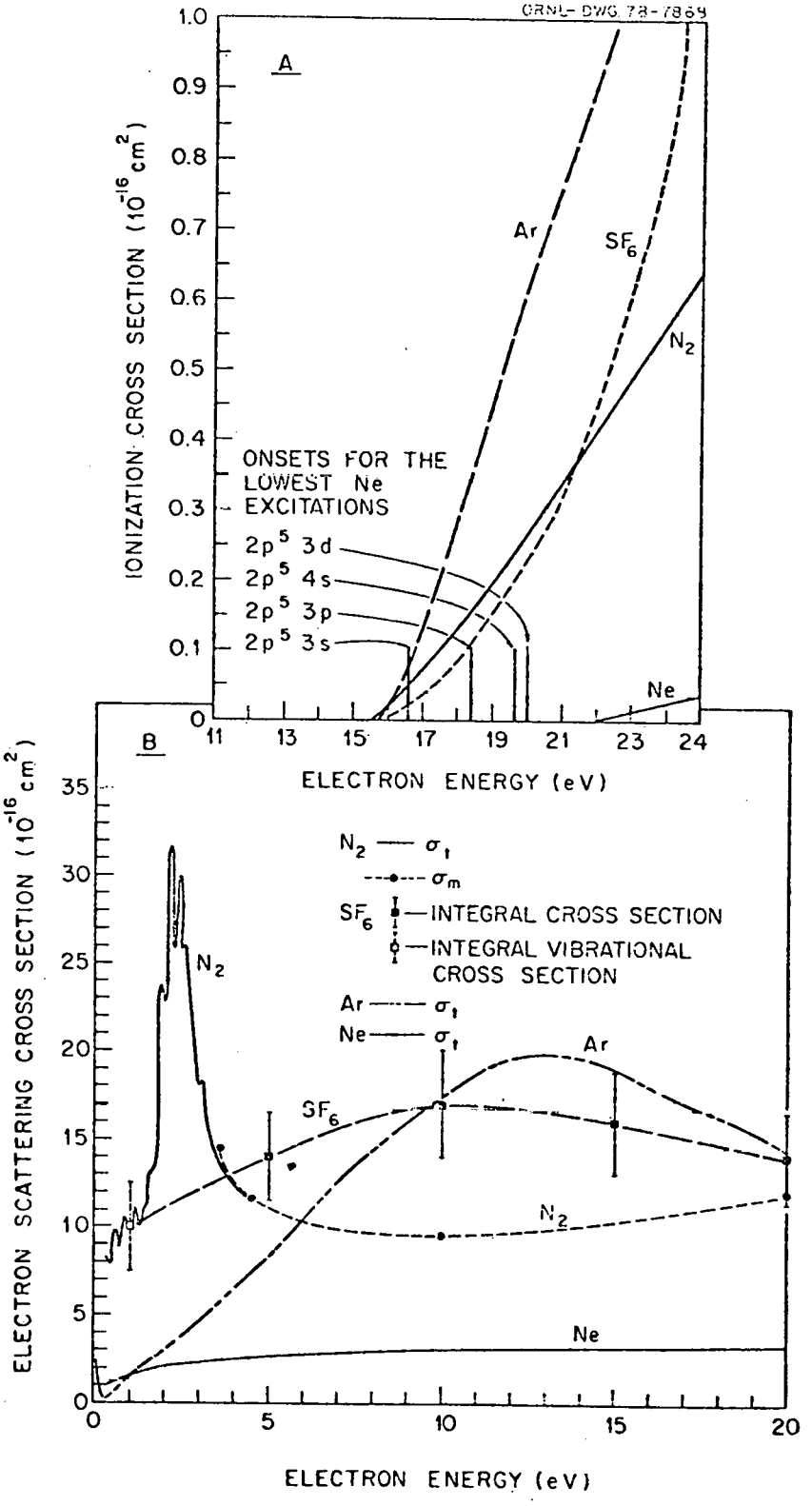
ORNL-DWG 78-7869
A
IONIZATION CROSS SECTION (10^{-16} cm^2)
Ar
SF_6
N_2
ONSETS FOR THE LOWEST Ne EXCITATIONS
$2p^5\,3d$
$2p^5\,4s$
$2p^5\,3p$
$2p^5\,3s$
Ne
ELECTRON ENERGY (eV)
B
ELECTRON SCATTERING CROSS SECTION (10^{-16} cm^2)
N_2 — σ_t
σ_m
SF_6 — INTEGRAL CROSS SECTION
INTEGRAL VIBRATIONAL CROSS SECTION
Ar — σ_t
Ne — σ_t
ELECTRON ENERGY (eV)

Fig. 5

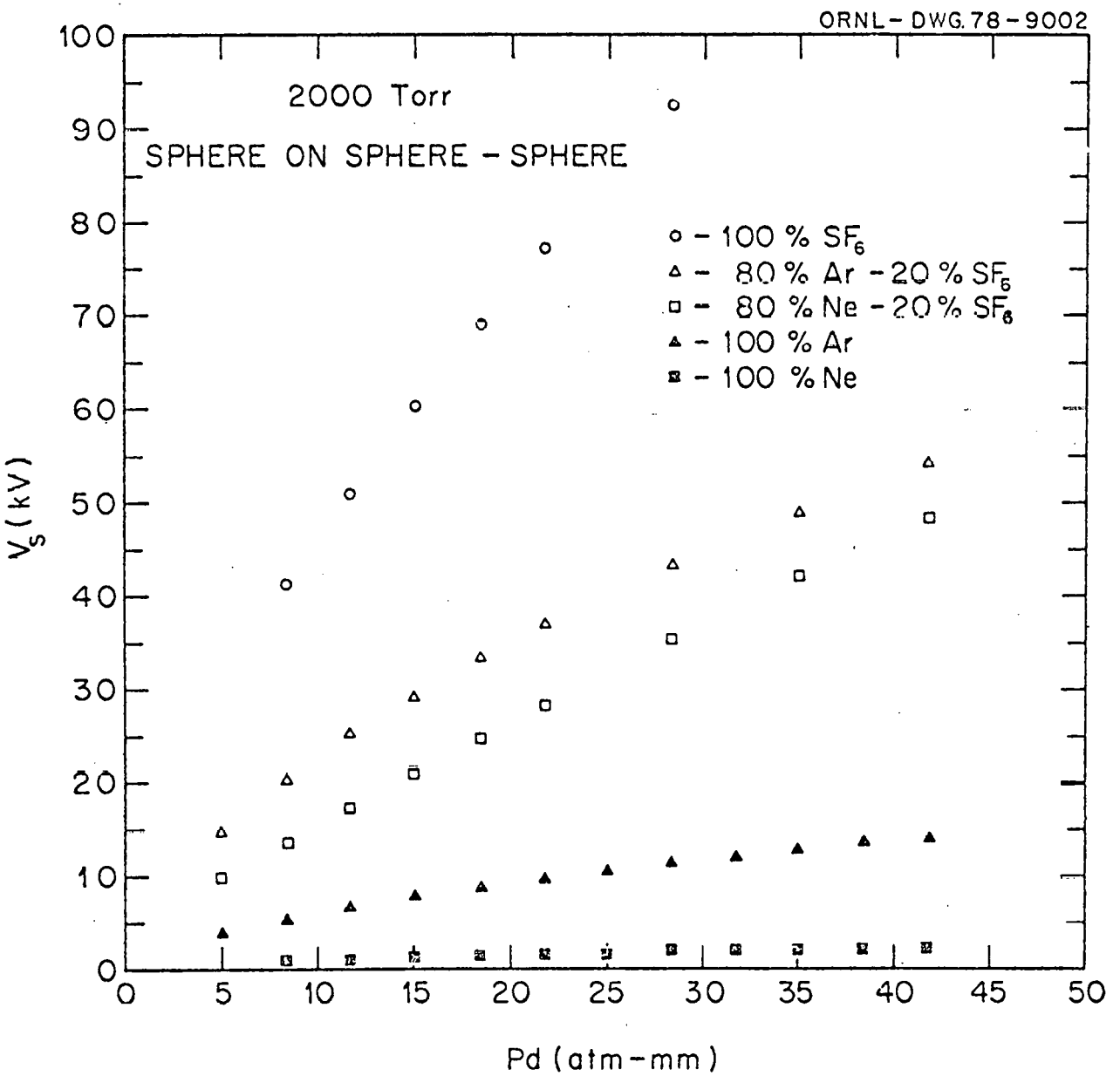
ORNL-DWG. 78-9002
2000 Torr
SPHERE ON SPHERE - SPHERE
○ - 100 % SF6
△ - 80 % Ar - 20 % SF6
□ - 80 % Ne - 20 % SF6
▲ - 100 % Ar
▣ - 100 % Ne
Vs (kV)
Pd (atm-mm)
0
10
20
30
40
50
60
70
80
90
100
0
5
10
15
20
25
30
35
40
45
50

Fig. 6

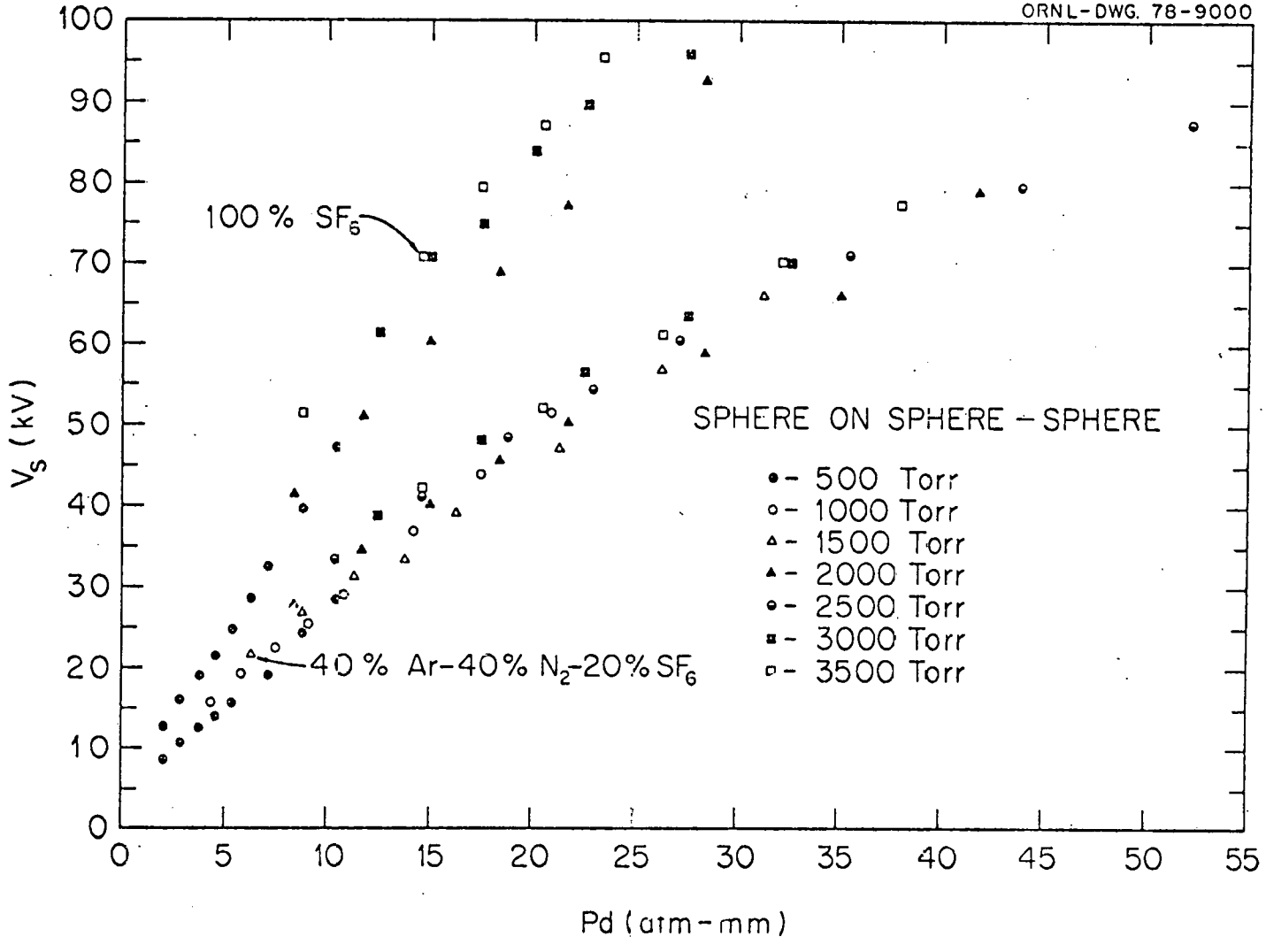
ORNL-DWG. 78-9000
100
90
80
70
60
50
40
30
20
10
0
V_S (kV)
0
5
10
15
20
25
30
35
40
45
50
55
Pd (atm-mm)
100 % SF_6
40 % Ar-40 % N_2-20 % SF_6
SPHERE ON SPHERE – SPHERE
● - 500 Torr
○ - 1000 Torr
△ - 1500 Torr
▲ - 2000 Torr
⊖ - 2500 Torr
■ - 3000 Torr
□ - 3500 Torr

Fig. 7

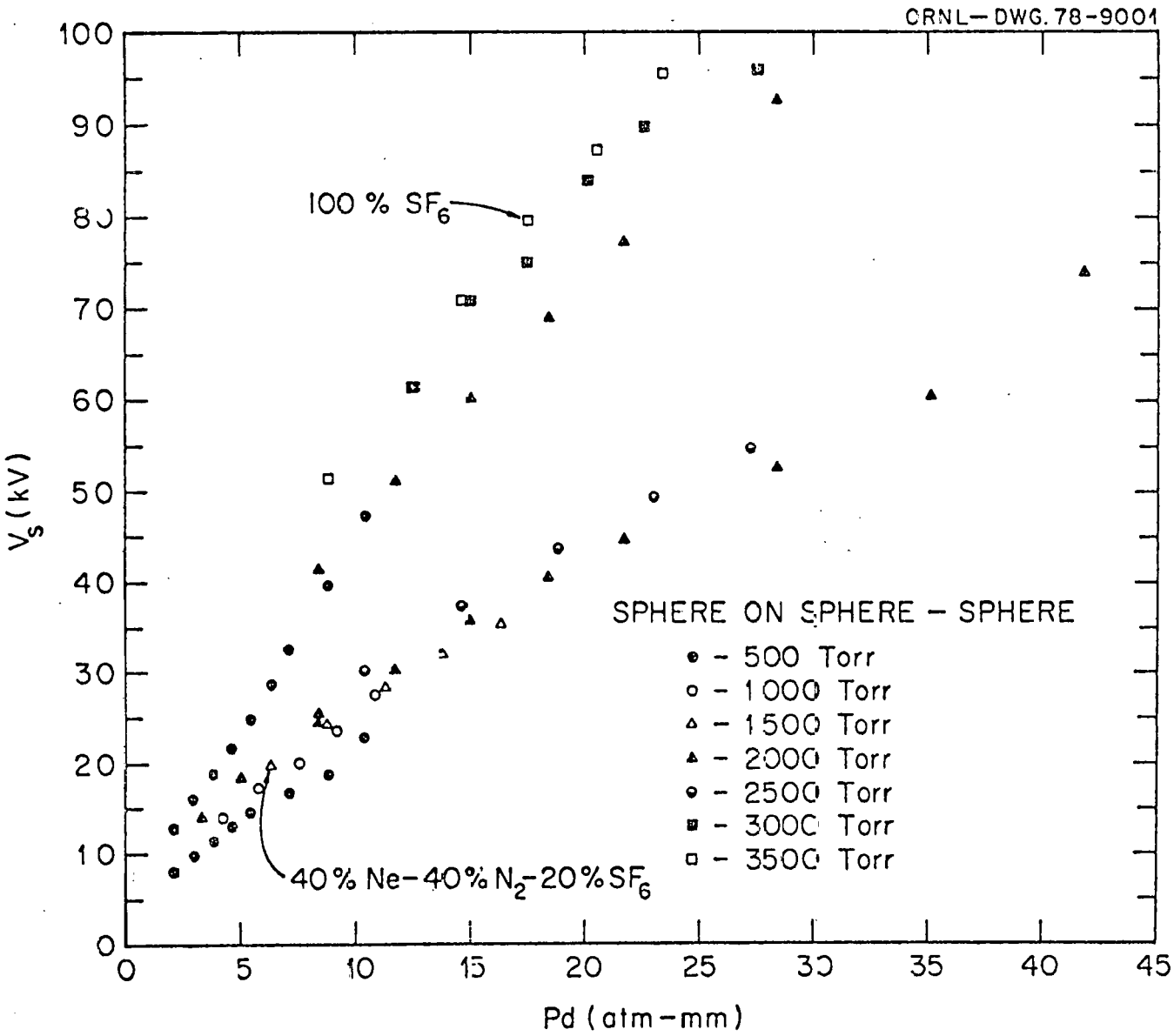
CRNL—DWG. 78-9001
100
90
80
70
60
50
40
30
20
10
0
V_s (kV)
0
5
10
15
20
25
30
35
40
45
Pd (atm-mm)
100 % SF_6
40% Ne–40% N_2–20% SF_6
SPHERE ON SPHERE – SPHERE
● – 500 Torr
○ – 1000 Torr
△ – 1500 Torr
▲ – 2000 Torr
⊙ – 2500 Torr
■ – 3000 Torr
□ – 3500 Torr

Fig. 8

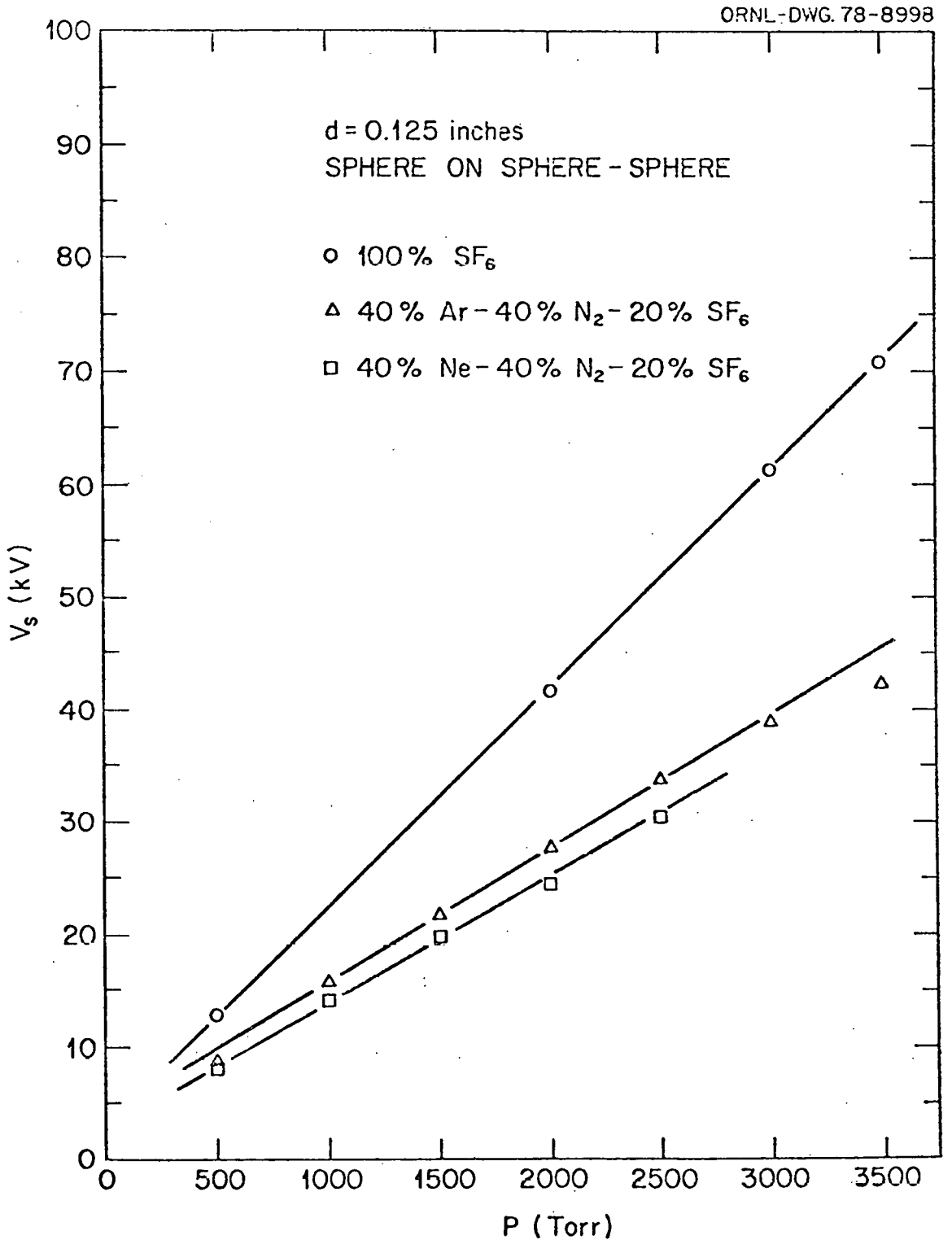
ORNL-DWG. 78-8998
d = 0.125 inches
SPHERE ON SPHERE - SPHERE
o 100% SF6
Δ 40% Ar - 40% N2 - 20% SF6
□ 40% Ne - 40% N2 - 20% SF6
Vs (kV)
P (Torr)
0
10
20
30
40
50
60
70
80
90
100
0
500
1000
1500
2000
2500
3000
3500

Fig. 9

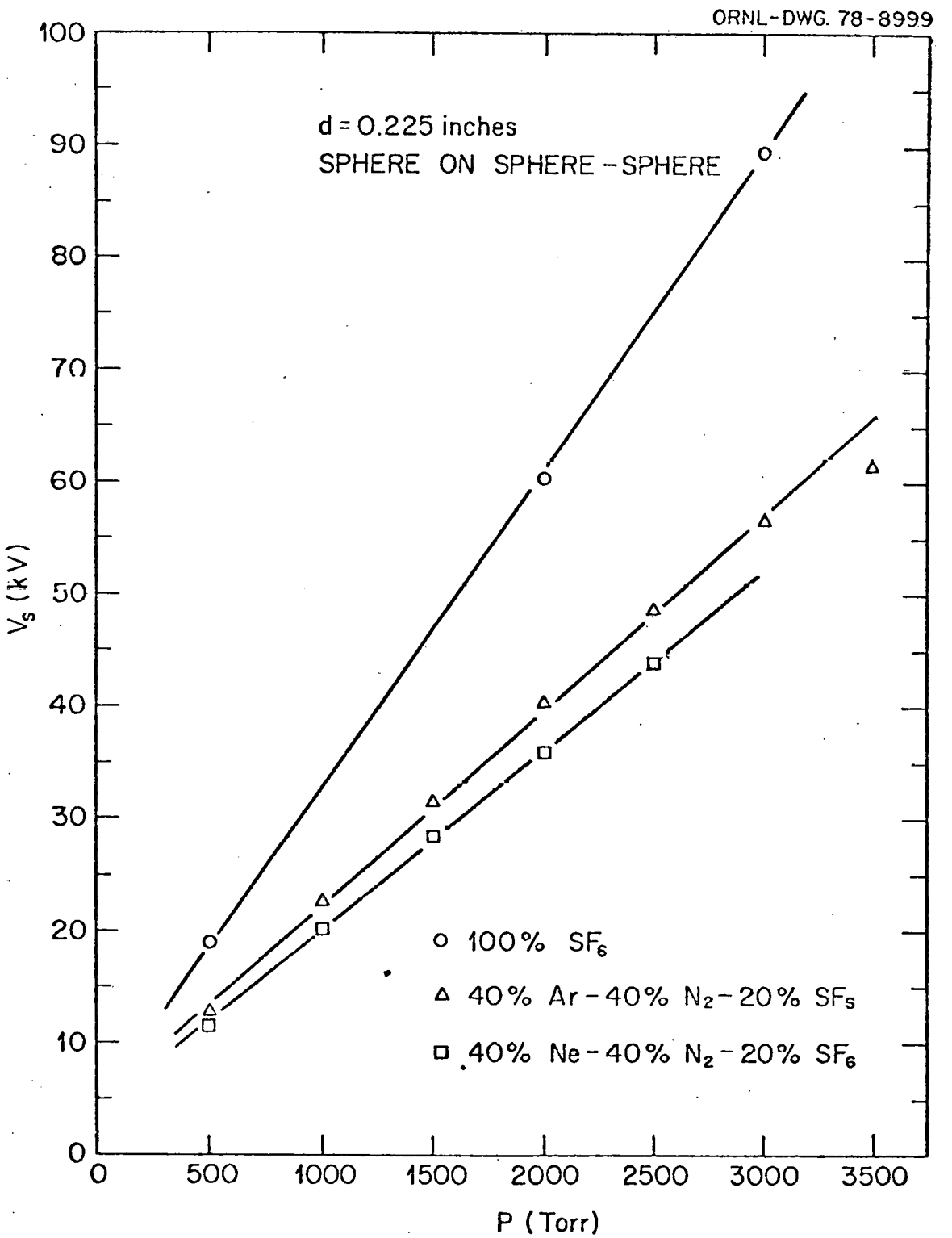
ORNL-DWG. 78-8999
d = 0.225 inches
SPHERE ON SPHERE - SPHERE
100% SF6
40% Ar - 40% N2 - 20% SF6
40% Ne - 40% N2 - 20% SF6
Vs (kV)
P (Torr)
0
10
20
30
40
50
60
70
80
90
100
0
500
1000
1500
2000
2500
3000
3500

Fig. 10

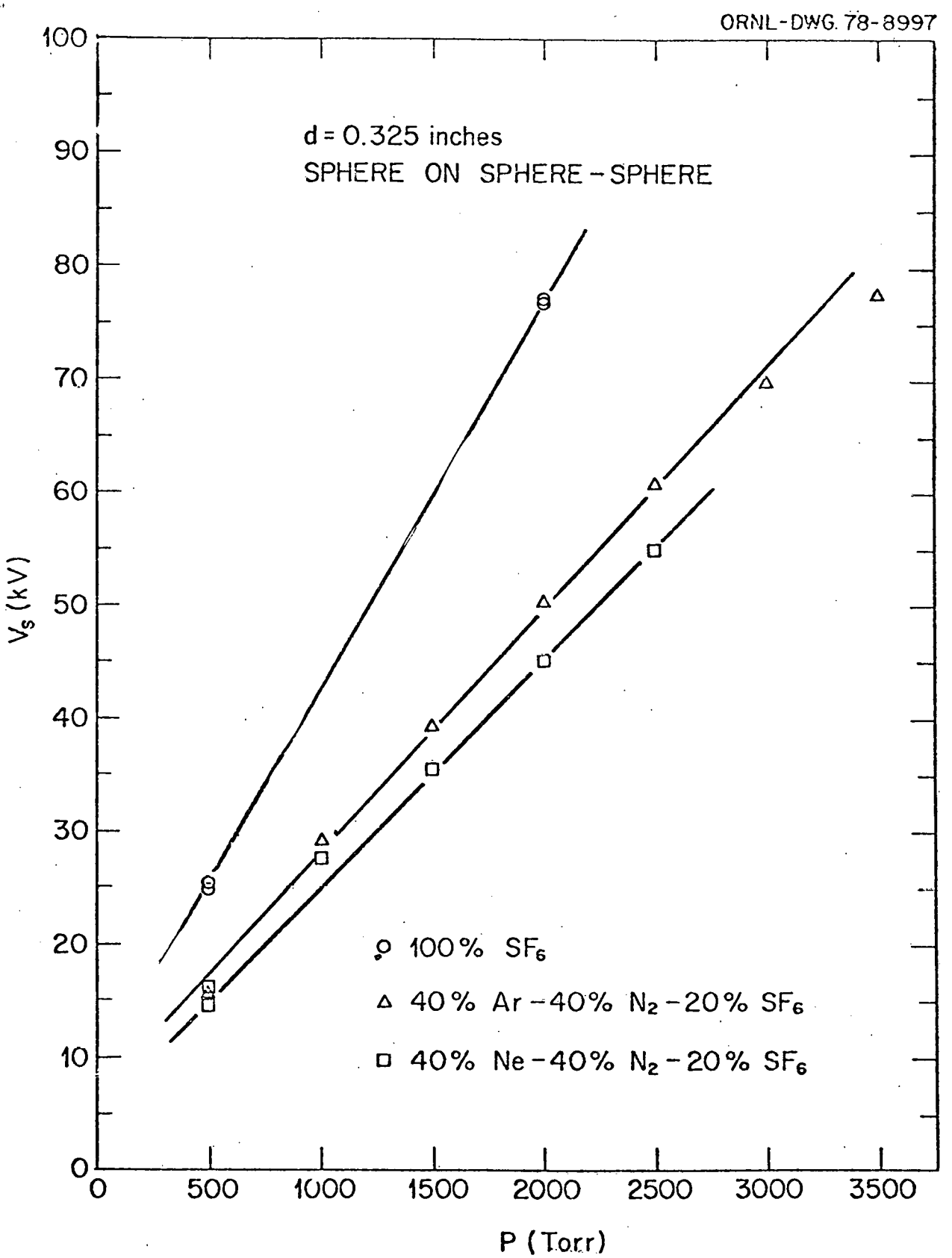
ORNL-DWG. 78-8997
d = 0.325 inches
SPHERE ON SPHERE - SPHERE
100% SF6
40% Ar - 40% N2 - 20% SF6
40% Ne - 40% N2 - 20% SF6
Vs (kV)
P (Torr)
0
10
20
30
40
50
60
70
80
90
100
0
500
1000
1500
2000
2500
3000
3500

Fig. 11

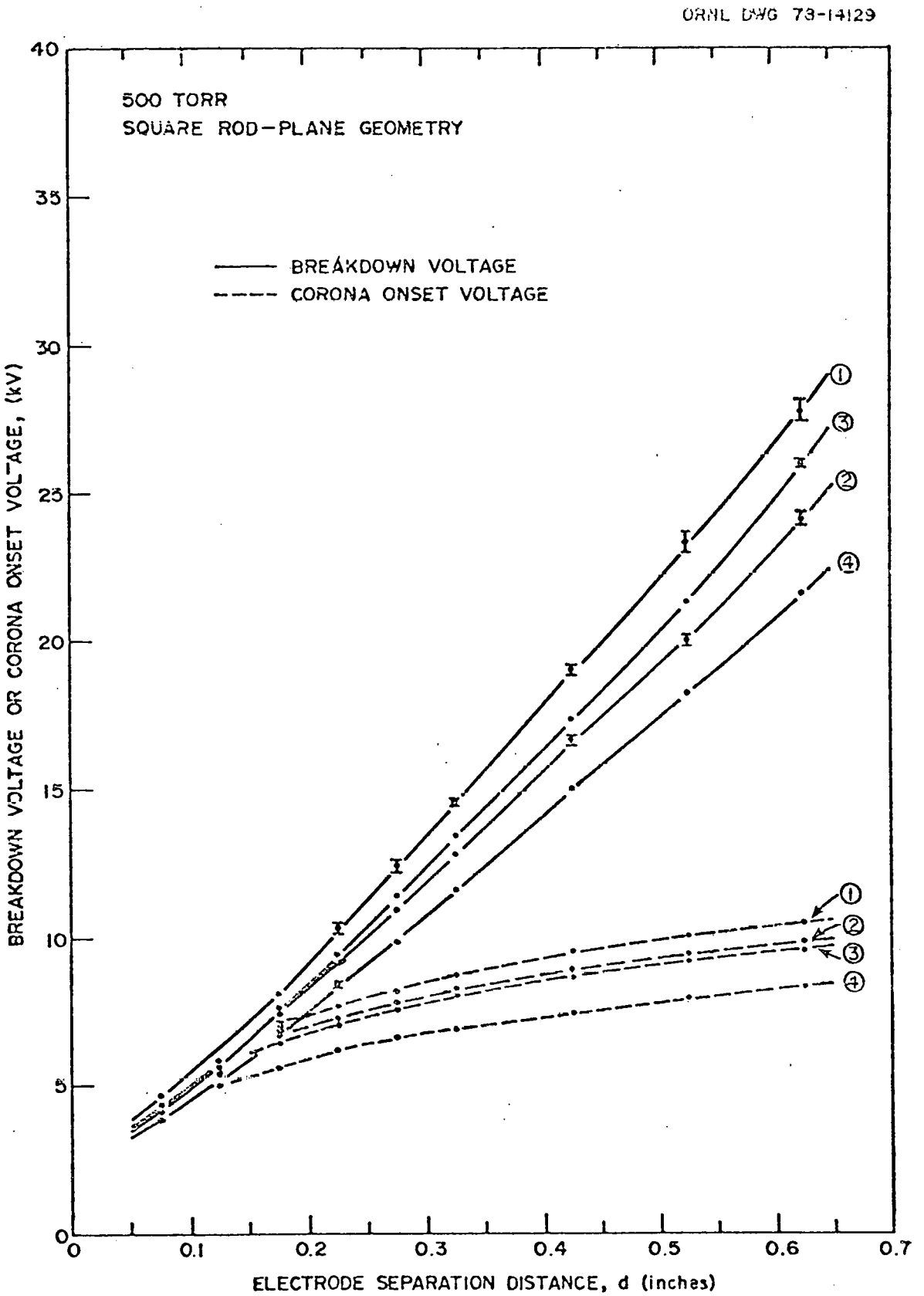
ORNL DWG 73-14129
500 TORR
SQUARE ROD-PLANE GEOMETRY
BREAKDOWN VOLTAGE
CORONA ONSET VOLTAGE
BREAKDOWN VOLTAGE OR CORONA ONSET VOLTAGE, (kV)
ELECTRODE SEPARATION DISTANCE, d (inches)
0
5
10
15
20
25
30
35
40
0
0.1
0.2
0.3
0.4
0.5
0.6
0.7
①
②
③
④

Fig. 12

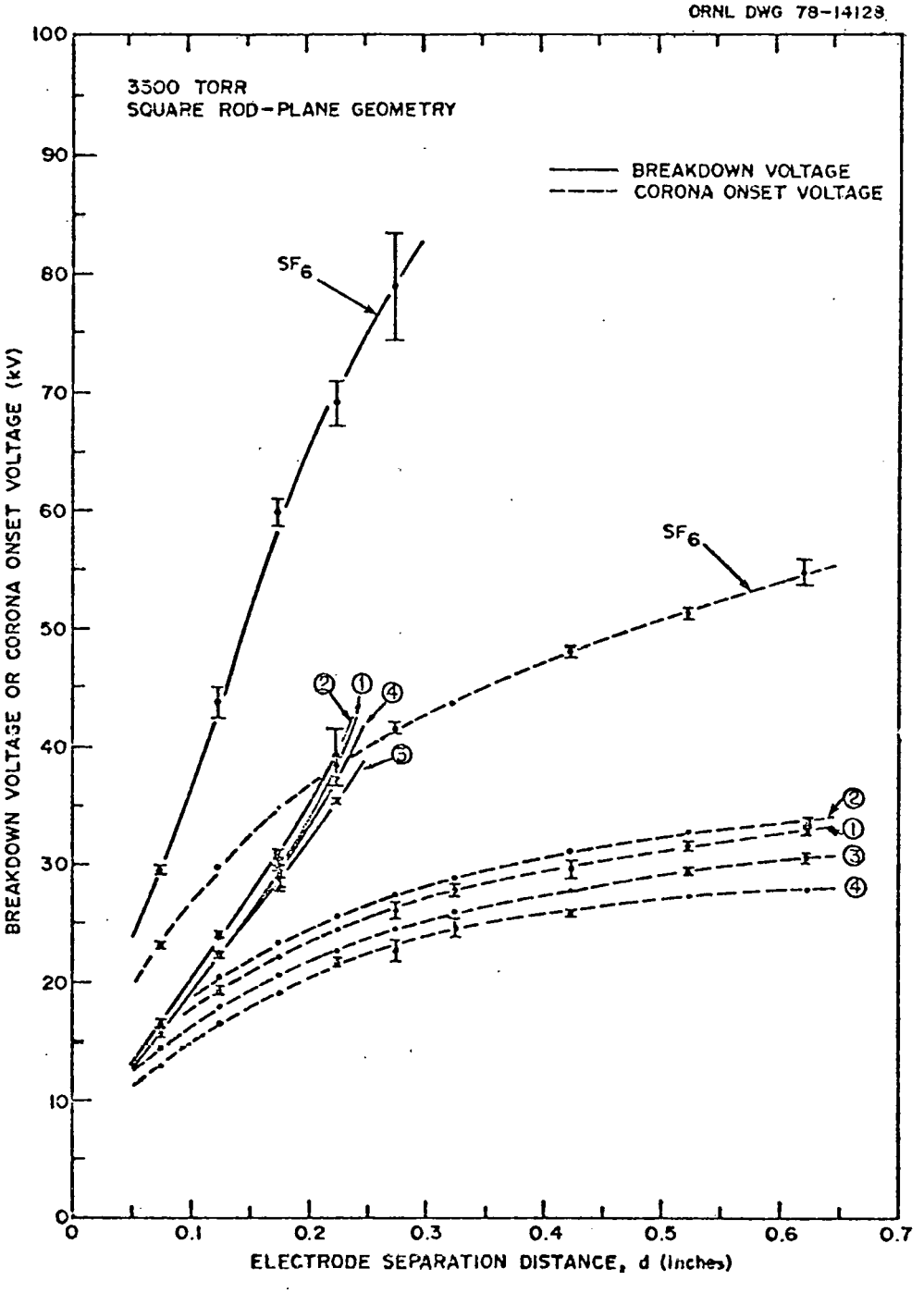
ORNL DWG 78-14128
3500 TORR
SQUARE ROD-PLANE GEOMETRY
BREAKDOWN VOLTAGE
CORONA ONSET VOLTAGE
SF6
SF6
BREAKDOWN VOLTAGE OR CORONA ONSET VOLTAGE (kV)
ELECTRODE SEPARATION DISTANCE, d (inches)
0
10
20
30
40
50
60
70
80
90
100
0.1
0.2
0.3
0.4
0.5
0.6
0.7

Fig. 13

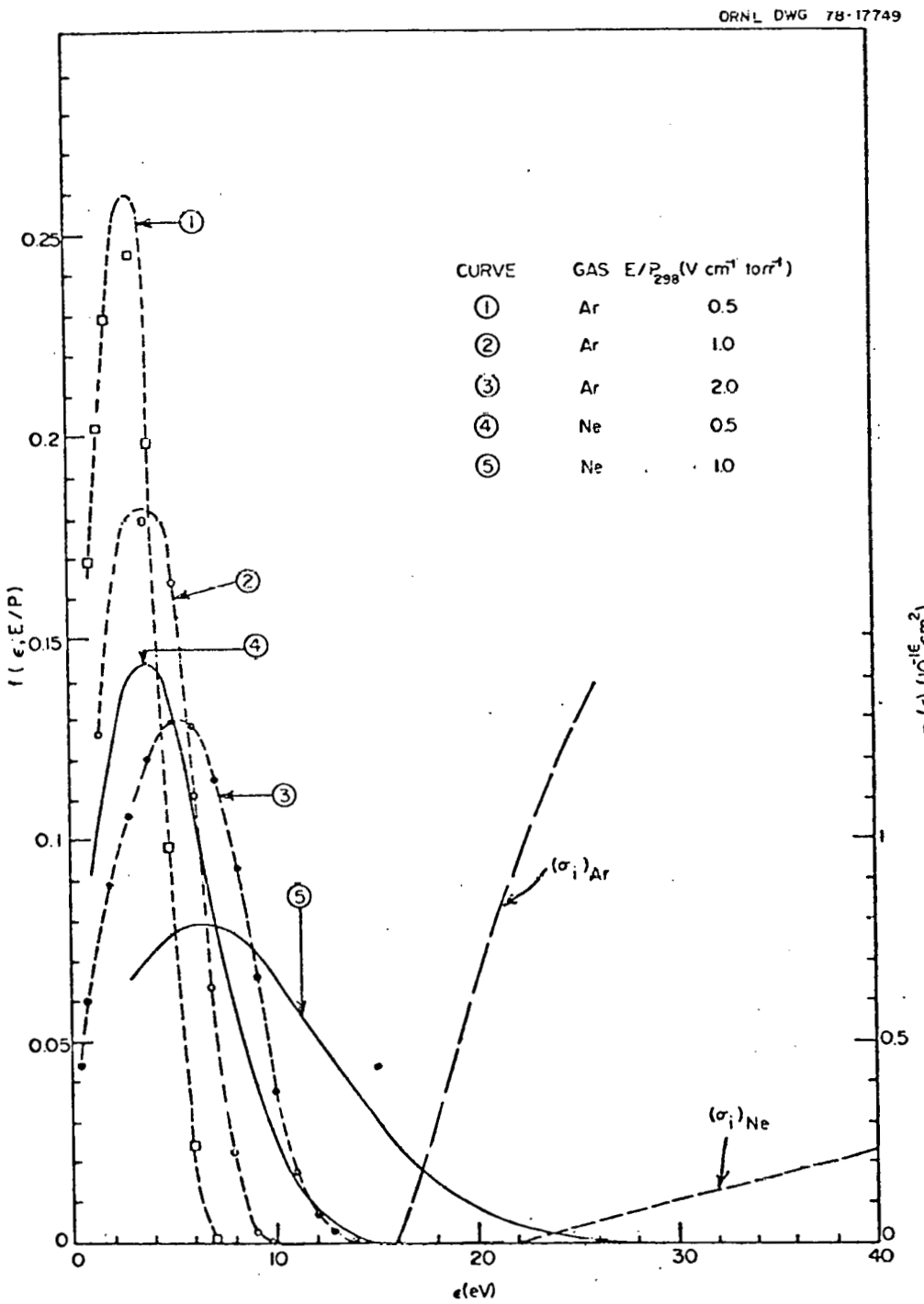
ORNL DWG 78-17749
CURVE GAS E/P298(V cm-1 torr-1)
① Ar 0.5
② Ar 1.0
③ Ar 2.0
④ Ne 0.5
⑤ Ne 1.0
f(ε,E/P)
σi(ε) (10-16cm2)
(σi)Ar
(σi)Ne
ε(eV)
0
0.05
0.1
0.15
0.2
0.25
0.5
1
10
20
30
40

Fig. 14

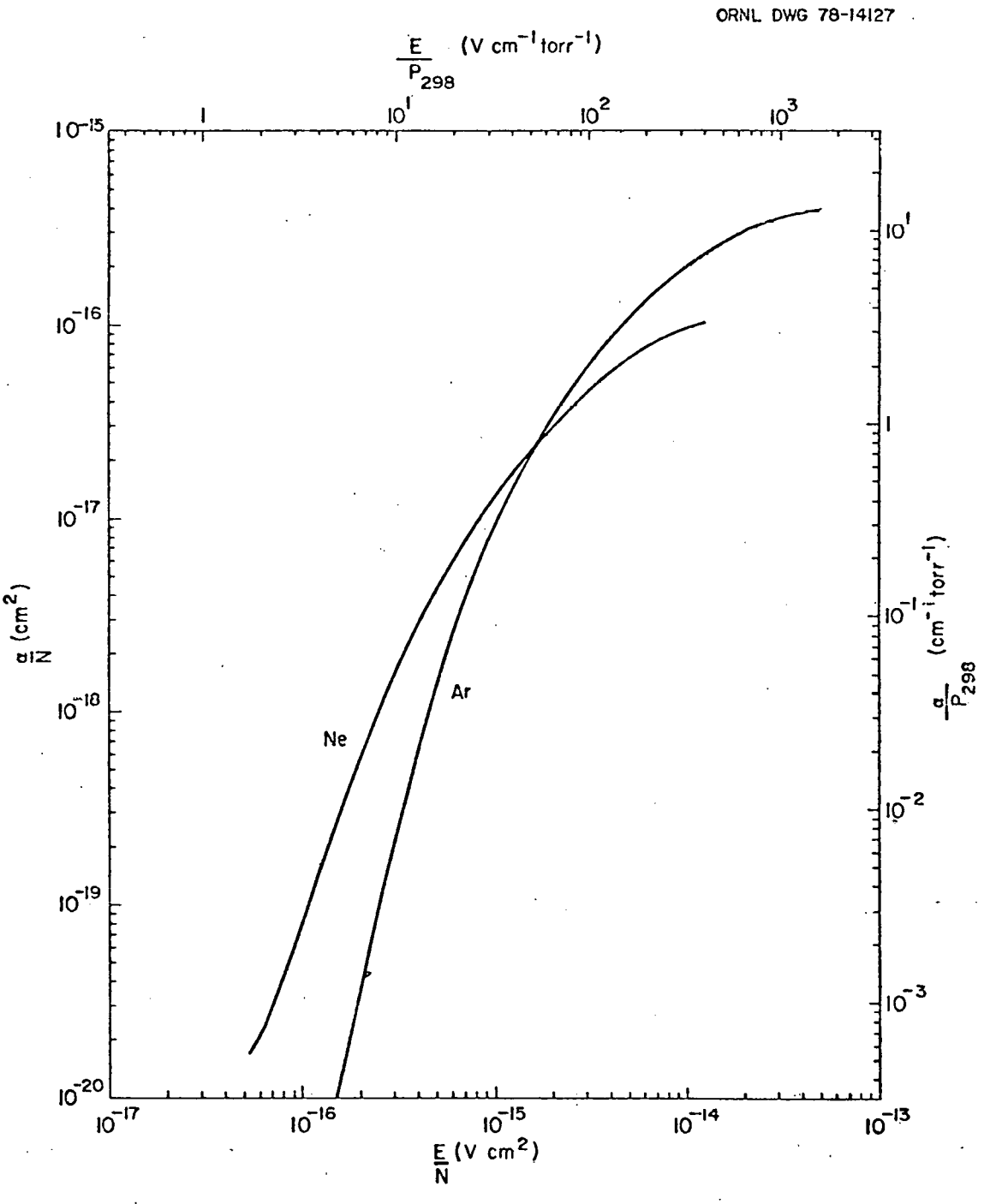
ORNL DWG 78-14127
E/P298 (V cm-1 torr-1)
1
10^1
10^2
10^3
10^-15
10^-16
10^-17
10^-18
10^-19
10^-20
α/N (cm^2)
10^1
1
10^-1
10^-2
10^-3
α/P298 (cm-1 torr-1)
Ne
Ar
10^-17
10^-16
10^-15
10^-14
10^-13
E/N (V cm^2)

Fig. 15

APPENDIX C

FIELD EMISSION FROM AN ATOMIC OR MOLECULAR NEGATIVE ION

Harold C. Schweinler

We present here a theoretical calculation of the transition probability per unit time of an electron from a negative ion state to a continuum state in free space under the influence of a static electric field. We have been able to carry out the calculation only for s states (spherically symmetrical) of the original negative ion.

We do not need any details of the internal structure of the molecular ion except that the energy of the highest-energy occupied level is $E_o = -(EA)$, where "EA" stands for "electron affinity." In fact, we can idealize the ion as a "spherical square well" of radius r_o and depth $-D_o$; the potential energy can be taken to be

$$V(r) = \begin{cases} -D_o & o < r < r_o \\ o & r_o < r \end{cases}$$

in the Schrödinger equation for the wave function ψ_o of the highest occupied level

$$-\frac{\hbar^2}{2m}\nabla^2\psi_o + V(r)\psi_o = E_o\psi_o. \qquad (1)$$

Here $\hbar$ is Planck's constant divided by 2π, m is the mass of the electron, and ∇^2 is Laplace's operator. We need only the solution in the external region $r > r_o$, namely, $\psi_o = C e^{-\kappa r}/r$. When this solution for ψ_o is substituted in Eq. (1), we find that $E_o = -\hbar^2\kappa^2/2m$, or $\kappa = [2m(EA)/\hbar^2]^{1/2}$. We choose C so that the probability of finding the electron outside of $r = r_o$ is a fraction f:

$$\int_{r_0}^{\infty} C^2\left(e^{-\kappa r}/r\right)^2 4\pi r^2 dr = f \qquad (2)$$

This gives $C = (\kappa f/2\pi)^{1/2} \exp(\kappa r_0)$. We think of f as a disposable parameter, in the general range of 0.02 to 0.20 or so.

When the electron is in free space subject only to the field F, its Schrödinger equation is

$$-\frac{\hbar^2}{2m}\nabla^2\psi + eFz\psi = E\psi \qquad (3)$$

Here the charge on the electron is -e, and we want the force on the electron to be in the +z direction, so F will be a negative number. To remind us that $F < 0$, we shall subsequently use the combination (-eF), which is of course positive. We shall take periodic boundary conditions in the x and y directions: $\psi(x + L_1, y, z) = \psi(x, y, z)$ and $\psi(x, y + L_2, z) = \psi(x, y, z)$. When we separate variables in Eq. (3), we find that the x and y dependence is given by $\exp i(k_x x + k_y y)$. The z dependence of Eq. (3) involves the Airy integral.

$$\mathrm{Ai}(\zeta) = \frac{1}{2\pi}\int_{-\infty}^{\infty} \exp i(w\zeta + w^3/3)dw \qquad (4)$$

This is a tabulated function, but we shall need only its asymptotic behavior for large $\zeta > 0$

$$\mathrm{Ai}(\zeta) \cong \tfrac{1}{2}\pi^{-1/2}\,\zeta^{-1/4}\exp(-2\zeta^{3/2}/3) \qquad (5)$$

(Several definitions of the Airy function are in use; ours is that of Mott and Massey.[1]) We find that the solution to Eq. (3) is proportional to

$$\exp i(k_x x + k_y y)\quad \mathrm{Ai}\left\{-B[z + \varepsilon/(-eF)]\right\}$$

where B is defined below and $\varepsilon = E - \hbar^2(k_x^2 + k_y^2)/2m$. For wave function

normalization a factor $(L_1L_2)^{-1/2}$ is required for the x and y dependence of this equation, and the periodic boundary equations require that k_xL_1 and k_yL_2 each be an integer times 2π. We shall, instead of summing over these discrete values of k_x and k_y, integrate with respect to k_x and k_y from negative infinity to infinity; this requires factors $L_1/2\pi$ and $L_2/2\pi$. The Airy function requires a coefficient A for "delta-function-in-energy" normalization, which is especially useful in our case. We shall not give details here; they can be found in Landau and Lifshitz[2] (but note that Landau and Lifshitz's Airy function is $\sqrt{\pi}$ times ours).

Putting all these considerations together, our adopted solution to Eq. (3) is

$$\psi_{k_xk_yE}(x, y, z) = (L_1L_2)^{-1/2} A \exp i(k_xx + k_yy)Ai\{-B[z + \varepsilon/(-eF)]\}$$

where $A = (2m/\hbar^2)^{1/3}(-eF)^{-1/6}$, $B = [2m(-eF)/\hbar^2]^{1/3}$, and $\varepsilon = E - \hbar^2(k_x^2 + k_y^2)/2m$. The normalization is (integration over all space)

$$\iiint \psi^*_{k_xk_yE} \psi_{k_x^1k_y^1E^1} dxdydz = (4\pi^2/L_1L_2)\delta(k_x - k_x^1)\delta(k_y - k_y^1)\delta(E - E^1) \qquad (6)$$

The problem which we want to solve is the time-dependent Schrödinger equation for the ion in a (strong) electric field, namely,

$$-(\hbar^2/2m)\nabla^2\psi + [V(r) + eFz]\psi = i\hbar\,\partial\psi/\partial t \qquad (7)$$

subject to initial conditions that the electron be in the ion at t = 0. For the wave function we take

$$\Psi = C_0(t)\psi_0 \exp(-iE_0t/\hbar) + \iiint C(k_xk_yEt)\psi_{k_xk_yE} \exp(-iEt/\hbar)(L_1L_2/4\pi^2)dk_xdk_ydE \qquad (8)$$

We find, upon substituting in Eq. (7), multiplying by $\psi^*_{k_x k_y E}$, integrating over all space, and integrating with respect to time,

$$C(k_x k_y E t) = \langle k_x k_y E | eFz | o \rangle \left\{ 1 - \exp i(E - Eo)t/\hbar \right\}/(E - Eo). \qquad (9)$$

Here we have used the Dirac notation for the matrix element

$$\langle k_x k_y E | eFz | o \rangle = \iiint \psi^*_{k_x k_y E}\, eFz\, \psi_o \, dxdydz \qquad (10)$$

Equation (10), it will soon be seen, will be needed only for $E = E_o$ (conservation of energy). For this case the integral over space can be evaluated; there remains the integral over the variable w used in defining the Airy function. In this latter integral, after an integration by parts, the resulting integral is of the same form as Eq. (4), which defined the Airy function! The result is

$$\langle k_x k_y E_o | eFz | o \rangle = -4\pi(\hbar^2/2m)AC(L_1 L_2)^{-1/2} Ai[(\kappa^2 + k_x^2 + k_y^2)/B^2] \qquad (11)$$

Our initial condition gave $C_o(o) = 1$, $C(k_x k_y E_o) = o$. The probability of being in any other state than ψ_o at a later time t is

$$P = \iiint |C(k_x k_y E t)|^2 (L_1 L_2/4\pi^2) dk_x dk_y dE \qquad (12)$$

From Eq. (9), $|C|^2$ contains the factor $\left| \left\{ 1 - \exp i(E - Eo)t/\hbar \right\}/(E - Eo) \right|^2$, which is shown[3] to be equivalent at moderate times t to $(2\pi/\hbar)t\ \delta(E - E_o)$. The proportionality to t enables us to define a probability per unit time, P/t. The $\delta(E - E_o)$ permitted us to replace E by E_o in going from Eq. (9) to Eq. (11). After the energy integration in Eq. (12) is performed, the k_x, k_y integration can be carried out because from Eq. (11) k_x and k_y enter in the combination $k_x^2 + k_y^2$, in the case of large argument of the Airy function [see Eq. (5)]. The result is

$$P/t = (\pi/\hbar)A^2C^2(eF)^2B^{-2\kappa^{-2}} \exp(-4\kappa^3/3B^3). \qquad (13)$$

This formula is easier to survey in terms of the atomic units of length $a_H = \hbar^2/me^2 = 0.53 \times 10^{-8}$ cm and energy $e^2/2a_H = 13.6$ eV, in terms of which the basic field strength is $e/a_H^2 \cong 5 \times 10^9$ volt/cm and the basic transition probability is $(e^2/2a_H)/\hbar \approx 2 \times 10^{16}$ sec^{-1}. Thus if we define $(\tilde{EA}) = (EA)/13.6$ eV, $\tilde{r}_o = r_o/a_H$, and $\tilde{F} = F/(5 \times 10^9$ volt/cm), Eq. (13) becomes

Transition probability per unit time =

$$P/t = [\Gamma \exp 2(\tilde{EA})^{1/2}\tilde{r}_o]2 \times 10^{16} \text{ sec}^{-1} \cdot \left\{(-\tilde{F})(\tilde{EA})^{-1/2} \cdot \exp[-2(\tilde{EA})^{3/2}/3(-\tilde{F})]\right\} \qquad (14)$$

Several comments are in order. First, the "outside" form of the wave function $\psi_o = C \exp(-\kappa r)/r$ was used throughout space in deriving Eq. (11). The Airy function is so small in the sphere $r < r_o$ that this procedure is justified; the main contribution to the integral comes from $r >> r_o$. Second, this calculation refers only to the case of spherically symmetrical wave functions ψ_o; it would be valuable to have a corresponding calculation for other angular momenta. However, I see no way of carrying out the latter calculation. When one considers that an elevenfold integration is implied by Eq. (12) (C and C* are each four-fold integrals), it was perhaps fortunate that the probability per unit time could be carried to a relatively simple final formula in the special case of spherical symmetry. Third, the initial bracketed expression in Eq. (14) can be considered to be a single parameter (of order unity); when thus viewed we have a one-parameter theory. Finally, the principal part of the variation in our final Eq. (14) arises from the exponential term.

REFERENCES

1. N. F. Mott and H.S.W. Massey, Theory of Atomic Collisions, 3rd edition (Clarendon Press, Oxford, 1965), p. 104.

2. L. D. Landau and E. M. Lifshitz, Quantum Mechanics, Vol. III (Pergamon Press, 1958), pp. 70-72 and 491.

3. See for example, W. Heitler, The Quantum Theory of Radiation, 3rd edition (Oxford University Press, 1954), p. 70.

APPENDIX D

UNION CARBIDE

INTERNAL CORRESPONDENCE

NUCLEAR DIVISION

POST OFFICE BOX Y, OAK RIDGE, TENNESSEE 37831

To (Name) Dr. L. G. Christophorou
Company Health and Safety Research Division
Location

Date June 30, 1978
Originating Dept.
Answering letter date

Copy to

Subject Acute inhalation toxicity of perfluoro-butene-2 in mice

On June 15, 1978, ten male BALB/C six-week-old mice whose average weight was 20.5 grams were exposed to perfluoro butene-2 at a nominal concentration of 1000 ppm in air at a total flow rate of 12 liters per minute in a 40 liter chamber. The flow rate of the test substance was determined by water displacement to be 12 cc per minute. This rate was reached at 21-1/2 hours and was found to be 10.6 cc per minute and was adjusted to 12 cc per minute. The chamber was allowed to equilibrate for 15 minutes before the mice were placed in the chamber for the exposure. The mice were observed for the first 2-1/2 hours at 15 to 20 min intervals and again at 21-1/2 hours. They were transferred to a mouse cage at 22 hours and 45 minutes.

No abnormal behavior was seen during the first 2-1/2 hours of exposure. At 21-1/2 hours the mice exhibited labored breathing and were almost too weak to move around and remained in this condition until removed from the exposure chamber. Two days after the beginning of the exposure 2 mice had died. On day 3, 5 more died and on day 4 and 5, 2 and 1 died respectively.

Perfluoro butene-2 is lethal to mice when exposed to 1000 ppm under the conditions described.

On June 22, 1978, ten, six-week-old male BALB/C mice were exposed to perfluoro butene-2 at a nominal concentration of 10^3 ppm in air at a total flow rate of 12 liters per minute in a 40 liter chamber. The flow rate of the perfluoro butene-2 was determined by water displacement to be 12 cc per minute before placing the mice in the chamber. This flow rate was checked at 2 hours and 7 hours. The chamber was allowed to equilibrate for 20 minutes after beginning the gas flow into the chamber and before timing was begun. The exposure was for eight consecutive hours. Both air and test substance were passed through a glass tube immersed in crushed ice.

The mice were observed hourly while in the chamber and the observations recorded. The mice ate, slept and investigated their surroundings in a manner judged to be typical of unexposed mice.

Dr. L. G. Christophorou June 30, 1978

After removal of the mice from the exposure chamber they were placed in a mouse cage. At the end of seven days the mice were alive, healthy and behaving normally.

No acute toxicity was detected when inhaled by mice under the conditions described.

M. E. Boling

M. E. Boling

MEB/jms

OK Well.

APPENDIX E

Paper Submitted for publication in the IEEE Transactions on Power Apparatus and Systems

APPLICATION OF BASIC GAS RESEARCH TO PRACTICAL SYSTEMS*

M. O. Pace, Member, IEEE C. C. Chan L. G. Christophorou

Atomic, Molecular and High Voltage Physics Group
Health and Safety Research Division
Oak Ridge National Laboratory, Oak Ridge Tennessee
and
University of Tennessee, Knoxville, Tennessee

Abstract - Improved gaseous dielectrics are being designed on the basis of knowledge of fundamental electron-molecule interactions. Within this program are herein reported breakdown measurements for four binary mixtures (SF_6/N_2, c-C_4F_8/N_2, 2-C_4F_8/N_2, and 2-C_4F_6/N_2) of various proportions for the practical conditions of cylindrical geometry, surface roughness, contamination by free conducting particles, and electrode material composition. Each of these binary mixtures teams together one gas that primarily de-energizes free electrons and one gas that removes free electrons from the dielectric by electron attachment. Under all conditions the binary mixtures containing SF_6 were the worst of the four tested, and this is explained in terms of fundamental electron-molecule interaction processes.

INTRODUCTION

Some initial, more basic, results of a systematic program to develop improved gas dielectrics for power system insulation through guidance from knowledge on basic electron-molecule interactions have been reported previously [1]. This paper reports initial results of a program of small scale, application-oriented, testing that has been phased into a wider program at Oak Ridge National Laboratory (ORNL) on gaseous and liquid dielectrics to: (1) screen proposed dielectrics concerning their behavior under power-apparatus conditions, (2) correlate behavior under power-apparatus conditions with basic electron-molecule interactions and uniform-field testing, and (3) identify appropriate dielectrics and engineering rules for their application.

The basic approach, as we have described earlier (e.g., Refs. [2] to [5]), is to inhibit breakdown by limiting the numbers and energies of free electrons in a gas under electric stress. The electron-molecule-photon interaction processes determining the breakdown initiation are quite complex [2,5,6], and sufficient quantitative information has been compiled only recently which helps identify good dielectrics. We have argued earlier [1] that improved dielectrics will be mixtures of several gases because (1) the free electrons collectively possess a wide range of energies while the most important basic processes of interest are resonant, and hence they are strong functions of energy; and (2) no single gas can have all the desirable electron-molecule interaction properties covering the entire range of electron energies.

The details of the basic part of the ORNL program on dielectrics have been presented elsewhere ([1] to [5]) and can be summarized as follows: the most important electron control mechanism in a gas under electric stress is electron attachment to gas molecules. Breakdown experiments indicate the best dielectrics are those that control electrons well at energies below the gas electronic excitation threshold energy, and the actual ionization process details are apparently less important than the attachment process in preventing breakdown [5]. Mixing gases is then advantageous since no one gas attaches electrons well for all the energies of the electrons present. Attachment becomes more difficult for all attaching gases at high electron energies (typically above 2 eV), so that gas components are included which can remove energy from electrons escaping the efficient low-energy attachment range, returning them to the energy region where attachment is effective and away from the ionization threshold. (There are many mechanisms for molecular absorption of electron energy, which are found in [6]).

The traditional Townsend and streamer models of breakdown employ lumped parameters such as the mean distance traveled by electrons before they either attach to, or ionize, a gas molecule; these parameters are determined by the many fundamental electron-molecule interactions but are not sufficiently detailed to suggest how mixtures should be formulated. However, these breakdown models (the streamer model being more successful in good gas dielectrics) are useful in formulating engineering design rules for the use of a given gas dielectric.

The characteristics and problems of power apparatus must dictate the usefulness of any gas dielectric. The development of improved gas dielectrics is, therefore, a trilogy: (1) discovery (based on fundamental research), (2) design [with rules derived from (1)] and (3) use in power systems (after appropriate screening on a small scale and proving on a larger scale).

This paper reports the initial tests of a comparative study of screening gas mixtures under the "practical" conditions of cylindrical geometry, varying surface roughness, contamination by free conducting particles, and varying conductor materials. Four different dielectric gases were chosen for their excellent electron attaching capabilities and dielectric strengths under uniform field testing [1,3,4]; each of these was mixed in various proportions with N_2, a gas which can absorb energy from electrons which escape the lower (≲2 eV) energy range where attachment is very efficient, returning them to that energy range. All experiments were at 1 atmosphere (101 kPa) pressure and room temperature (≈21°C).

APPARATUS AND PROCEDURE

Electrodes

A typical concentric-cylinder electrode system employed in the present study is shown in Fig. 1. The

*Research sponsored by U.S. Department of Energy under contract W-7405-eng-26 with Union Carbide Corporation.

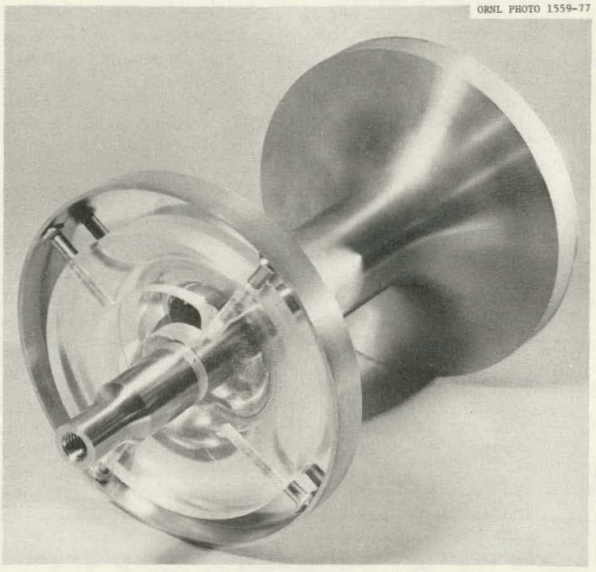

Fig. 1. Concentric cylinder electrode system.

outer cylinder was machined from one solid brass piece to effect a central cylindrical region of 2-cm (inner) radius and 10-cm length. At each end the outer cylinder very smoothly flares to a larger radius of approximately 8 cm, providing a surface to which is attached a Plexiglas disc, which positions the inner electrode. Typical inner cylinders are shown in Fig. 2; the smaller ones have Plexiglas bushings to adapt them to the Plexiglas holders. The outer cylinder is at ground potential, and the inner cylinder is connected to high voltage. It has been visually confirmed that breakdowns do occur in the central inter-cylinder region and not on the Plexiglas discs or the cylinder ends. The same outer cylinder is used in all experiments, but different inner electrodes are used to allow comparisons of the effects of electrode radius, surface roughness, and material composition. For studies of particle effects, additional Plexiglas discs are inserted at each end of the small central inter-electrode region to prevent particle escape. It should be noted that the data taken with the present system are intended for comparing different mixtures and effects for a given inner electrode radius, since the field fringing from the cylinder ends varies with inner radius; this effect may be reflected in the data when the radius is changed. The data should be used with caution for other purposes.

Chamber and Cage

The electrodes are mounted in a stainless steel chamber, visible in Fig. 3, inside a shielding cage. The electrode axis is aligned toward a quartz window in the chamber end for observation of breakdown and particle motion. Ultraviolet light from a 60W deuterium lamp is directed through the window by a partially conducting front surface mirror without interfering with observation. The chamber volume is 60 liters.

High voltage is introduced into the chamber by a 300-kV cable feedthrough with O-ring seals. The ground electrode is insulated from the chamber through a 30-kV ceramic feedthrough and is grounded outside the chamber. Attached to the chamber are appropriate connections for gas inlets, a pressure gauge, a pumping system comprised of a mechanical and a diffusion pump with liquid N_2 baffle, and a liquid N_2 cooled stainless steel flask for temporarily liquifying some test gases for re-use.

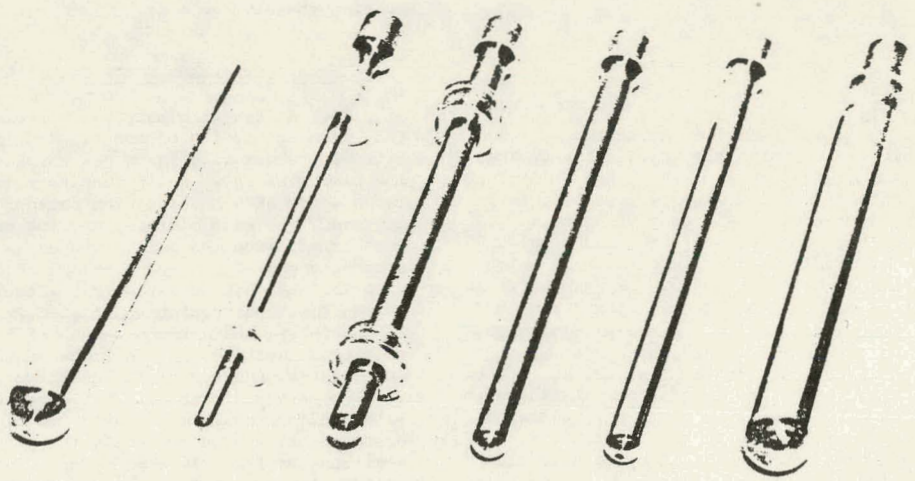

Fig. 2. Some inner electrodes for concentric cylinder electrode system. (Smaller sizes have bushings for mounting.)

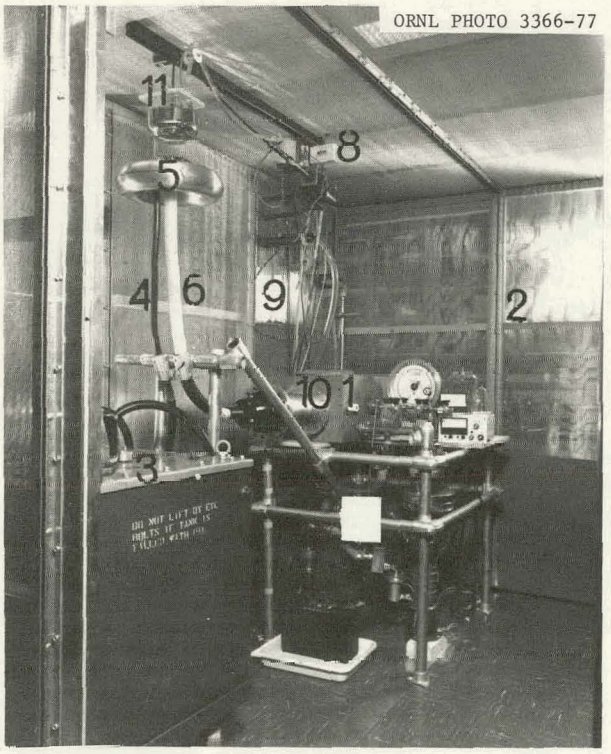

Fig. 3. Interior of shielding cage. (Instrumentation and controls are outside.) (1) chamber; (2) rear cage wall; (3) ±150 kV dc supply; (4) HV cable out of supply; (5) HV diverter gap electrode on corona shield; (6) HV cable into chamber; (7) vacuum pumps; (8) diverter gap motor and trigger source; (9) cage feedthrough panel; (10) HV feedthrough into chamber; (11) ground electrode of diverter gap.

Electrical Apparatus

In Fig. 3 is shown the double layer copper mesh cage that isolates the spark electrical noise. The single system ground is located on the cage feedthrough panel, which contains radio-frequency rejection feedthroughs for instrumentation and control signals.

The high voltage power supply provides 0 to ±150 kV dc by means of a voltage doubler circuit in which vacuum diodes charge two series 0.006 μF capacitors in oil. Also in the oil is a 300 MΩ resistor string, which forms a 1000:1 divider with external resistance to ground for voltage measurement, and a 100 kΩ resistor string in series with the high voltage output.

In conducting the breakdown measurements the high voltage is sampled repeatedly by a digital voltmeter, as the high voltage is slowly increased at the rate of $\sim$100 Vs^{-1}. When breakdown is sensed by an automated controller [1] it disables the digital voltmeter sampling, thus preserving the voltage reading just prior to breakdown. The meter sampling rate and high voltage rise rate are chosen to make the error negligible ($\sim$5 V) between this preserved reading and the actual breakdown voltage. The automated controller can also control the high voltage, raising it at an appropriate, slow rate and lowering it quickly upon breakdown, and then restarting the cycle after an appropriate delay. The breakdown is sensed by voltage on resistors in the electrode connection to ground, but an optical spark pickup is also incorporated which employs a lens, a light pipe, and a phototransistor in tandem.

In order to limit discharge energy in the test gap (upon breakdown) more quickly than by just reducing the power supply input, a triggered air gap (numbers 5 and 11 in Fig. 3) shorts the HV line, between power supply and chamber, to ground in tens of microseconds. This gap is formed by two 6-in.-diameter stainless steel hemispheres, the lower (high voltage) one resting on a 300-kV corona ring while the upper one (ground electrode) is movable through a motor driven chain suspension. The gap is triggered by a 50-kV spark applied to an insulated tungsten rod inside a hole in the center of the ground electrode, as in a "trigatron" gap.

Experimental Procedure

The test electrodes are carefully cleaned and mounted, and the chamber is pumped to a vacuum level of $\sim 10^{-4}$ Pa ($\sim 10^{-9}$ atmospheres). Test gases are admitted via previously evacuated lines and vacuum quality valves to form mixtures expressed according to partial pressures. The total mixture pressure is always 1 atmosphere. The diverter gap is set by the motor and manually test-fired at high voltage near the anticipated breakdown level. The high voltage is set (either automatically by a feedback system or manually) to begin at a "base" value below the anticipated breakdown level, rise slowly ($\lesssim$100 Vs^{-1}) until breakdown occurs, and then quickly return to the "base" value. Upon breakdown the automatic controller preserves the last voltmeter reading just before breakdown and fires the diverter gap. After a suitable pause the controller repeats the cycle. In particle-effects studies two investigators participate, one at the control panel and the other at the chamber window. The latter visually verifies that every recorded breakdown is produced by a single free particle as in power apparatus [7-11] and not by some peculiar mechanism (e.g., by two aligned particles or by particles clinging to the insulating particle barrier). Trapped particles (e.g., those particles clinging to Plexiglas or spot-welded to an electrode) are freed by letting the remaining (free) particles bounce at a voltage below breakdown or by pulsing the high voltage.

BREAKDOWN MEASUREMENTS IN CYLINDRICAL GEOMETRY

Four different binary gas mixtures have been studied, each consisting of one electron-attaching gas and nitrogen, whose role is to de-energize electrons reaching higher energies and return them to the lower energy range where attachment by the partner gas is most effective. For each mixture, various compositions have been tried, from the pure nitrogen to the pure electron attaching gas.

The attaching gases were SF_6 (sulfur hexafluoride), c-C_4F_8 (perfluorocyclobutane), 2-C_4F_8 (perfluorobutene-2) and 2-C_4F_6 (hexafluoro-2-butyne). Electron attachment cross sections as functions of electron energy for these gases, uniform field breakdown data for them and their binary mixtures with nitrogen, have been given in [1]. Sulfur hexafluoride attaches electrons well at energies below $\sim$0.4 eV, while the other gases attach electrons efficiently over a much wider energy range, $\sim$0.0 to 1.4 eV. All of the other perfluorocarbon gases tested displayed higher breakdown strengths than SF_6, and this was attributed to their ability to control electrons over a wider energy range than SF_6 does. It was also observed that as SF_6 was increasingly substituted for nitrogen in the SF_6/N_2 mixture (at a constant total pressure), the dielectric strength saturated (at $\sim$20% SF_6) and was not appreciably increased by further substitution of SF_6 for N_2 even though pure SF_6 has a

uniform field dielectric strength ∿2.5 times that of pure N_2. The perfluorocarbon/nitrogen mixtures did not exhibit this saturation effect, but instead, they always gave improvement as the perfluorocarbon content was increased at constant total pressure. This saturation was attributed [1] to the fact that SF_6 captures electrons efficiently only at very low energies (≲0.4 eV) and saturation is, thus, reached once a large number of electrons in this energy range is attached. Pedersen [12] has endeavored to approximate theoretically the shape of the breakdown voltage vs percent of SF_6 in N_2 curve (uniform field data, Fig. 4), but here the observed saturation effect is noticeably stronger than his prediction.

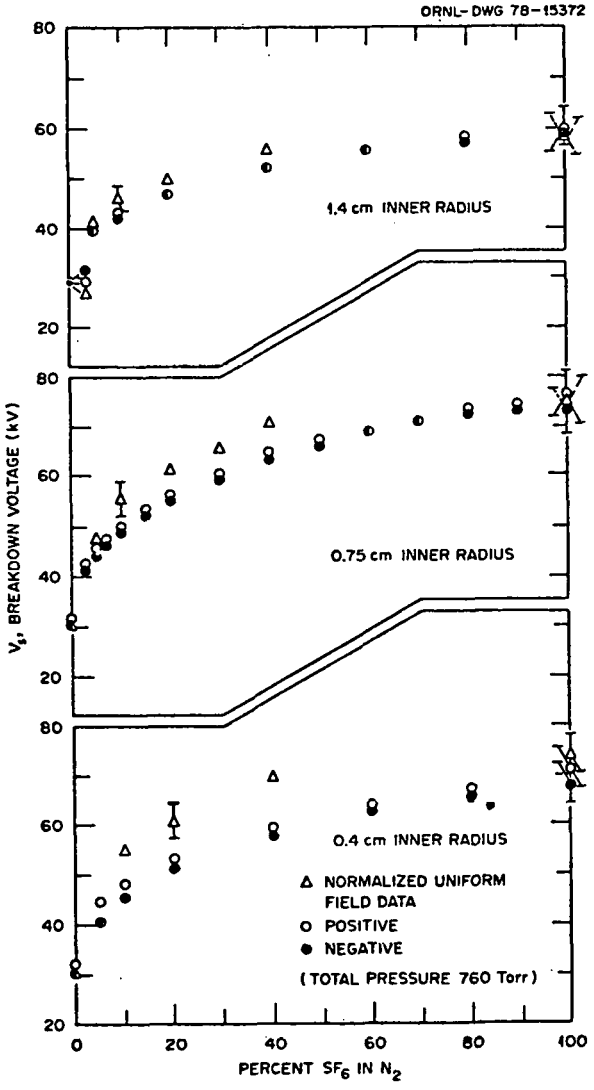

Fig. 4. Breakdown voltages in three cylindrical geometries for SF_6/N_2 mixtures at 1 atmosphere and ∿21°C. Mixtures are identified by the percentage of SF_6 by pressure. The uniform field breakdown curve has been normalized to each point for pure N_2 with negative polarity.

Nitrogen acted as an appropriate partner for each attaching gas because N_2 de-energizes electrons with energies of approximately 2 to 3 eV, [2-5] thus "guarding" the range just above that where the electron attaching gases are effective.

Figures 4 to 7 show breakdown voltages (for both inner-cylinder polarities) for mixtures of SF_6/N_2, c-C_4F_8/N_2, 2-C_4F_8/N_2, and 2-C_4F_6/N_2, respectively and for smooth, stainless steel inner cylindrical electrodes of 1.4, 0.75 , and 0.4 cm radii. These three radii correspond respectively to increasingly nonuniform fields and to ratios of outer electrode radius ÷ inner electrode radius of 0.5 e, e, and 2 e (where e = 2.72). For the sake of comparing curve shapes, the graphs also contain data on uniform field breakdown voltage versus percent of electron attaching gas in N_2, normalized to the point for pure N_2 for negative polarity. The error bars in Figs. 4 to 7 show combined estimated systematic and observed random errors; the relative values would be less uncertain. The observed random error was standard deviation ÷ mean of at least ten observations and was ≲3% for each plotted data point.

In the SF_6/N_2 data of Fig. 4, the saturation effect we elaborated upon earlier is evident in the normalized uniform field curves. This characteristic saturation however, is not as pronounced in the data taken with the cylindrical electrode geometry, and it seems to be less pronounced as the field becomes more nonuniform (in the order 1.4-, 0.75-, and 0.4-cm radii).

In the fluorocarbon/N_2 results in Figs. 5 to 7 the curve of breakdown voltage versus percent of attaching gas in N_2 is always nearly a straight line. Each fluorocarbon/N_2 mixture is still better than the SF_6/N_2 mixture for all cylindrical electrode geometries tested. In Figs. 5 to 7 is seen an occasional tendency for the negative breakdown voltage to exceed slightly the positive breakdown value, which did not occur in the SF_6 data; this is tentatively attributed to negative corona due to the greater electron capture ability of the fluorocarbons.

In Figs. 4 to 7, it can be seen that the breakdown voltage is the highest for the 0.75-cm inner-electrode radius. This is in agreement with the fact that with (infinitely long) concentric cylinders with a given voltage between them and a given outer radius, the lowest field on the inner electrode surface occurs for an outer radius ÷ inner radius ratio of e. It should be noted that the effect of field fringing at the open ends of the electrodes is to lower the field inside, and this effect is more pronounced for smaller inner radii; hence the observed breakdown voltage for the 0.4-cm inner-electrode radius is almost as high as that for the 0.75-cm inner-electrode radius. The data are useful for comparing the effects various factors have on the breakdown strengths with any one inner radius, and for comparing the shapes of the breakdown voltage vs percentage of attaching gas in N_2 curves as one varies the inner-electrode radius (and thus the degree of field nonuniformity).

Finally, in Fig. 8 we plot the breakdown voltage, V_s, as a function of percent of attaching gas in N_2 for the 0.4-cm inner-electrode radius and negative polarity . Based on these data and the overall capability of those gases to remove electrons via attachment in the energy range 0 to ∿1.4 eV (i.e., the energy integrated electron attachment cross section) [12], it appears that the larger the overall capability for electron removal of an attaching gas additive, the less the breakdown strength of the mixture suffers in nonuniform fields. From similar data using inner-electrodes with other (1.4- and 0.75-cm) radii it was observed that as the field becomes more nonuniform (i.e., as the inner-electrode radius decreases from 1.4 to 0.75 and 0.4 cm) the percent of perfluorocarbon additive in N_2 at which the V_s is roughly equal to the V_s of the SF_6/N_2 mixture, decreases. For example, for

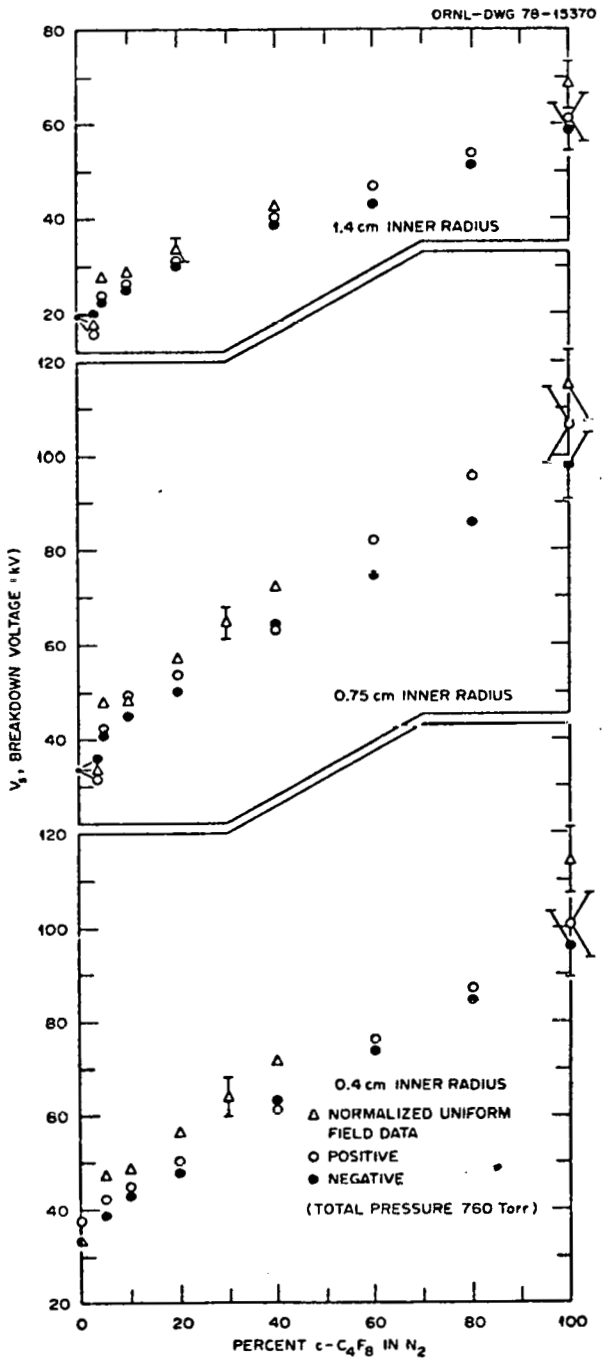

Fig. 5. Breakdown voltages in three cylindrical geometries for c-C_4F_8 (perfluorocyclobutane)/N_2 mixtures at 1 atmosphere and ∿21°C. Mixtures are identified by the percentage of c-C_4F_8 by pressure. The uniform field breakdown curve has been normalized to each point for pure N_2 with negative polarity.

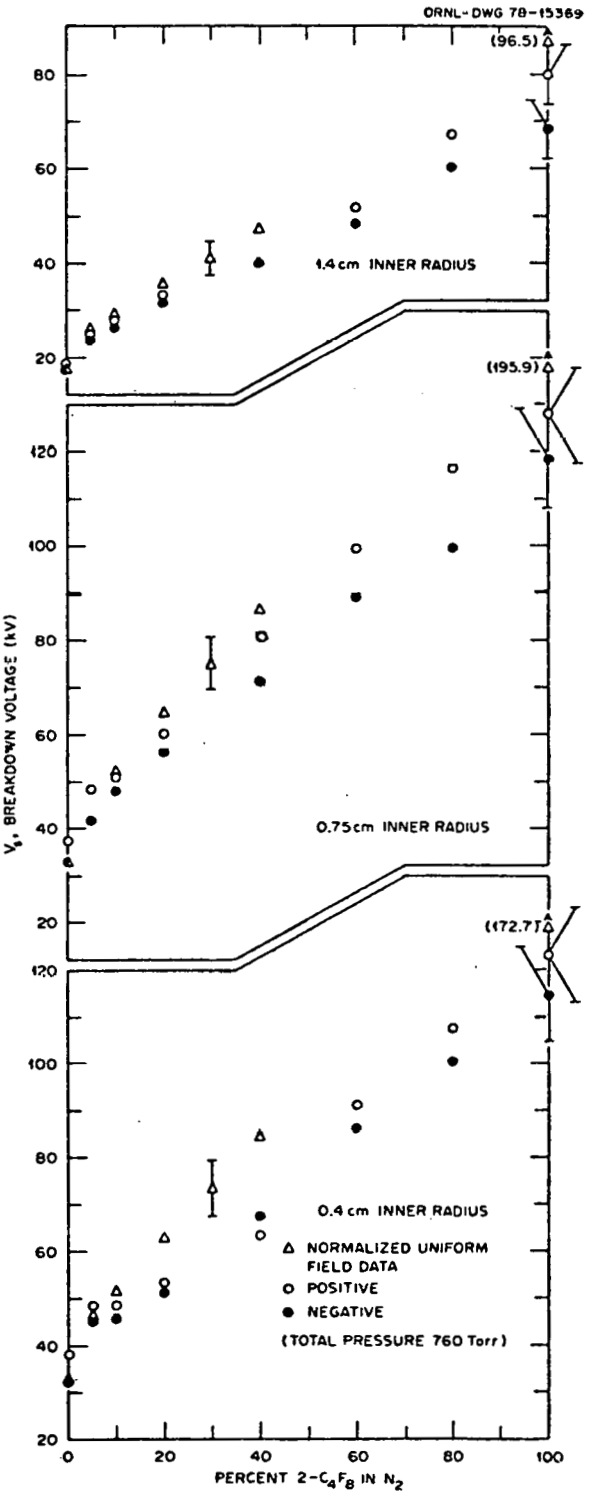

Fig. 6. Breakdown voltages in three cylindrical geometries for 2-C_4F_8 (perfluorobutene-2)/N_2 mixtures at 1 atmosphere and ∿21°C. Mixtures are identified by the percentage of 2-C_4F_8 by pressure. The uniform field breakdown curve has been normalized to each point for pure N_2 with negative polarity.

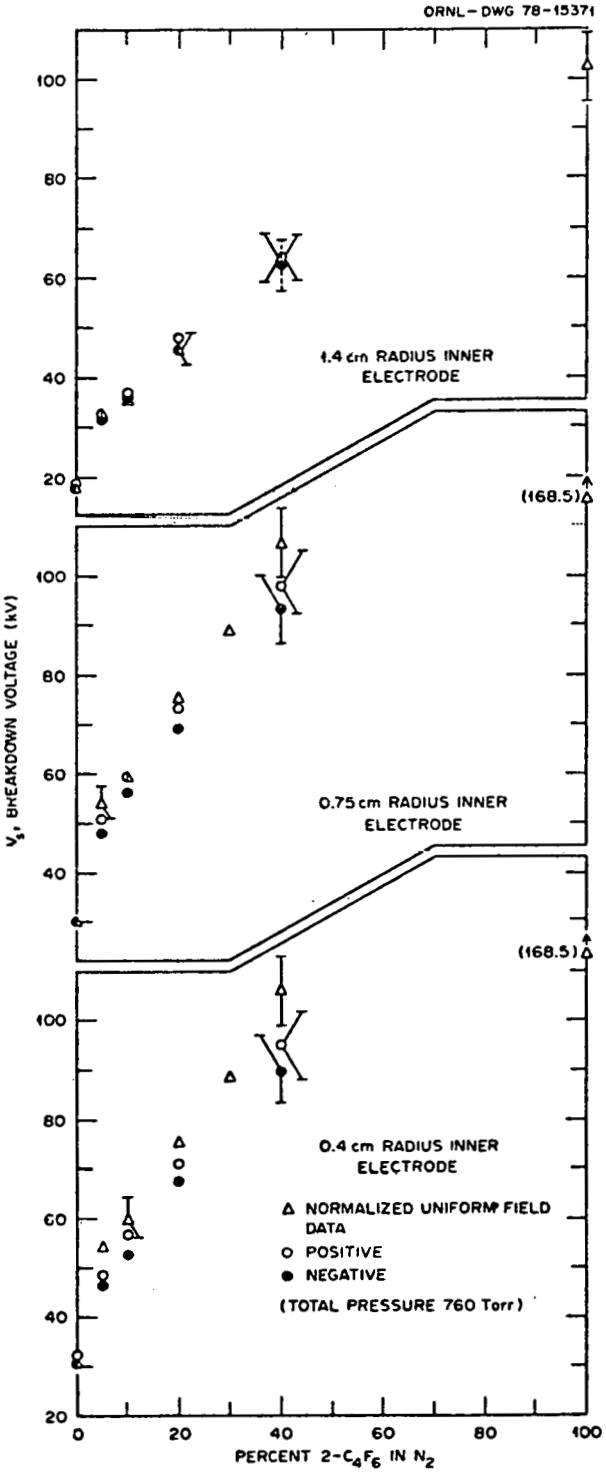

Fig. 7. Breakdown voltages in three cylindrical geometries for 2-C_4F_6 (hexafluoro-2-butyne)/N_2 mixtures at 1 atmosphere and ∿21°C. Mixtures are identified by the percentage of 2-C_4F_6 by pressure. The uniform field breakdown curve has been normalized to each point for pure N_2 with negative polarity.

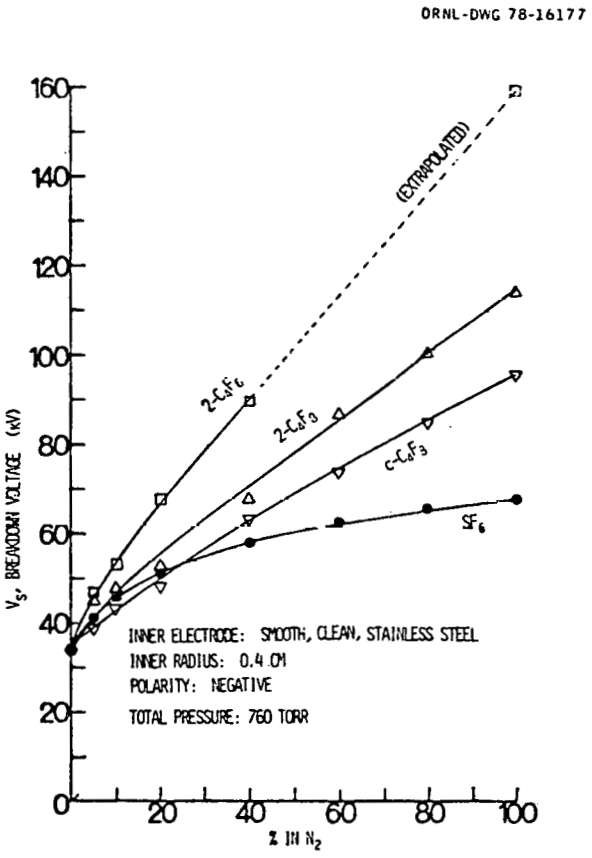

Fig. 8. Breakdown voltages of all attaching gas/N_2 binary mixtures studied, with negative polarity on the 0.4-cm-radius inner cylindrical electrode at 1 atmosphere and ∿21°C. Mixtures are identified by the percentage of attaching gas by pressure. (The 2-C_4F_6/N_2 curve has been extrapolated for the percentage of 2-C_4F_6 > 40%.)

the c-C_4F_8 mixture the breakdown voltage vs percent of c-C_4F_8 in N_2 crosses the similar curve for the SF_6/N_2 mixture at ∿66, ∿42 and ∿28%, at inner-electrode radii of 1.4, 0.75, and 0.4 cm, respectively. Similarly, for the 2-C_4F_8/N_2 mixtures the respective percentages are 51, 17, and 0%. This indicates the superiority of the perfluorocarbon/nitrogen mixtures over the SF_6/N_2 mixtures under these conditions of nonuniform fields.

MEASURED EFFECTS OF SURFACE ROUGHNESS

To study the effect of surface roughness on the dielectric strength of the four mixtures of attaching gases with nitrogen, preliminary breakdown measurements for both polarities were made for three stainless steel

inner cylindrical electrodes of 0.75-cm radius. The only difference between the three inner electrodes was their surfaces: (1) polished to a mirror finish, (2) the same as (1) except for a 0.004-in.-deep groove spiralled around a 2-in. length in the central electrode region, and (3) the same as (1) except for a 0.020-in.-deep groove spiralled around a 2-in. length in the central electrode region. Those breakdown results are shown in Figs. 9 to 12. The error bars indicate the combination of estimated systematic errors and observed random error, the latter (≤3%) being the standard deviation ÷ the mean for at least ten breakdowns. Relative values should contain less error than implied by the error bars.

The results in Figs. 9 to 12 indicate that each fluorocarbon tested is still superior to SF_6 in the face of roughness. Comparisons among the four figures reveal that the mixture with approximately 5% of attaching gas is fairly insensitive to this degree of roughness for each attaching gas, for both polarities. In the case of roughness, extreme nonuniform fields may prevail and, in these cases, in addition to electron attachment and electron slowing down, the electron-impact induced ionization could be important.

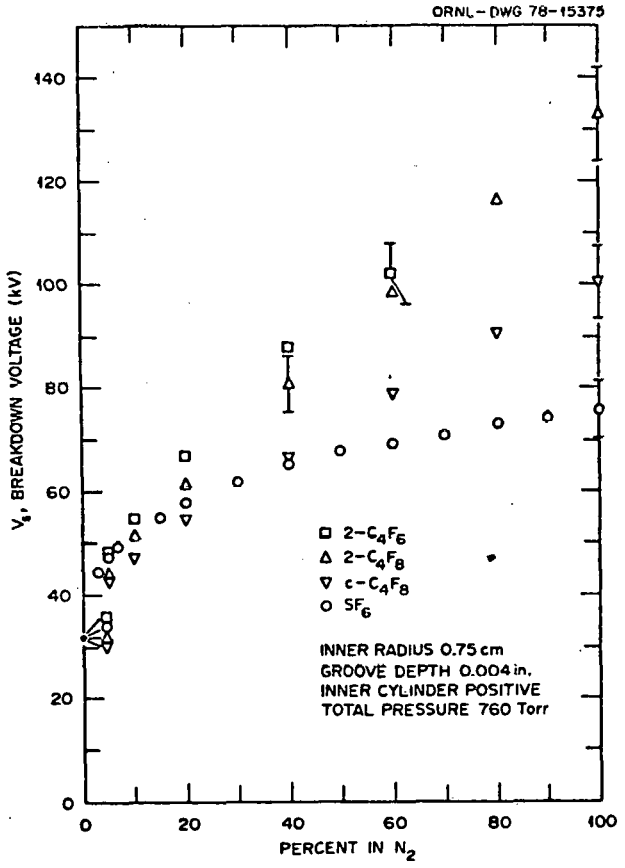

Fig. 9. Breakdown voltages for the four attaching gas/N_2 binary mixtures for inner electrode roughness of 0.004 in. and positive polarity at 1 atmosphere and ∿21°C. Mixtures are identified by the percentage of attaching gas by pressure.

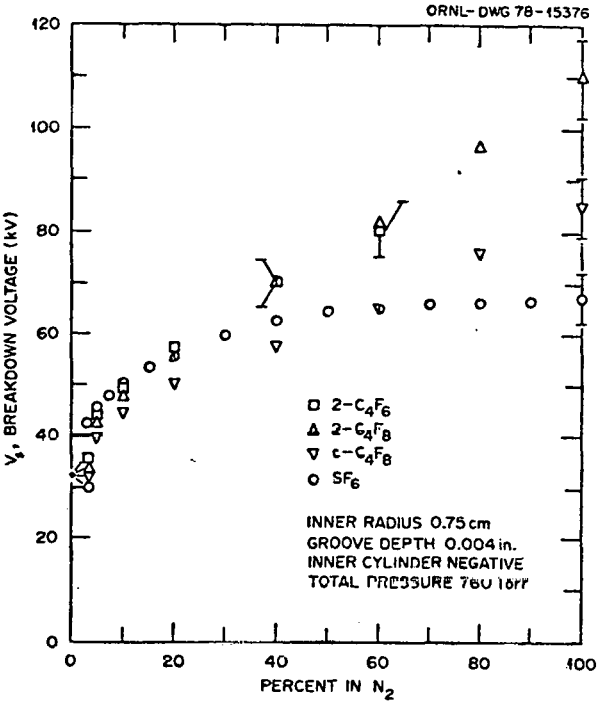

Fig. 10. Breakdown voltages for the four attaching gas/N_2 binary mixtures for inner electrode roughness of 0.004 in. and negative polarity at 1 atmosphere and ∿21°C. Mixtures are identified by the percentage of attaching gas by pressure.

MEASURED EFFECT OF ELECTRODE MATERIAL

To study the effect of inner electrode material on the dielectric strength of the four electron attaching gas/N_2 mixtures, breakdown measurements were made with three inner electrodes each with 1.4-cm radius and smooth surface, but of three different materials, namely, stainless steel, aluminum, and copper. Again each fluorocarbon/N_2 mixture was better than the corresponding SF_6/N_2 mixture; since negligible effect of electrode material composition on the breakdown voltage was found, no graphs are given, and the reader is referred to the results already presented in Figs. 4 to 7 for the stainless steel inner electrode of radius 1.4 cm. Some small differences were observed between electrodes of different material, but those were within the experimental error.

MEASURED EFFECTS OF CONTAMINATING PARTICLES

Considerable research has been performed on particle contamination in gas-insulated systems, (e.g., [7] to [11]) and accordingly we considered it desirable to investigate the behavior of the mixtures SF_6/N_2, c-C_4F_8/N_2, 2-C_4F_8/N_2, and 2-C_4F_6/N_2 in the presence of free long conducting particles. Five copper particles were therefore confined in the central inter-electrode region (Fig. 1) by additional discs of Lexan with 2-cm outer radius and a central hole for the 0.75 smooth stainless steel electrode. These particle barriers were inserted into the ends of the small (2-cm) radius cylindrical region. The Plexiglas discs seen in Fig. 1 were left in place to position the electrode correct-

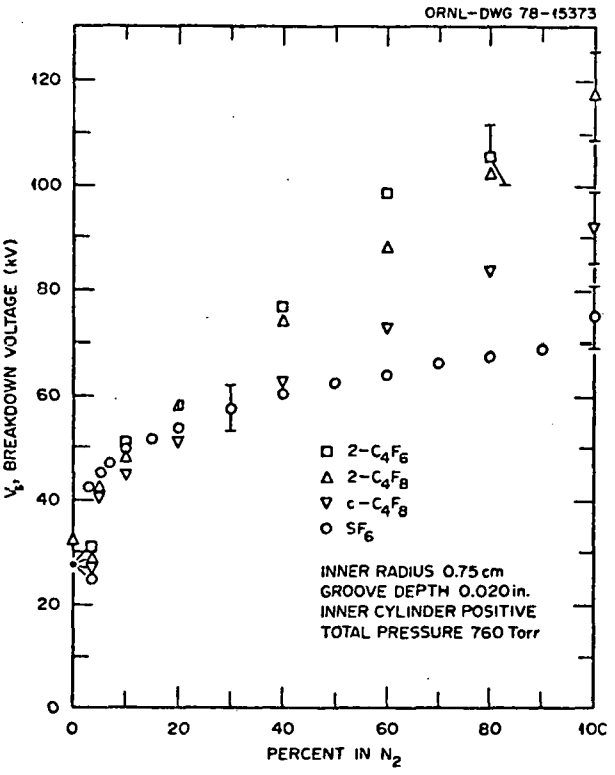

Fig. 11. Breakdown voltages for the four attaching gas/N_2 binary mixtures for inner electrode roughness of 0.020 in. and positive polarity at 1 atmosphere and ∿21°C. Mixtures are identified by the percentage of attaching gas by pressure.

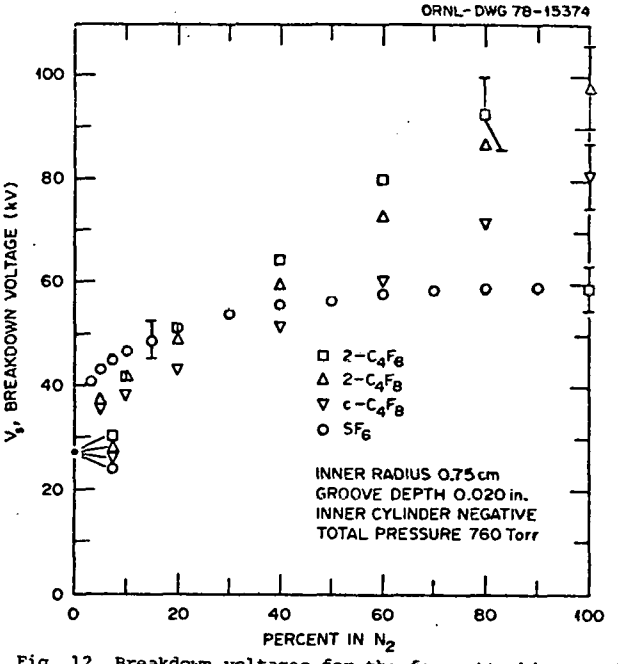

Fig. 12. Breakdown voltages for the four attaching gas/N_2 binary mixtures for inner electrode roughness of 0.020 in. and negative polarity at 1 atmosphere and ∿21°C. Mixtures are identified by the percentage of attaching gas by pressure.

ly. It was verified that the breakdown voltage (without particles) was unchanged by the additional particle barrier discs. In this arrangement the breakdown strength of each mixture could be compared to the case of the same electrode without particles, and also the breakdown strengths of different mixtures could be compared in the presence of particles.

The particles exhibited the same modes of behavior as reported by others ([7]-[11]). As the voltage was slowly raised, the particles would suddenly leave their positions (on the bottom inside surface of the outer cylinder) and assume a bouncing motion between the electrodes. If breakdown did not occur during the bouncing motion, at higher voltage the particles would assume the "firefly" motion of hovering very close to the negative electrode and moving slowly along the surface with an attitude perpendicular to that surface. As the voltage was raised levitation occurred at 17.0 ± 1.5 kV, and as the voltage was lowered motion ceased at 7.0 ± 1.5 kV, independently of the gas mixture.

Preliminary breakdown voltages for various proportions of the mixtures SF_6/N_2, c-C_4F_8/N_2, 2-C_4F_8/N_2, and 2-C_4F_6/N_2 are shown in Figs. 13 and 14 for 5 copper particles, each 1/8 in. long by 0.015 in. diameter with the smooth stainless steel inner electrode. The error bars show estimated systematic errors combined with observed random error; the latter, defined as standard deviation ÷ mean for at least five values, was 5%. For each reading recorded it was visually observed that the breakdown was caused by a single free particle (see discussion in experimental section).

With contaminating particles the fluorocarbons were again better than SF_6, which still exhibited somewhat its saturation effect seen without particles. Of course all curves in Figs. 13 and 14 are constrained to coincide at the left (0%) end.

SUMMARY AND CONCLUSIONS

Small scale comparative breakdown tests have been made on four types of binary gas dielectric (SF_6/N_2, c-C_4F_8/N_2, 2-C_4F_8/N_2, 2-C_4F_6/N_2) mixtures, of various proportions, corresponding to conditions of geometry, surface, material, and contamination that approximate those in power apparatus and are sources of problems. Each binary mixture consisted of one gas that attaches electrons well at some low energy in the range from 0 to ∿1.4 eV and also one gas (N_2) that de-energizes electrons escaping the attachment range as they reach 2 to 3 eV and returns them to the energy region of efficient capture. All tests conducted so far were for a total gas pressure of 1 atmosphere (101 kPa) and at room temperature (∿21°C).

In the tests with three coaxial cylinder geometries, as well as in previous uniform field measurements, SF_6/N_2 mixtures were found to have lower breakdown voltages than the other three. As SF_6 was increasingly substituted for nitrogen (with total pressure constant) a saturation effect was observed. Both of these characteristics of the SF_6/N_2 mixtures are attributed to the fact that SF_6 attaches electrons effectively only in a limited (≤0.4 eV) electron energy range compared to the perfluorocarbons studied.

The surface-roughness effect studies have shown that the perfluorocarbon/N_2 mixtures are better than the SF_6/N_2 mixtures. For each of the four mixtures the least sensitive proportions to roughness were approximately 5% attaching gas + 95% nitrogen, though for all but SF_6 the mixtures with more attaching gas offered

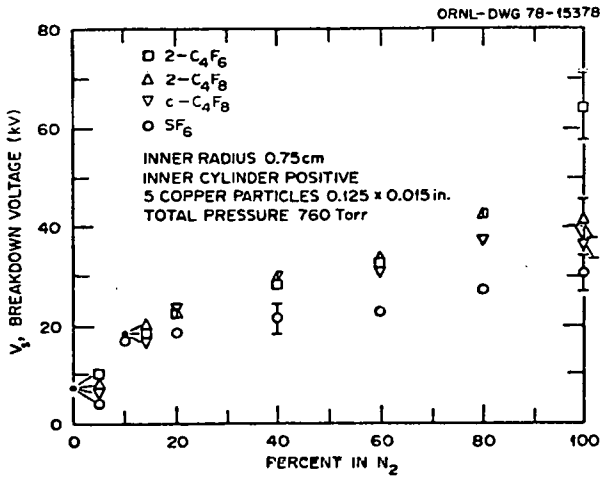

Fig. 13. Breakdown voltages for the four attaching gas/N_2 binary mixtures with contaminating free wire particles at positive polarity, 1 atmosphere, and ∿21°C. Mixtures are identified by the percentage of attaching gas by pressure.

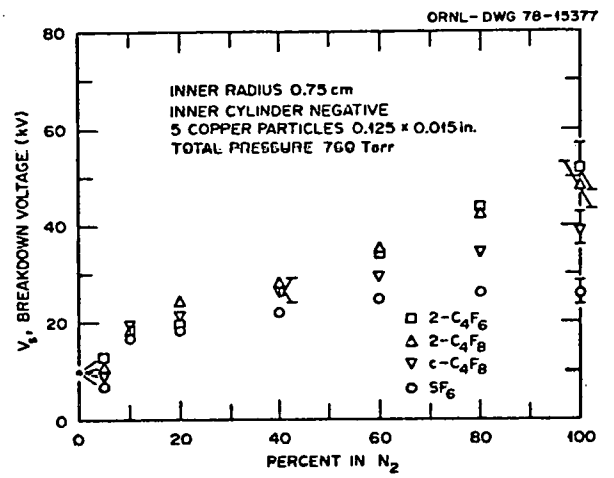

Fig. 14. Breakdown voltages for the four attaching gas/N_2 binary mixtures with contaminating free wire particles at negative polarity, 1 atmosphere, and ∿21°C. Mixtures are identified by the percentage of attaching gas by pressure.

substantial improvement in breakdown voltage.

No significant effect of electrode material was found for inner electrodes that were identical except for their material composition: stainless steel, copper, and aluminum.

In studies of the effects of free conducting particles, the perfluorocarbon/N_2 mixtures were better than the SF_6/N_2 mixtures. For each mixture the introduction of particles was more deleterious than the introduction of surface roughness, but which is the worse problem depends, of course, on the particular roughness and particle chosen. The particle behavior for all four mixtures did coincide with that observed by others for SF_6.

In the future we will examine pressure effects, other gases besides N_2 for the efficient de-energizing of electrons, other electron attaching gases, and mixtures of more than two gases. For the few best mixtures, engineering design rules must be developed and larger scale testing must be performed.

REFERENCES

[1] M. O. Pace, L. G. Christophorou, D. R. James, R. Y. Pai, R. A. Mathis, and D. W. Bouldin, "Improved Unitary and Multicomponent Gaseous Insulators," IEEE Transactions on Electrical Insulation, vol. EI-13, pp. 31-36, February 1978.

[2] L. G. Christophorou, "Elementary Electron-Molecule Interactions and Negative Ion Resonances at Subexcitation Energies and their Significance in Gaseous Dielectrics," Proceedings of the XIII International Conference on Phenomena in Ionized Gases, Berlin, September 11-17, 1977, Vol. II (1978).

[3] D. R. James, L. G. Christophorou, R. Y. Pai, M. O. Pace, R. A. Mathis, I. Sauers, and C. C. Chan, "Dielectric Strengths of New Gases and Gas Mixtures," Gaseous Dielectrics (Proceedings of the International Symposium on Gaseous Dielectrics, Knoxville, Tennessee, March 6-8, 1978) pp. 224-251, (Oak Ridge National Laboratory Report CONF-780301).

[4] L. G. Christophorou, D. R. James, R. Y. Pai, R. A. Mathis, I. Sauers, M. O. Pace, D. W. Bouldin, A. A. Christodoulides, and C. C. Chan, High Voltage Research (Breakdown Strengths of Gaseous and Liquid Insulators), June 1978. (ORNL/TM-6384).

[5] L. G. Christophorou, "The Use of Basic Physical Data in the Design of Multicomponent Gaseous Insulators," Proceedings of the V International Conference on Gas Discharges, Liverpool, England, September 11-15, 1978. London: Institution of Electrical Engineers.

[6] L. G. Christophorou, Atomic and Molecular Radiation Physics. New York: Wiley Interscience, 1971.

[7] C. M. Cooke, "Particle Contamination in Compressed Gas Insulation, Limitations and Control," Gaseous Dielectrics (Proceedings of the International Symposium on Gaseous Dielectrics, Knoxville, Tennessee, March 6-8, 1978) pp. 162-189, (Oak Ridge National Laboratory Report CONF-780301).

[8] R. E. Wootton and F. T. Emery, "Effect of Duration of Voltage Application and Number of Conducting Particles on the AC Breakdown Strength of Compressed SF_6 in a Coaxial System," Gaseous Dielectrics (Proceedings of the International Symposium on Gaseous Dielectrics, Knoxville, Tennessee, March 6-8, 1978), pp. 206-223, (Oak Ridge National Laboratory Report CONF-780301).

[9] R. Nakata, "Particle Scavenging Studies Leading to the Development of a HVDC Gas Bus System," Proceedings of the Conference on Electrical Insulation and Dielectric Phenomena, Colonie, New York, October 17-20, 1977, paper E-20.

[10] A. H. Cookson, P. C. Bolin, H. C. Doepken, Jr., R. E. Wootton, C. M. Cooke, and J. G. Trump, "Recent Research in the United States on the Effect of Particle Contamination in Reducing the Breakdown Voltage in Compressed Gas-Insulated Systems," 1976 Session of CIGRE, August 25-September 2, 1976, Paris, France, paper 15-09.

[11] C. M. Cooke, R. E. Wootton, A. H. Cookson, "Influence of Particles on AC and DC Electrical Performance of Gas Insulated Systems at Extra High Voltage," IEEE Transactions on Power Apparatus and Systems, vol. PAS-96, May/June, pp. 768-777.

[12] A. Pedersen, "Estimation of Breakdown Voltage in Compressed, Strongly Electronegative Gases and Gas Mixtures," Proceedings of the Conference on Electrical Insulation and Dielectric Phenomena, Colonie, New York, October 17-20, 1977, paper E-2.

[13] A. A. Christodoulides, L. G. Christophorou, R. Y. Pai, and C. M. Tung, "Electron Attachment to Perfluorocarbon Compounds. Part I: c-C_4F_6, 2-C_4F_6 1,3-C_4F_6, c-C_4F_8 and 2-C_4F_8, J. Chem. Phys. (submitted for publication).

Marshall O. Pace (S'62-M'70) [redacted] He received the following degrees in electrical engineering: B.S. (Magna Cum Laude), 1963, University of South Carolina; M.S., 1965, Massachusetts Institute of Technology; Ph.D., 1970, Georgia Institute of Technology.

Now Professor of Electrical Engineering at the University of Tennessee, M. O. Pace has also worked at Columbia Products Co., NASA, and Oak Ridge National Laboratory. He has conducted research for the U.S. Atomic Energy Commission, National Science Foundation, U.S. Department of Energy, NASA, Carrier Corp., and Carborundum Corp. His interests are in high voltage and other physical electronics problems.

He is a member of IEEE, Power Engineering Society, CIGRE, Tau Beta Pi, Sigma Xi, and Phi Beta Kappa.

Ching C. Chan was [redacted] He received the B.S. degree in Electrical Engineering from the University of Tennessee in 1977, and is completing the M.S. degree working as a Graduate Research Assistant in the area of gaseous dielectrics for power apparatus. His interests are in plasma and power apparatus and systems.

Mr. Chan worked 12 months at Florida Power and Light Co. as a Cooperative student at the University of Tennessee.

L. G. Christophorou is Professor of Physics at the University of Tennessee and Head of the Atomic, Molecular and High Voltage Physics Group at the Oak Ridge National Laboratory.

THIS PAGE

WAS INTENTIONALLY

LEFT BLANK

INTERNAL DISTRIBUTION

1-2. Central Research Library
3. Document Reference
4-6. Laboratory Records
7. Laboratory Records, R.C.
8. ORNL Patent Office
9. Merl Baker
10. R. D. Birkhoff
11. D. W. Bouldin
12. J. G. Carter
13-57. L. G. Christophorou
58. H. H. Hubbell
59-60. D. R. James
61. C. M. Jones
62. S. V. Kaye
63. H. M. Long
64. R. A. Mathis
65. M. M. Menon
66-67. M. O. Pace
68-69. R. Y. Pai
70. H. Postma
71. C. R. Richmond
72. M. W. Rosenthal
73. H. C. Schweinler
74. S. W. Schwenterly
75. J. H. Whealton
76. H. A. Wright
77. N. F. Ziegler
78. A. Zucker

EXTERNAL DISTRIBUTION

79. D. Allen, Division of Electric Energy Systems, Department of Energy, Washington, D. C. 20545
80. D. Blanc, Universite Paul Sabatier, Centre de Physique Atomique, 118, route de Narbonne, 31077 Toulouse Cedex, France.
81. J. D. Craggs, Department of Electrical Engineering, The University of Liverpool, Brownlow Hill, P.O. Box 147, Liverpool L69 3BX, England.
82. K. Dimoff, Institut National de la Recherche Scientifique, Universite du Quebec, Case Postale 1020, Varennes, Quebec, JOL 2PO, Canada.
83. J. Dutton, Department of Physics, University College of Swansea, University of Wales, Singleton Park, Swansea SA2 8PP, United Kingdom.
84. J. Gracia, Energy Research and Development, Department of Energy, Oak Ridge Operations Office Office, Oak Ridge, Tennessee 37830.
85. O. Farish, Department of Electrical Engineering, University of Strathclyde, Glasgow, C1, 1XW, Scotland.
86. R. W. Flugum, Division of Electric Energy Systems, Department of Energy, Washington, D.C. 20545.
87-97. T. F. Garrity, Division of Electric Energy Systems, Department of Energy, Washington, D.C. 20545.
98. J. M. Googe, Department of Electrical Engineering, The University of Tennessee, Knoxville, Tennessee 37916.
99. D. Mayhew, Office of the Controller, Department of Energy, Washington, D.C. 20545.
100. J. McKeown, Assistant Administrator for Conservation, Department of Energy, Washington, D.C. 20545.

101. T. Nitta, Mgr. Switchgear Engineering, Switchgear Department, Mitsubishi Corporation, 80 Nakano, Minami Shimizu, Amagasaki, Hyogo, Japan.
102. Office of Assistant Manager, Energy Research and Development, Department of Energy, Oak Ridge Operations Office, Oak Ridge, Tennessee 37830.
103. W. Pfeiffer, Institut fur Hochspannungs-und Meßtechnik, 6100 Darmstadt, Schloßgraben 1, Germany.
104. J. J. Phillips, Tennessee Valley Authority, 1310 Commerce Union Bank Building, Chattanooga, Tennessee 37401
105. V. Tahiliani, Electric Power Research Institute, P.O. Box 10412, Palo Alto, California 94303.
106. J. P. Vora, Division of Electric Energy Systems, Department of Energy; Washington, D.C. 20545.
107-133. Technical Information Center, Oak Ridge, Tennessee 37830.

☆ U.S. GOVERNMENT PRINTING OFFICE: 1979-748-189/360